

INFORMATION TO USERS

This manuscript has been reproduced from the microfilm master. UMI films the text directly from the original or copy submitted. Thus, some thesis and dissertation copies are in typewriter face, while others may be from any type of computer printer.

The quality of this reproduction is dependent upon the quality of the copy submitted. Broken or indistinct print, colored or poor quality illustrations and photographs, print bleedthrough, substandard margins, and improper alignment can adversely affect reproduction.

In the unlikely event that the author did not send UMI a complete manuscript and there are missing pages, these will be noted. Also, if unauthorized copyright material had to be removed, a note will indicate the deletion.

Oversize materials (e.g., maps, drawings, charts) are reproduced by sectioning the original, beginning at the upper left-hand corner and continuing from left to right in equal sections with small overlaps. Each original is also photographed in one exposure and is included in reduced form at the back of the book.

Photographs included in the original manuscript have been reproduced xerographically in this copy. Higher quality 6" x 9" black and white photographic prints are available for any photographs or illustrations appearing in this copy for an additional charge. Contact UMI directly to order.

UMI

A Bell & Howell Information Company
300 North Zeeb Road, Ann Arbor MI 48106-1346 USA
313/761-4700 800/521-0600

**A NEW CDP COORDINATE SYSTEM FOR THE SORTING,
VELOCITY ANALYSIS, AND IMAGING OF CROSSWELL
REFLECTION DATA**

A DISSERTATION
SUBMITTED TO THE DEPARTMENT OF GEOPHYSICS
AND THE COMMITTEE ON GRADUATE STUDIES
OF STANFORD UNIVERSITY
IN PARTIAL FULFILLMENT OF THE REQUIREMENTS
FOR THE DEGREE OF
DOCTOR OF PHILOSOPHY

Nicholas Kimble Smalley

November 1997

UMI Number: 9837150

Copyright 1998 by
Smalley, Nicholas Kimble

All rights reserved.

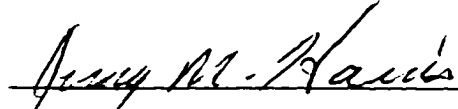
UMI Microform 9837150
Copyright 1998, by UMI Company. All rights reserved.

This microform edition is protected against unauthorized
copying under Title 17, United States Code.

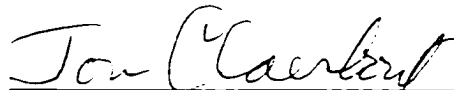
UMI
300 North Zeeb Road
Ann Arbor, MI 48103

@ Copyright by Nicholas Kimble Smalley 1998
All Rights Reserved

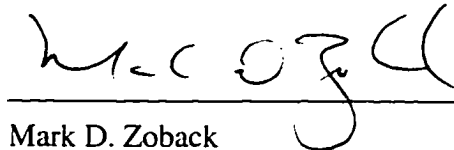
I certify that I have read this dissertation and that in my opinion it is fully adequate, in scope and quality, as a dissertation for the degree of Doctor of Philosophy.


Jerry M. Harris (Principal Adviser)

I certify that I have read this dissertation and that in my opinion it is fully adequate, in scope and quality, as a dissertation for the degree of Doctor of Philosophy.


Jon F. Claerbout

I certify that I have read this dissertation and that in my opinion it is fully adequate, in scope and quality, as a dissertation for the degree of Doctor of Philosophy.


Mark D. Zoback

Approved for the University Committee on Graduate Studies:


Thomas Wasow

Abstract

A new method of crosswell reflection imaging is presented in this dissertation. This method is based on a method of CDP sorting and velocity analysis that parallels surface seismic reflection imaging. A point to point mapping operator is applied to CDP sorted data with a stacking velocity model obtained from crosswell reflection velocity analysis. The approach is tested on wide offset synthetic and field data sets, both of which had 2-d variation in velocity and geological structure. We obtained coherent reflection images in both cases.

We start by deriving CDP coordinate systems for the crosswell and VSP geometries in a similar fashion to the midpoint - offset coordinate system for the surface seismic geometry. We do this by deriving the CDP equation for an arbitrary seismic geometry, and then specializing the coordinates to the crosswell and VSP geometries. We can then solve for the coordinates which represent CDP gathers and an independent parameter, which gives us a CDP coordinate system for the crosswell and VSP geometries. The crosswell CDP coordinate system is a polar coordinate system, where the angular coordinate is the CDP coordinate, and the radial distance coordinate represents a measure of the vertical distance the source and receiver are from the reflector.

The new CDP polar coordinate system gives us the basis for a reflection velocity analysis procedure based on the moveout of the phase of the reflection data in CDP gathers. This is similar to the NMO stacking velocity based procedure in surface seismic reflection velocity analysis, where our objective is to align the phase of the crosswell reflection data to optimize the stack. Due to the changing depths of sources and receivers in the crosswell geometry, we need to assign multiple stacking velocities for a single CDP. This makes the crosswell reflection velocity analysis procedure more complicated than surface seismic, where only one stacking velocity is required for a single CDP.

By optimizing the reflection data for stack over a 2-d grid of CDPs, we can obtain coherent reflection events across the entire survey in a medium with small 2-d variation in

velocity ($< 20\%$). The alignment of the phase of the reflection data over a 2-d grid of CDPs gives the crosswell CDP sorting and velocity analysis imaging method an advantage over other crosswell reflection imaging methodologies. Many other methodologies use direct and reflected traveltimes tomography to find the imaging velocities. These methods have been shown to give coherent reflection images in some cases, particularly in 1-d media. However, by not directly aligning the phase of the reflection data in CDP gathers, even small changes in velocity that are not discerned in the velocity model can lead to a loss of coherency in the final stack.

Acknowledgments

Wow ! I'm finally finished. It's been very challenging but very rewarding. There are many people I'd like to thank and acknowledge for their guidance, friendship, and support. First of all I'd like to thank my advisor Jerry Harris. Jerry provided me with financial support through the Seismic Tomography Project (STP) consortium, excellent computer resources (both software and hardware), the opportunity to work on many interesting projects, and excellent guidance in my research. Jerry always showed good judgment on when to give me advice, challenge me, and when to leave me alone. Jerry's support not only helped me to successfully complete my thesis, but also gave me the skills and confidence that enabled me to obtain an excellent job opportunity for my post graduate life. I would also like to thank Bob Langen of Chevron for his support over the years. Bob served as the STP faculty member during Jerry's sabbatical year. Bob was always very supportive, and always had time to listen to me. Bob's experience and suggestions greatly helped both me and the STP group as a whole.

I would also like to thank several other faculty members for their support. I took two classes in exploration geophysics from Jon Claerbout during my first year at Stanford. These classes provided me with an excellent background in geophysical seismic data processing and wave propagation, and served as a foundation for my research. It was always pleasant to talk to Jon, and he was very supportive of me and my work. Mark Zoback was the department chairman for most of my years at Stanford. He was always willing to listen to the progress I was making on my research, and showed a lot of enthusiasm about my work. Additionally, Mark was very supportive and instrumental to the work I did along with Susan Owen on the Graduate Student Advisory Committee (GSAC). It was clear that Mark was fully committed to improving student life and student-faculty interaction within the department. I would also like to thank Lynn Orr for his development of and commitment to the GSAC. I thank Biondo Biondi and Martin Blunt for agreeing to be part of the my defense committee (particularly on such short notice !)

Youli Quan was my office mate for most of my years at Stanford. Youli was always nice, considerate, and helpful. The friendship with him as well as his wife Li and his daughter Cindy made my life much more enjoyable during my stay here. Guan Wang was also a very good friend who was always very helpful with computer questions and technical issues, and with whom I shared many intelligent (and often highly animated!) conversations. I would also like to thank the other members of STP for their friendship and support including Le-Wei Mo, Ricardo Castellini, and Ann Wiley. Other good friends I have known included Ginger Barth and Dale Richards. I would also like to thank all the people (far too numerous to list everyone) with whom I have shared friendship, good conversation, and knowledge.

I would really like to thank my parents, Dr. Anthony and Anna Smalley, and my brother Nathan Smalley for their love and support. Even though my parents were 2000 miles away in Texas their phone calls always gave me a lift. Additionally, their editing of my thesis as well as coming out to California to support me during my defense helped me so much during a time where the pressure was very high.

During the last several months I developed a special friendship with Qing (Keena) Yan. We met over the internet earlier this year (she is working toward a Ph.D. in molecular biology at the University of Arizona). Her e-mails of encouragement meant so much to me while I was working night and day to get finished. I feel very lucky to have become friends with such a kind, intelligent, and sweet person.

Many other people have been very helpful to me in my academic life. Mark van Schaack was always helpful with questions concerning ProMAX and data acquisition, and also served as the system administrator for three years. Spyros Lazaratos successful work in crosswell reflection imaging served as a chief motivation for my work in this same area. Additionally, Spyros was generous with his knowledge on wave propagation and crosswell data processing. Caroline Lambert was very helpful during her tenure as STP computer administrator. Sonya Williams, Marianne Ehlers, and Linda Farwell were very helpful with administrative issues.

Finally, I would like to thank George Trebaol and Luther Smith for the job opportunity they made me at TRW. Knowing I had an excellent (and high paying !) job waiting for me upon graduation gave me considerable encouragement during the long and grueling dissertation writing days.

Table of Contents

1	Introduction	1
1.1	Background.....	1
1.2	Previous work on Crosswell Reflection Imaging.....	2
1.3	The Goals of this Thesis.....	2
1.3.1	Crosswell CDP Coordinate System	3
1.3.2	Crosswell Reflection Velocity Analysis.....	3
1.3.3	Crosswell Reflection Imaging On a Synthetic Data Set	5
1.3.4	Crosswell Reflection Imaging On a Real Data Set.....	6
2	CDP Coordinate Systems for Surface Seismic, Crosswell, and VSP Geometries	8
2.1	Introduction	8
2.2	Arbitrary Geometry CDP Definition	9
2.3	Specific Geometry CDP Definition	10
2.3.1	Surface Seismic	10
2.3.2	Crosswell	10
2.3.3	VSP.....	11
2.4	Reflection Traveltime Equations.....	12
2.4.1	Surface Seismic	12
2.4.2	Crosswell	13
2.4.3	VSP.....	13
2.5	Parameterizing the CDP Gathers	13
2.5.1	Surface Seismic	14
2.5.2	Crosswell.....	15

2.5.3	VSP	16
2.6	CDP Traveltime Equations.....	17
2.6.1	Surface Seismic	18
2.6.2	Crosswell	18
2.6.3	VSP.....	18
2.7	CDP Traveltime Moveout Corrections	19
2.7.1	Surface Seismic	19
2.7.2	Crosswell	19
2.7.3	VSP.....	20
2.8	Stacking the Reflection Data	23
2.9	Conclusions	23
3	Crosswell Reflection Velocity Analysis.....	24
3.1	Introduction	24
3.2	Velocity Analysis in a Constant Velocity Medium	25
3.3	Variable Velocity Reflection Traveltime Equations.....	28
3.3.1	Evaluation of the crosswell traveltime Taylor Series Expansion	32
3.4	Variable Velocity Moveout Corrections	33
3.5	Variable Velocity Reflection Velocity Analysis.....	37
3.5.1	Synthetic Example	38
3.6	Estimating Reflection Depth	42
3.6.1	Synthetic Example	44
3.6.2	Variable Velocity	47
3.6.3	Synthetic Example	48
3.7	Conclusions	49
4	Crosswell CDP Reflection Imaging - Synthetic Data Set.....	53
4.1	Introduction	53
4.2	Data Set Description	53
4.3	Reflection Imaging Algorithm	54
4.4	Raw Data.....	55
4.5	Pre-Processed Reflection Data	55
4.6	Reflection Velocity Analysis.....	58
4.6.1	CDP Sorting of the Reflection Data.....	58

4.6.2	Reflection Depth Determination	60
4.6.3	Alignment of Reflection Event	63
4.6.4	Stacking Velocity Grid	63
4.7	CDP Imaging Algorithm	65
4.7.1	Starting Reflection Depth and Reflection Depth Loop	65
4.7.2	CDP Sorting	66
4.7.3	Interpolation of Stacking Velocities	69
4.7.4	HNMO and VLMO corrections	69
4.8	Stack over CDP Gathers and Final Reflection Image.....	69
4.9	Conclusions	71
5	Crosswell CDP Reflection Imaging - Field Data Set.....	72
5.1	Introduction	72
5.2	Field Data Description	73
5.3	Pre-Processed Reflection Data	73
5.4	Reflection Velocity Analysis.....	74
5.4.1	CDP Sorting of the Reflection Data.....	74
5.4.2	Reflection Depth Determination	74
5.4.3	Alignment of the Reflection Event	79
5.4.4	Velocity Analysis for CDP's in the middle of the survey	79
5.4.5	Stacking Velocity Grid	82
5.5	Final Reflection Image Stack	84
5.6	Conclusions	88
	References	89

List of Tables

1.1	CDP coordinate systems	17
-----	------------------------------	----

List of Figures

1.1	Crosswell CDP gather, CDP coordinate system, and stacking coordinates	4
1.2	Replacement of a series of interval velocities with a single stacking velocity	5
1.3	2-d grid of stacking velocities	6
2.1	Reflection geometry for arbitrary source and receiver location	9
2.2	CDP gathers in terms of surface seismic coordinates and geometry	11
2.3	CDP gathers in terms of crosswell coordinates and geometry	12
2.4	CDP gathers in terms of VSP coordinates and geometry	13
2.5	Surface seismic and crosswell CDP coordinate systems	14
2.6	Rotated VSP coordinates and VSP CDP coordinate system	15
2.7	Traveltime curves for surface seismic, crosswell, and VSP CDP gathers	19
2.8	Moveout Corrections for surface seismic, crosswell, and VSP geometries	21
2.9	Traveltime curves after the horizontal moveout correction	22
2.10	Traveltime curves after horizontal and vertical moveout corrections	22
2.11	Final reflection images	23
3.1	Surface Seismic and Crosswell CDP gathers in variable velocity media	25
3.2	CDP- HNMO gathers for different velocity estimates	27
3.3	CDP- VLMO gathers for different velocity estimates	28
3.4	Surface Seismic reflection geometry for variable velocity media	29
3.5	Crosswell reflection geometry for variable velocity media	31
3.6	Crosswell experiment used to evaluate the Taylor Series expansion	32
3.7	Comparison of two term traveltime and the true traveltime	34
3.8	The stacking velocity value for two extreme apertures.....	37
3.9	Replacement of a series of interval velocities with a single stacking velocity	38
3.10	Crosswell reflection velocity analysis procedure	39

3.11	Synthetic model	40
3.12	Velocity analysis results from the synthetic model	41
3.13	Comparison between velocity analysis and true stacking velocities.....	42
3.14	Reflection depth error	44
3.15	Synthetic model	44
3.16	Stacking velocity and the derivative of the stacking velocity	46
3.17	Synthetic model	49
3.18	Adjusted stacking velocity derivative	50
3.19	Adjusted stacking velocity derivative	51
4.1	2-d velocity synthetic model	54
4.2	Crosswell reflection imaging algorithm	55
4.3	CSGs from the synthetic model	56
4.4	Upgoing and downgoing reflection geometry	57
4.5	f-k filter.....	57
4.6	CSGs after upgoing and downgoing reflection pre-processing	58
4.7	Reflection velocity analysis algorithm	59
4.8	Three different CDP locations and their reflective raypaths	59
4.9	Four CDP gathers	60
4.10	CDP traveltimes gathers for the correct and erroneous reflector depths	62
4.11	Four CDP gathers at an incorrect assumed reflector depth	62
4.12	1-d tomogram of the synthetic model	63
4.13	Alignment of a reflection event	64
4.14	Stacking velocities determined from velocity analysis	65
4.15	Stacking velocity grid	66
4.16	Comparison of crosswell and surface seismic stacking velocity grids.....	67
4.17	CDP imaging algorithm	67
4.18	Pre-processing used to image regions of the survey	68
4.19	Point to point mapping.....	68
4.20	3-d interpolation of the stacking velocities	69
4.21	Final reflection image stack	70
5.1	Data Set Geometry	73
5.2	CRG of the field data, and after pre-processing for downgoing reflections	75
5.3	4 CDP gathers	76
5.4	CDP - VLMO gathers for 3 assumed reflection depths	77

5.5	1-d tomogram velocity model	78
5.6	Alignment of a reflection event	80
5.7	Stacking velocities determined from velocity analysis	81
5.8	CDP - VLMO gather in the middle of the survey with and without add. proc.	81
5.9	CDP - VLMO gather in the middle of the survey	82
5.10	Stacking velocity grid	83
5.11	Final reflection image stack using CDP sorting and velocity analysis	85
5.12	Final reflection image stack from the XSP - CDP algorithm	86
5.13	2-d SIRT tomogram	87

Chapter 1

Introduction

1.1 BACKGROUND

The use of full waveform crosswell data has increased over the last several years. One of the main reasons for this is the high frequency content of crosswell data. The high frequency content allows for much higher resolution of the subsurface than other seismic geometries such as surface seismic and Vertical Seismic Profile (VSP). The high resolution potential of crosswell data has made it an integral part of reservoir characterization (Lines, et. al, 1995). The most common imaging method using crosswell data has been tomographic traveltimes inversion or tomography. Tomography uses the traveltimes of the direct arrival of the seismic traces. The traveltimes are inverted to obtain a velocity model (Harris, et. al, 1990). While traveltimes tomography can often provide a useful image of the medium, it only uses the traveltimes of the direct arrivals. In order to take full advantage of the high frequency content of crosswell data, we need to use more of the wavefield. For example, diffraction tomography (Harris and Wang, 1996) uses most of the crosswell wavefield.

More recently there has been a focus on using the reflection arrival of the crosswell wavefield to image the medium. Crosswell reflection imaging presents some unique problems in sorting, wavefield separation, and velocity analysis. The crosswell geometry has sources and receivers that vary in depth, giving another dimension to the sorting and stacking problem. Additionally, crosswell data has great complexity. It has many different wave modes, many of which directly interfere with the reflection data, and need to be removed in order to image the medium with reflection data. Both the complex wavefield of crosswell data and the crosswell geometry present a challenge in obtaining a velocity model for reflection imaging.

1.2 PREVIOUS WORK ON CROSSWELL REFLECTION IMAGING

Some well developed migration algorithms have been applied to crosswell reflection imaging. One of these is Kirchhoff migration (Mo, 1993), (Qin and Schuster, 1993). This algorithm used direct arrival traveltime tomography to obtain the velocity model for reflection imaging. This migration algorithm handles all possible dips, but also requires full aperture to fully collapse the Fresnel zone. Since the crosswell geometry does not have full aperture, this method often leaves artifacts in the final image, and smears noise over the migration ellipse. The work based upon the XSP-CDP method (Lazaratos, 1993), which is an adaptation of the VSP-CDP method (Wyatt and Wyatt, 1981), heavily emphasized wavefield separation to isolate the reflection data from the rest of the crosswell wavefield, and used a point to point mapping operator to image the crosswell reflection data. This method produced a number of high resolution reflection images. However, this method only used direct arrival traveltime tomography and sonic log velocities, and did not use the reflection data to obtain the velocity model for reflection imaging. The CDRATT (Combined Direct and Reflection Arrival Traveltime Tomography) reflection imaging procedure used a combined least squares inversion of the direct and reflected arrival traveltimes to obtain a velocity model for reflection imaging (Van Schaack, 1997). This procedure also used a point to point mapping operator to image the reflection data. However, it does not solve for the velocities that directly align the phase of the reflection data. Another recent method (Stewart, R.R, and Marchisio, G., 1991) used the traveltime moveout of the reflection data in the Common Midpoint Domain to find stacking velocities to image the reflection data. However, this method does not perform velocity analysis in CDP gathers, such as is the case with surface seismic reflection velocity analysis.

1.3 THE GOAL OF THIS THESIS

The goal of this thesis is to improve the crosswell reflection stack by finding a 2-d set of stacking velocities that will optimize the final stack. This method closely parallels the surface seismic reflection velocity analysis procedure of aligning the phase of the reflection events to maximize the semblance of the data in CDP gathers. By allowing the stacking velocities to change laterally and vertically, we can find the optimum reflection stack where there is small to moderate 2-d velocity variation. The benefits of this methodology are:

- 1) It optimizes the stack of the reflection data by finding the stacking velocities that the reflection data itself indicates are best for stack.

- 2) It can take into account 2-d variation in the stacking velocities.
- 3) It can handle wider well spacings where we are more likely to have 2-d changes in the stacking velocities.

This thesis uses many of the same attributes that made the XSP-CDP mapping algorithm successful, including wavefield separation and the point to point mapping operator. Additionally, it improves upon the XSP-CDP method by defining crosswell CDP gathers, and by using the moveout of reflection data in the CDP gathers to find an improved velocity model for reflection imaging. It also improves upon the CDRATT method by finding the velocity model that directly aligns the phase of the reflection data for stack.

We do this by defining a new CDP coordinate system for crosswell reflection data (Chapter 2), a method for reflection velocity analysis using this CDP coordinate system (Chapter 3), and a reflection mapping method that uses the CDP coordinate system and a 2-d grid of stacking velocities to sort, image, and stack the reflection data resulting in a final reflection image on a wide offset crosswell survey (Chapters 4 and 5).

1.3.1 Crosswell CDP Coordinate System

In Chapter 2, a new CDP coordinate system for crosswell reflection data is derived by first finding the crosswell source and receiver pairs that yield CDP reflection points (figure 1.1(a)), and then parameterizing the problem by assigning a variable to the CDP gathers and an independent parameter (figure 1.1(b)). This is done in parallel for the surface seismic, crosswell, and VSP geometries. By writing the reflection traveltime equation in terms of the crosswell CDP coordinate system, we are able to define moveout corrections for the source and receiver offset for a given CDP. This allows us to align the reflection data for stack (figure 1.1(c)).

1.3.2 Crosswell Reflection Velocity Analysis

In Chapter 3, we make use of the CDP coordinate system derived in Chapter 2 by deriving a velocity analysis procedure based on the moveout of the reflection data in the CDP gathers. The moveout of the reflection data in CDP gathers is a function of the actual velocity of the medium and the applied moveout velocity. In order to obtain the correct

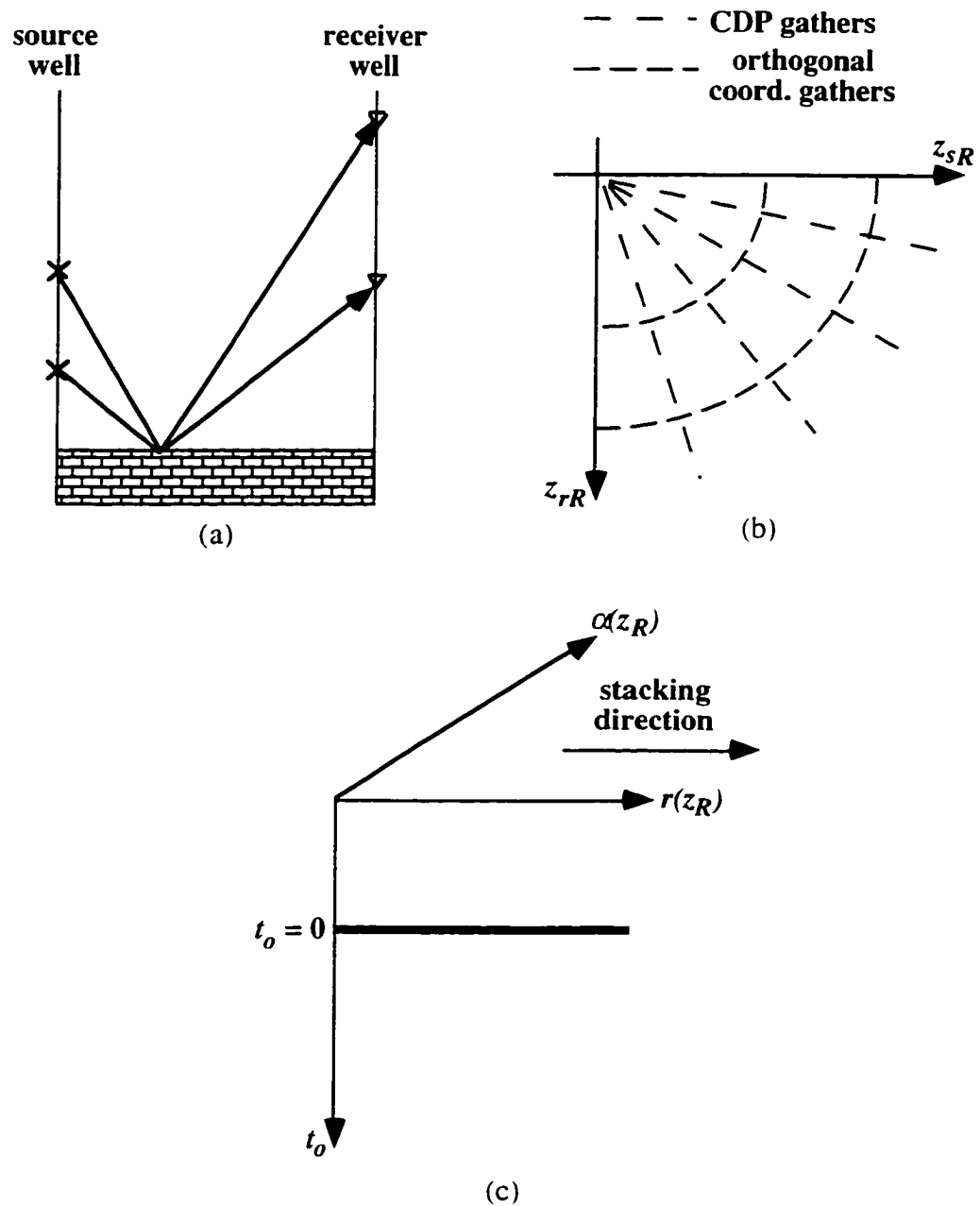


Figure 1.1: (a) A crosswell CDP gather. By keeping the ratio of the source distance and the receiver distance from the reflection constant, we obtain a CDP gather in constant velocity media. (b) The crosswell CDP coordinate system. It is a polar coordinate system $[\alpha(z_R), r(z_R)]$, where $\alpha(z_R)$ is the CDP coordinate and $r(z_R)$ is the orthogonal coordinate, z_{sR} and z_{rR} are the distance from the source to the reflection and from the receiver to the reflection respectively, and z_R is the reflection depth. (c) A crosswell CDP gather after source and receiver moveout corrections have been made. The reflection event is aligned for stack.

moveout for reflection data in CDP gathers, the correct velocity must be applied in making the moveout corrections. In a variable velocity medium we can replace a series of interval velocities with a single stacking velocity to make the traveltime moveout corrections (figure 1.2). Additionally, we use Fermat's principle to approximate the raypath location by the common ratio gathers (figure 1.2). By performing moveout corrections for all source and receiver pairs for a given CDP, we are able to align the reflection data to obtain the optimal stack. We also show in this chapter how to find the reflection depth, and the necessity to incorporate prior information to find the reflection depth.

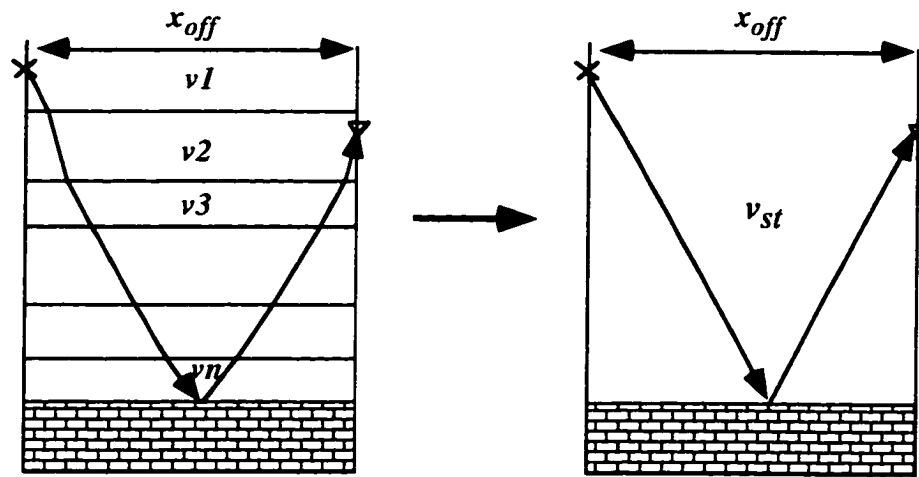


Figure 1.2: Replacement of a series of interval velocities with a single stacking velocity. This allows for the use of common ratio gathers to define CDPs and the use of a single stacking velocity (v_{st}) to perform the moveout corrections.

1.3.3 Crosswell Reflection Imaging On a Synthetic Data Set

By combining the CDP sorting procedure discussed in Chapter 2, and the reflection velocity analysis procedure discussed in Chapter 3, we were able to define a new algorithm for crosswell reflection imaging in Chapter 4. The new algorithm takes the data from the recorded time series all the way through to a final reflection image. This includes:

- 1) Wavefield separation to isolate the reflection data from the rest of the crosswell wavefield.
- 2) Sorting into CDP gathers.

- 3) Reflection velocity analysis to find the stacking velocities that will optimize the stack.
- 4) A point to point mapping operator using the 2-d grid of stacking velocities (figure 1.3) to create the final stack.

We applied this algorithm to a finite difference generated synthetic data set that has 2-d velocity variation that ranges from 13 kft/sec to 15.5 kft/sec. It is this degree of 2-d velocity variation for which this reflection imaging algorithm is developed. A coherent and accurate stack is produced for the entire survey.

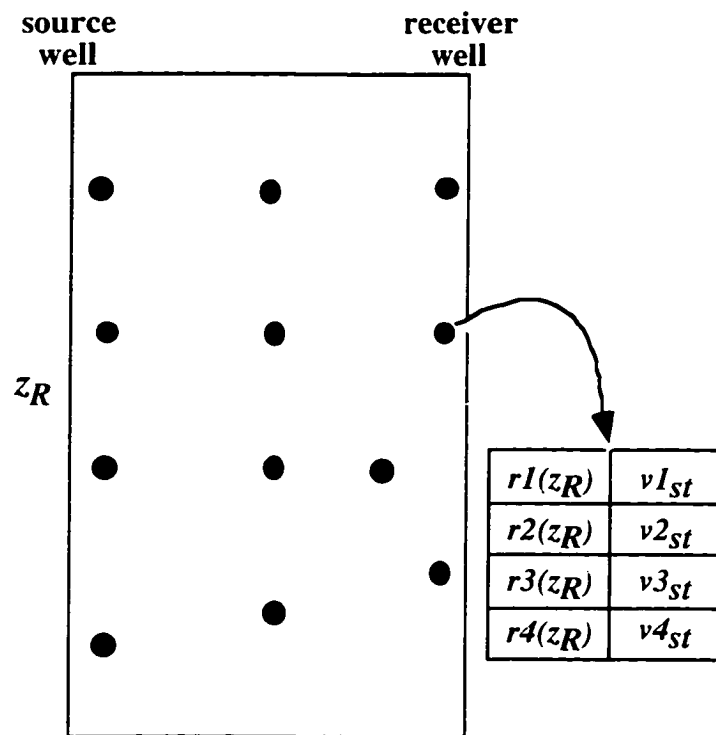


Figure 1.3: A 2-d grid of stacking velocities, in which each point where CDP reflection velocity analysis was performed (solid circles) has a vector of stacking velocities. By generating a 2-d grid of stacking velocities through CDP reflection velocity analysis, we can obtain a reflection image for the entire survey. The crosswell geometry requires that each CDP point has multiple stacking velocities in a variable velocity medium. This differs from the surface seismic geometry, where only one stacking velocity is used at each CDP point.

1.3.4 Crosswell Reflection Imaging On a Real Data Set

We applied the same reflection algorithm discussed in Chapter 4 to a real data set in chapter 5. This data set has small 2-d variation in velocity (<10 %) and a well spacing of

1225 ft. The real data set has a number of problems dealing with signal to noise. This requires 2-d Fourier filtering both to isolate the reflection data in the pre-processing stage, and additional filtering in CDP gathers to isolate the reflection data for velocity analysis. Velocity analysis was performed over a 2-d grid of reflection points. We obtained a high resolution reflection image for the final stack. We compared this image to a XSP-CDP stacked image. While both images show similar structure, the image using CDP reflection velocity analysis yields a more coherent overall stack.

Chapter 2

CDP Coordinate Systems for Surface Seismic, Crosswell, and VSP Geometries

2.1 INTRODUCTION

One of the most basic concepts of improving subsurface images using seismic data is to improve the signal to noise ratio through stacking. In surface seismic reflection imaging, this is achieved by combining the data in a way that allows us to sum together energy coming from a common depth point in space. This concept is Common Depth Point (CDP) stacking. In CDP stacking the signal is summed from those sources and receivers that have the same reflection point. It is beneficial with any seismic geometry to find the set of sources and receivers that under certain conditions will sample the same reflection point, so that the concept of CDP stacking can be used. Once the source and receiver pairs that yield the same reflection point are known, we want to write the reflection traveltime equation pertaining to that specific geometry in terms of the CDP location and an independent parameter or variable. By doing this, we can correct for the traveltime moveout of the source and receiver pairs for a given CDP in terms of the independent parameter, allowing the data to be stacked. In this chapter we start by deriving the lateral reflection point location for sources and receivers with arbitrary locations. We then look at surface seismic, crosswell, and Vertical Seismic Profile (VSP) geometries to find their respective CDP equations, and derive CDP traveltime equations and moveout corrections to obtain a framework for stacking and imaging.

2.2 ARBITRARY GEOMETRY CDP DEFINITION

An arbitrary source and receiver location is shown in figure 2.1. Assuming constant velocity, we can write the following trigonometric equations:

$$\tan \phi = \frac{x - x_s}{z_R - z_s}, \quad (2.1)$$

$$\tan \phi = \frac{x_r - x}{z_R - z_r}, \quad (2.2)$$

where ϕ is the angle of incidence of the reflection raypath, z_s and z_r are the source and receiver depths, x_s and x_r are the lateral locations of the source and receiver, z_R is the reflection depth, and x is the lateral location of the reflection point.

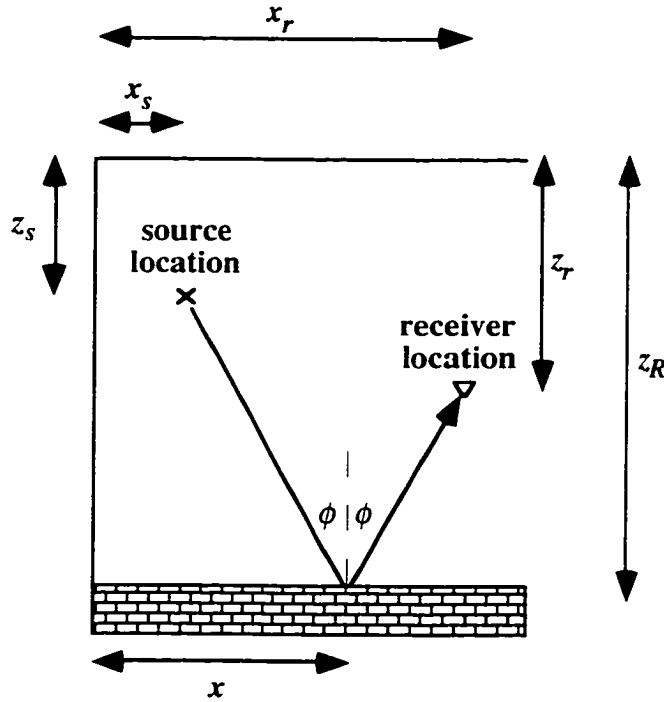


Figure 2.1: Arbitrary source and receiver location reflection geometry for a constant velocity medium.

By solving equations (2.1) and (2.2) for x , we obtain the following expression for the lateral location of the reflection point:

$$x = \frac{x_r(z_R - z_s) + x_s(z_R - z_r)}{[(z_R - z_s) + (z_R - z_r)]}. \quad (2.3)$$

By holding x constant in equation (2.3), we can obtain the set of source and receiver locations that yield the same reflection point locations for any given source and receiver geometry.

2.3 SPECIFIC GEOMETRY CDP DEFINITIONS

Equation 2.3 gives us the CDPs for any given source and receiver geometry. In this section, we examine the set of source and receiver pairs that yield CDPs for specific seismic geometries. These geometries include surface seismic, crosswell, and VSP. Each of these geometries allows for simplification to equation (2.3) and for reduction in the number of variables. This allows us to graph in two dimensions the set of sources and receivers that yield the same CDPs for each of these seismic geometries.

2.3.1 Surface Seismic

For the surface seismic geometry we make the following simplifications to equation (2.3):

$$z_s = 0, z_r = 0. \quad (2.4)$$

Equation (2.3) now simplifies to

$$x = \frac{x_r + x_s}{2}. \quad (2.5)$$

Therefore our remaining variables are (x_s, x_r) . Figure 2.2(a) shows the coordinates that correspond to CDP gathers in surface seismic space (x_s, x_r) (constant values of x in equation (2.5)). We see that CDP gathers correspond to lines in surface seismic space (x_s, x_r) . Figure 2.2(b) shows a surface seismic CDP gather.

2.3.2 Crosswell

For the crosswell geometry, we can simplify equation (2.3) by writing the following:

$$x_s = 0, x_r = x_{off} \text{ (well spacing)}. \quad (2.6)$$

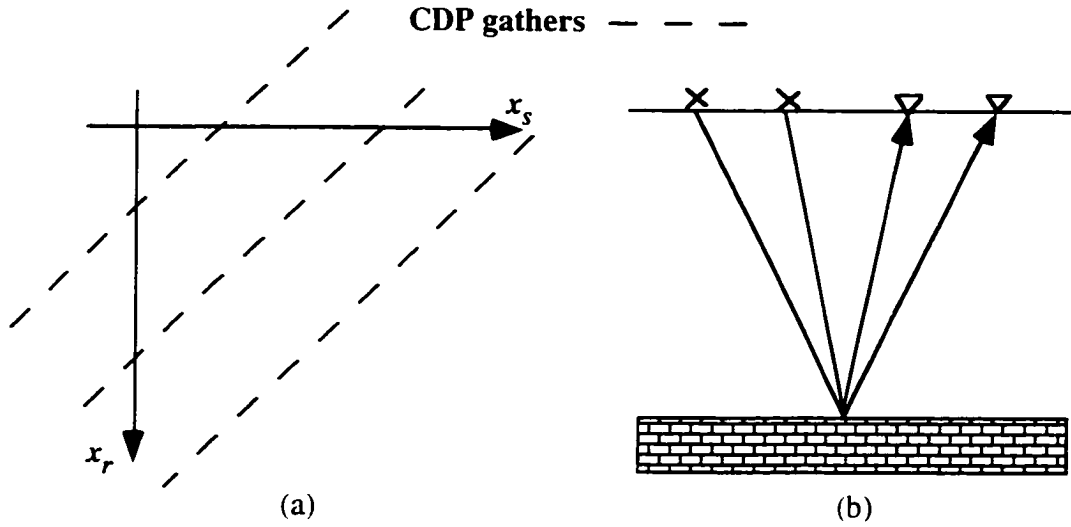


Figure 2.2: CDP gathers in terms of surface seismic coordinates (a) and the surface seismic geometry (b).

Now equation (2.3) reduces to

$$x = \frac{x_{off}}{1 + \frac{z_{rR}}{z_{sR}}}, \quad (2.7)$$

where $z_{rR} = z_R - z_r$ and $z_{sR} = z_R - z_s$. Figure 2.3(a) shows the coordinates that correspond to common reflection points or CDP gathers in crosswell space (z_{sR}, z_{rR}) . These CDP gathers are lines that radiate from the origin. We see that as well as the source and receiver depths, the crosswell problem is parameterized by the reflection depth z_R . Figure 2.3(b) also shows a crosswell CDP gather.

2.3.3 VSP

For the VSP geometry, we can simplify equation (2.3) by writing the following:

$$z_s = 0, x_r = 0. \quad (2.8)$$

Now equation (2.3) reduces to

$$x = \frac{x_s}{1 + \frac{z_R}{z_{rR}}}, \quad (2.9)$$

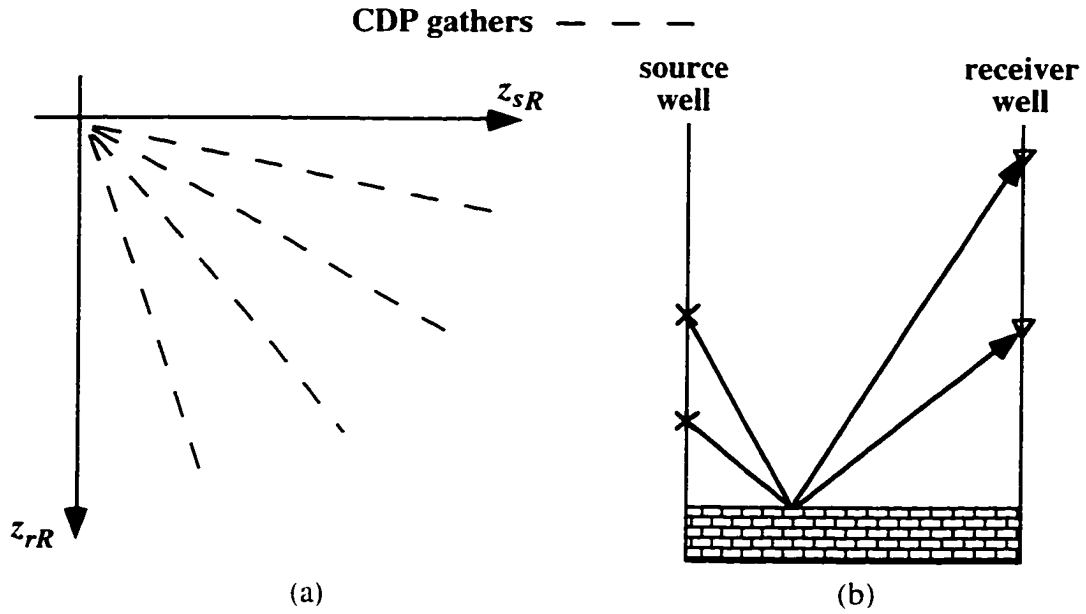


Figure 2.3: CDP gathers in terms of crosswell coordinates (a), and the crosswell geometry (b).

where $z_{rR} = z_R - z_r$. Figure 2.4(a) and equation (2.9) show that the CDP gathers in (x_s, z_{rR}) space are hyperbolas. This is shown in more detail in section 2.5.3. We can take note of the similarities between equation (2.9) for the VSP geometry and equation (2.7) for the crosswell geometry. By substituting x_s for x_{off} , z_R for z_{rR} , and z_{rR} for z_{sR} in equation (2.7) we obtain equation (2.9). Therefore we can consider the VSP geometry to be a special case of the crosswell geometry, or vice versa. In similar fashion to the crosswell CDP gathers, the VSP CDP gathers are parameterized by reflection depth. Figure 2.4(b) also shows a VSP CDP gather. The sources that give the CDP locations change in lateral location in a hyperbolic fashion.

2.4 TRAVELTIME EQUATIONS

Knowing the set of sources and receivers that correspond to CDP reflection points is very useful. However before the CDP reflection data can be stacked, we have to correct for the different locations of the source and receiver pairs that yield different traveltimes for the same CDP reflection point. The traveltimes for each of the previously discussed geometries for a constant velocity medium (velocity = v) are given below.

2.4.1 Surface Seismic

$$t = \frac{\sqrt{(2z_R)^2 + (x_s - x_r)^2}}{v} \quad (2.10)$$

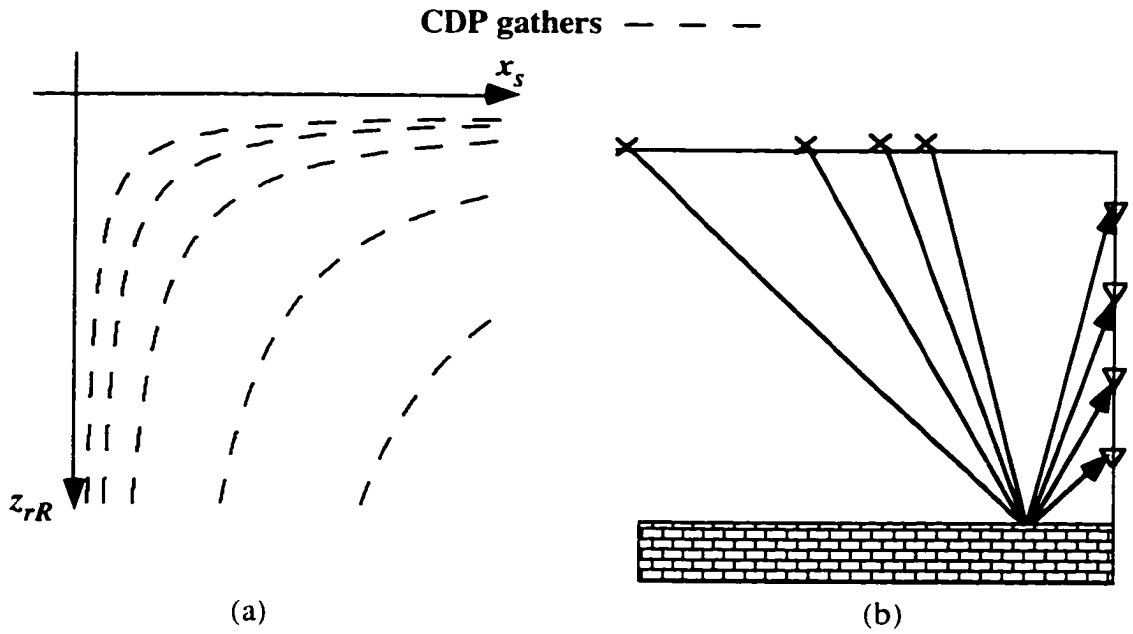


Figure 2.4: CDP gathers in terms of VSP coordinates (a), and the VSP geometry (b).

2.4.2 Crosswell

$$t = \frac{\sqrt{(z_{sR} + z_{rR})^2 + x_{off}^2}}{v} \quad (2.11)$$

2.4.3 VSP

$$t = \frac{\sqrt{(2z_{rR})^2 + x_s^2}}{v} \quad (2.12)$$

We now need to rewrite equations (2.10 - 2.12) in terms of a CDP coordinate and another independent parameter so that we can determine how the reflection traveltime changes for a given CDP. We can use the CDP coordinate geometry from the previous section to determine an independent parameter for each of the seismic geometries.

2.5 PARAMETERIZING THE CDP GATHERS

In order to write CDP traveltime equations for each geometry, we have to rewrite equations (2.10) - (2.12) in terms of a CDP coordinate and another independent coordinate or parameter. Therefore we need a way to parameterize the CDP curves in terms of an

independent variable for each of the seismic geometries. For all the proceeding geometries, the CDP gathers are represented by a family of curves with a characteristic shape. Our objective is to use the shape of these curves to define a CDP coordinate system for each geometry.

2.5.1 Surface Seismic

In the case of surface seismic the CDP lines have a slope of 1 in (x_s, x_r) space (figure 2.2(a)), and correspond to common midpoint gathers. Each of the CDP or common midpoint lines are parameterized by using the orthogonal set of curves which are lines corresponding to common offset gathers (figure 2.5(a)). The coordinates (y, h) correspond to midpoint and offset respectively, and are defined in terms of the (x_s, x_r) coordinates as follows (Claerbout, 1985):

$$y = \frac{x_s + x_r}{2} \quad (2.13)$$

$$h = \frac{x_r - x_s}{2} \quad (2.14)$$

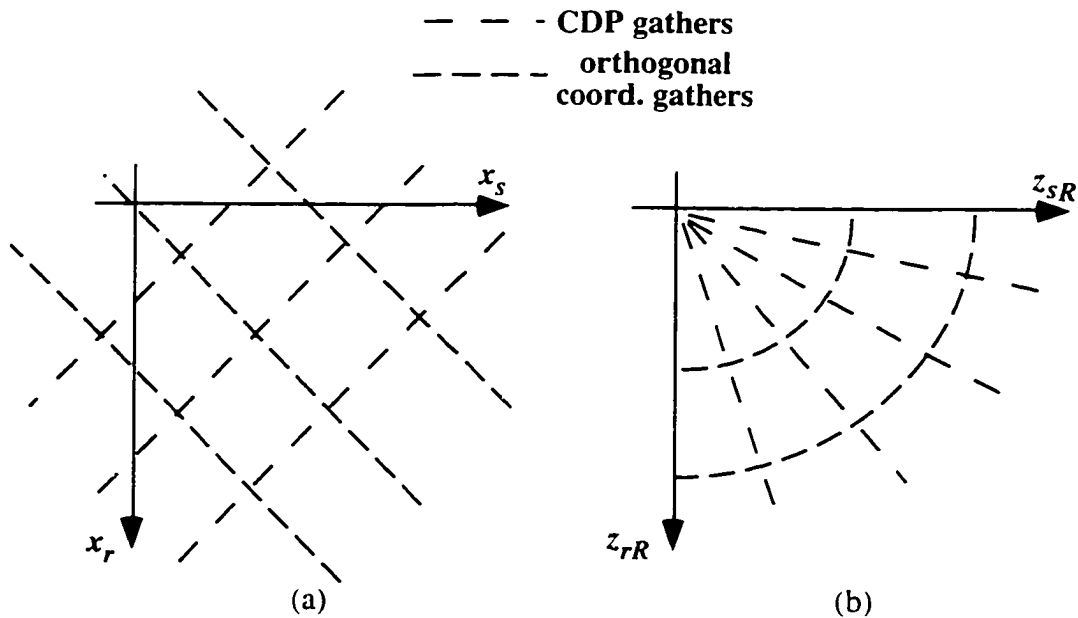


Figure 2.5: Surface seismic CDP coordinate system (a), and the crosswell CDP coordinate system (b). The surface seismic CDP coordinate system is rectangular, and the crosswell CDP coordinate system is polar and parameterized by reflection depth.

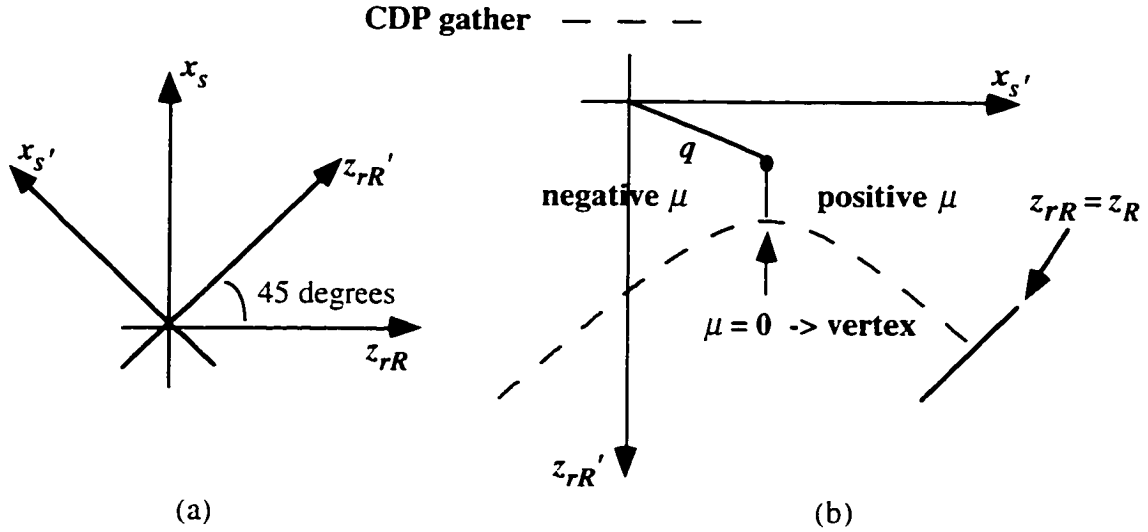


Figure 2.6: VSP coordinate system rotation (a), and the VSP CDP coordinate system (b). The VSP coordinate system is hyperbolic and is parameterized by reflection depth and CDP location.

2.5.2 Crosswell

The crosswell geometry has CDP gathers that radiate from the origin in (z_{sR}, z_{rR}) space (figure 2.3(a)). Each of these lines makes a constant angle with either axis. This suggests that we can parameterize the crosswell CDP gathers by drawing a family of curves each with constant radial distance from the origin (i.e. circles) (Figure 2.5(b)). Therefore we can define a set of crosswell CDP coordinates $[\alpha(z_R), r(z_R)]$ as follows:

$$\tan \alpha(z_R) = \frac{z_{rR}}{z_{sR}}, \quad (2.15)$$

$$r(z_R) = \sqrt{z_{sR}^2 + z_{rR}^2}. \quad (2.16)$$

We can rewrite the original coordinates in terms of the new CDP polar coordinates:

$$z_{sR} = r(z_R) \cos \alpha(z_R), \quad (2.17)$$

$$z_{rR} = r(z_R) \sin \alpha(z_R). \quad (2.18)$$

2.5.3 VSP

As stated previously, equation (2.9) forms hyperbolas in (x_s, z_{rR}) space for constant values of x . The axis of symmetry is located 45 degrees from the two axes. This suggests that the best way to parameterize the CDP curves for the VSP geometry is with hyperbolic coordinates. In order to rewrite equation (2.9) in the form of a basic hyperbolic equation, we define a new set of coordinates (x_s', z_{rR}') rotated 45 degrees from the (x_s, z_{rR}) coordinates (figure 2.6(a)). Rewriting equation (2.9) in terms of the rotated coordinate system yields

$$\frac{[x_s' - \frac{\sqrt{2}}{2}(z_{rR} + x)]^2}{xz_R} - \frac{[z_{rR}' - \frac{\sqrt{2}}{2}(z_{rR} - x)]^2}{xz_R} = 1. \quad (2.19)$$

We see from equation (2.19) that the center of the hyperbola is located at $[\frac{\sqrt{2}}{2}(z_{rR} + x), \frac{\sqrt{2}}{2}(z_{rR} - x)]$ in (x_s', z_{rR}') space, and that the vertex is located at a distance $\sqrt{xz_R}$ from the hyperbola's center (figure 2.6(b)). Therefore the center of the hyperbola is a function of both the reflection depth and lateral reflection point location. We now define the hyperbolic coordinates $[q(z_R, x), \mu(z_R, x)]$ as follows:

$$x_s' - x_o = q \cosh \mu, \quad (2.20)$$

$$z_{rR}' - z_o = q \sinh \mu, \quad (2.21)$$

where $q = \sqrt{xz_R}$, $x_o = \frac{\sqrt{2}}{2}(z_{rR} + x)$, $z_o = \frac{\sqrt{2}}{2}(z_{rR} - x)$, $\cosh \mu = \frac{x_s' - \frac{\sqrt{2}}{2}(z_{rR} + x)}{\sqrt{xz_R}}$, and

$$\sinh \mu = \frac{z_{rR}' - \frac{\sqrt{2}}{2}(z_{rR} - x)}{\sqrt{xz_R}}.$$

By transforming back to our original coordinates we find that

$$q \cosh \mu = \frac{\sqrt{2}}{2}[(z_{rR} + x_s) - (z_{rR} + x)], \quad (2.22)$$

$$q \sinh \mu = \frac{\sqrt{2}}{2} [(z_{rR} + x_s) - (z_R - x)]. \quad (2.23)$$

We can now solve for the coordinates (x_s, z_{rR}) in terms of the hyperbolic coordinates and using the exponential definitions for $\cosh \mu$ and $\sinh \mu$:

$$x_s = \frac{\sqrt{2}}{2} (q e^{\mu} + 2z_R), \quad (2.24)$$

$$z_{rR} = \frac{\sqrt{2}}{2} (q e^{-\mu} + 2 \frac{q^2}{z_R}). \quad (2.25)$$

The coordinate systems for the surface seismic, crosswell, and VSP geometries are summarized in table 1.1.

Table 1.1: CDP Coordinate Systems

seismic geometry	CDP coordinate system	CDP coordinate	orthogonal (stacking) coordinate
surface seismic	rectangular	y	h
crosswell	polar	$\alpha(z_R)$	$r(z_R)$
VSP	hyperbolic	$q(x, z_R)$	$u(x, z_R)$

2.6 CDP TRAVELTIME EQUATIONS

We have now defined a set of CDP coordinates for each of the seismic geometries. One of the coordinates represents the CDP point, and the other is an independent parameter representing different source and receiver pairs for the same CDP point. We use these CDP coordinates to rewrite equations (2.10 - 2.12) to give us the reflection traveltime equations from which we can define CDP moveout corrections.

2.6.1 Surface Seismic

The well known CDP moveout equation for surface seismic reflection data is

$$t = \frac{2 \sqrt{z_R^2 + h^2}}{v}. \quad (2.26)$$

Figure 2.7(a) shows the traveltimes for a CDP gather as a function of offset.

2.6.2 Crosswell

Using equations (2.17) and (2.18), and substituting into equation (2.11), we obtain the crosswell CDP traveltimes equation:

$$t = \frac{\sqrt{r^2(z_R)[1 + \sin(2\alpha(z_R))] + x_{off}^2}}{v}. \quad (2.27)$$

Figure 2.7(b) shows the traveltimes for a CDP gather (constant $\alpha(z_R)$) as a function of $r(z_R)$. This equation is a hyperbola. As $r(z_R)$ approaches infinity, the slope of the traveltimes curve approaches $\frac{\sqrt{1 + \sin(2\alpha(z_R))}}{v}$. This is the asymptote of the hyperbola.

This corresponds to sources and receivers located at an infinite distance above or below the reflector.

2.6.3 VSP

Using equations (2.24) and (2.25) and substituting into equation (2.12), we obtain the VSP CDP traveltimes equation:

$$t = \frac{\frac{\sqrt{2}}{2} \cdot \sqrt{(qe^\mu + 2z_R)^2 + (\sqrt{2}z_R + qe^{-\mu} + 2\frac{q^2}{z_R})^2}}{v}. \quad (2.28)$$

Figure 2.7(c) shows the traveltimes curve for a CDP gather (constant q) as a function of μ for the VSP geometry. As μ approaches infinity the lateral source location approaches an

infinite distance from the receiver well. When μ is negative it has finite range as the receiver can go no higher than the surface. For a receiver at the surface $z_{rR} = z_R$.

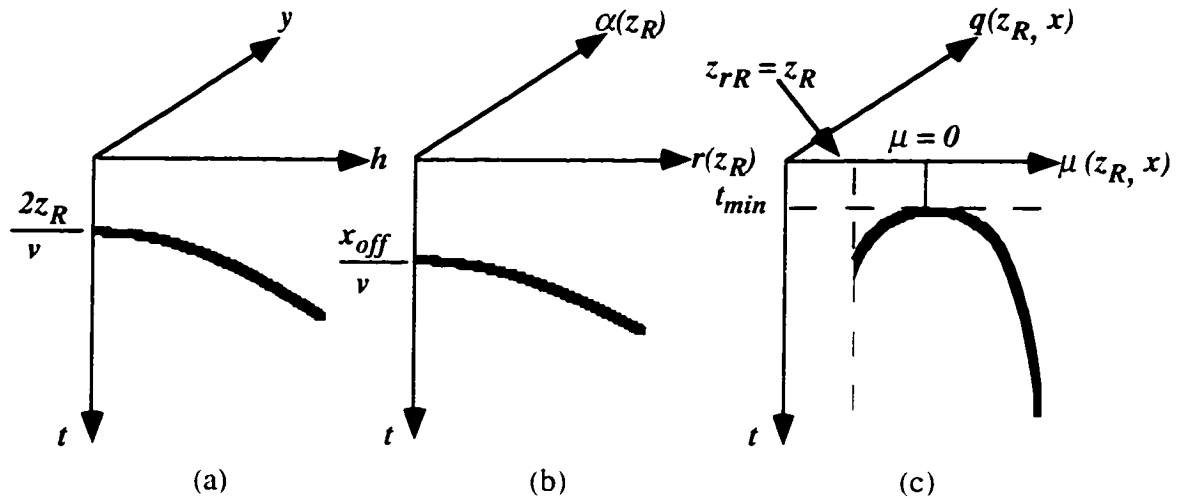


Figure 2.7: Traveltime curves for CDP gathers in terms of the surface seismic (a), crosswell (b), and VSP (c) CDP coordinates. The surface seismic and crosswell CDP traveltime curves are hyperbolic, and the VSP CDP traveltime curve is exponential.

2.7 CDP TRAVELTIME MOVEOUT CORRECTIONS

Now that we have derived CDP traveltime equations, we can define moveout corrections for each of the geometries. This allows us to make the traveltime corrections for each individual CDP gather, so that stacking the data optimizes the signal to noise ratio.

2.7.1 Surface Seismic

The well-defined NMO correction is shown in figure 2.8(a). The NMO corrected traveltime is given by (figure 2.10(a))

$$t = t_o = \frac{2z_R}{v}. \quad (2.29)$$

2.7.2 Crosswell

The crosswell geometry has an additional complication with both a horizontal and a vertical offset in the sources and receivers. We start by defining a moveout correction for the horizontal offset of the sources and receivers (the well spacing). We define this as the

Horizontal Normal Moveout (HNMO) correction. Figure 2.8(b) shows the HNMO correction. The HNMO traveltime is given by (Figure 2.9(a))

$$t_{ho} = \frac{z_{sR} + z_{rR}}{v}, \quad (2.30)$$

or in terms of the crosswell CDP coordinate system:

$$t_{ho} = \frac{r(z_R)\sqrt{1 + \sin(2\alpha(z_R))}}{v}. \quad (2.31)$$

We also have to correct for the vertical offset of the sources and receivers relative to the reflection depth. We define this correction as the Vertical Linear Moveout correction (VLMO). Figure 2.8(b) shows the VLMO correction. The VLMO traveltime is given by (figure 2.10(b))

$$t_o = 0. \quad (2.32)$$

The VLMO traveltime is zero since the vertical correction of the sources and receivers is down to the reflector depth.

2.7.3 VSP

In a similar fashion to crosswell, we perform a two step correction for the offset of the sources and receivers. First we correct for the horizontal offset by defining the Horizontal VSP Moveout (HVMO) correction (figure 2.8(c)). The HVMO corrected traveltime is given by (figure 2.9(b))

$$t_{ho} = \frac{\frac{\sqrt{2}}{2} \cdot (\sqrt{2}z_R + qe^{-\mu} + 2\frac{q^2}{z_R})}{v}. \quad (2.33)$$

Next, we correct for the vertical offset of the sources and receivers by defining the correction Vertical VSP Moveout (VVMO) correction (figure 2.8(c)). The VVMO corrected traveltime is given by (figure 2.10(c))

$$t_o = 0. \quad (2.34)$$

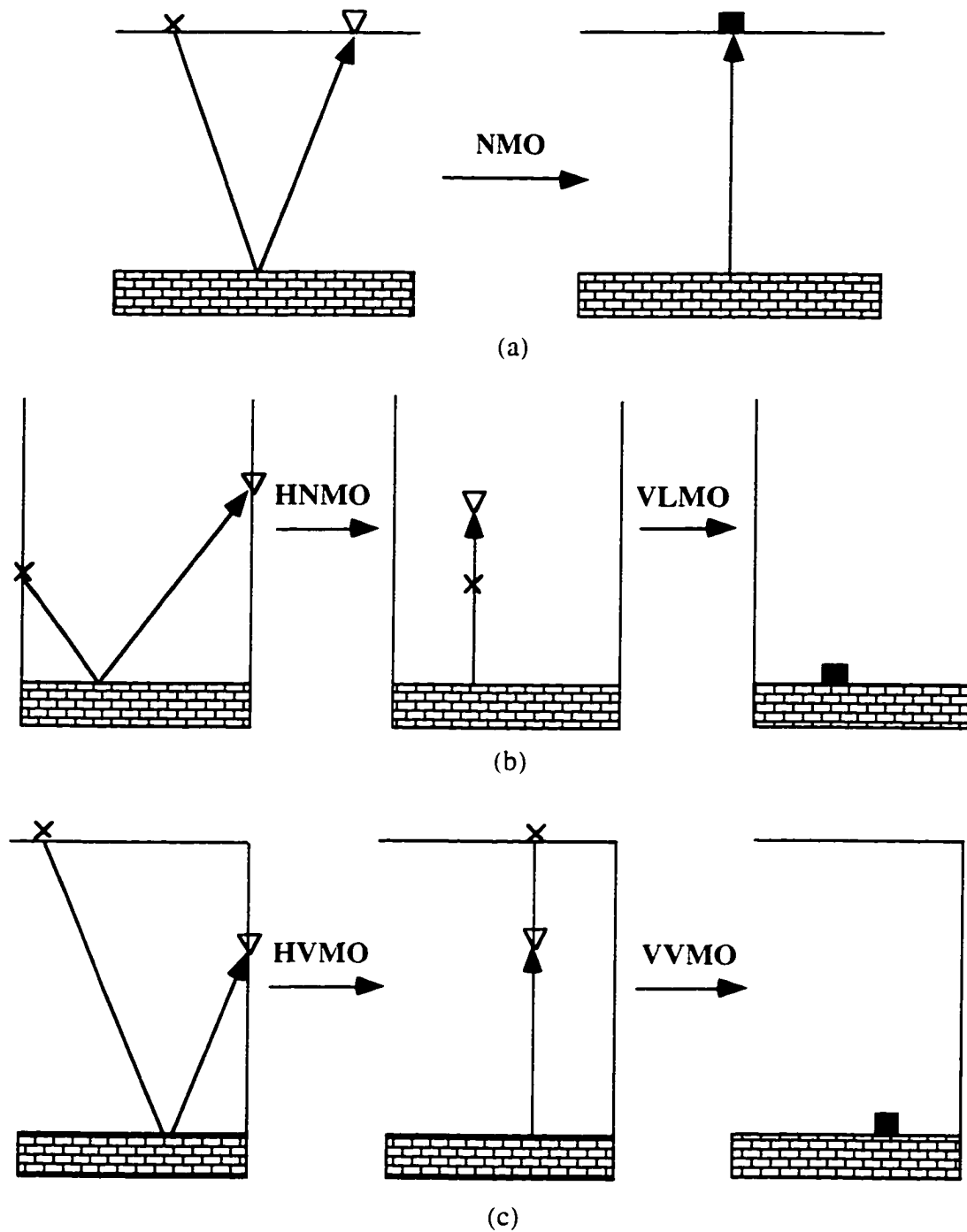


Figure 2.8: Moveout corrections for the surface seismic (a), crosswell (b), and VSP (c) geometries. The surface seismic geometry requires a one step moveout correction due to the horizontal offset of the sources and receivers, while the crosswell and VSP geometries require two step corrections for the horizontal and vertical offsets of the sources and receivers.

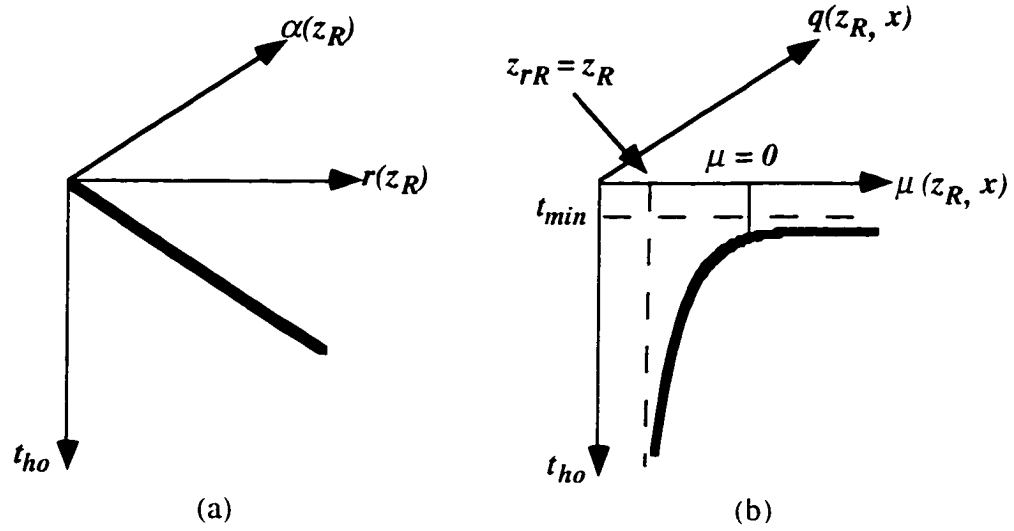


Figure 2.9: Crosswell (a) and VSP (b) CDP gathers after the HNMO and HVMO corrections. These are the CDP gathers after the horizontal moveout corrections have been made.

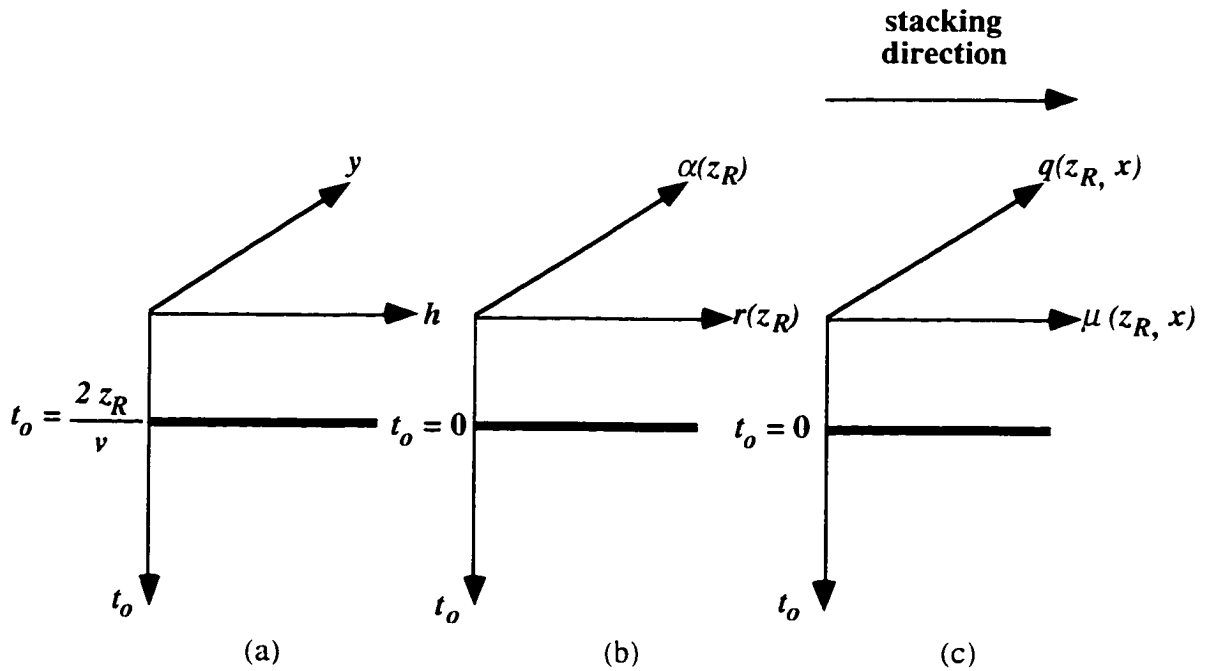


Figure 2.10: Surface Seismic (a), Crosswell (b), and VSP (c) CDP gathers after the NMO, VLMO and VVMO corrections. These are the CDP gathers after both the horizontal and vertical moveout corrections have been made. These CDP gathers are ready to be stacked.

The VVMO traveltimes are zero since the vertical correction of the sources and receivers is down to the reflector depth.

2.8 STACKING THE REFLECTION DATA

Once the data is aligned in the CDP gathers (figure 2.10), the data can be summed over the stacking coordinate to obtain a final image for the reflection event for all three geometries (figure 2.11).

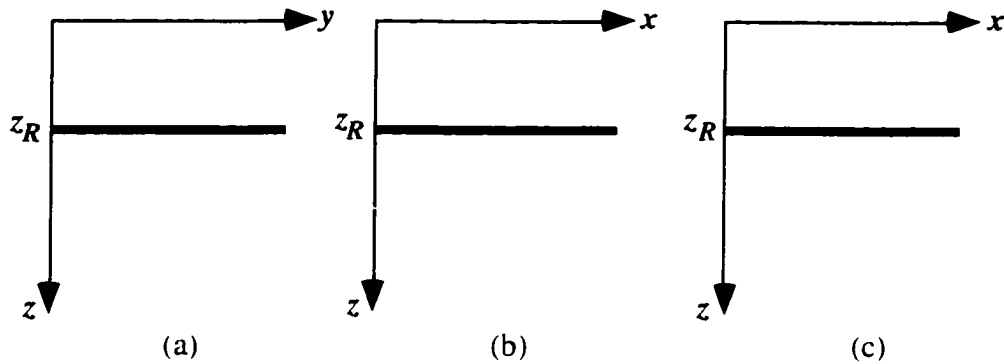


Figure 2.11: Final images for reflection events after summing the data over the stacking coordinate for the surface seismic (a), crosswell (b), and VSP (c) geometries. We have replaced the coordinate representing the CDP point with the spatial coordinate x for the crosswell and VSP geometries.

2.9 CONCLUSIONS

We have shown that we can define CDP gathers for the surface seismic, crosswell, and VSP geometries. Since the CDP gathers form a characteristic shape, we are able to parameterize each of the CDP gathers in terms of a coordinate system for each geometry. By using the CDP coordinates in the traveltimes equations for each geometry, we are able to write CDP traveltimes equations, and define traveltimes moveout corrections. This gives us the basis for reflection velocity analysis and the stacking and imaging of reflection data for each of these geometries.

Chapter 3

Crosswell Reflection Velocity Analysis

3.1 INTRODUCTION

In the previous chapter we derived a new CDP coordinate system for sorting and stacking crosswell reflection data. As was shown in the previous chapter, the traveltime and moveout correction equations all depend on the velocity of the medium. When dealing with actual crosswell data, the velocity varies as a function of position and is not exactly known. This chapter shows how to modify the traveltime and moveout equations for a medium of unknown variable velocity, and how to perform velocity analysis to align the reflection data for stack. Finding an accurate velocity model is very important for reflection imaging. The location of a time sample in image space is very sensitive to the velocity model (Lazaratos, 1993). The objective of aligning data in the stacking direction is analogous to surface seismic reflection velocity analysis. However, the crosswell reflection velocity analysis problem requires consideration of two additional factors. First, the geometry indicates that more than one stacking velocity is needed for each reflection point, since the sources and receivers which yield the same CDP transverse different vertical layers (figure 3.1b). By contrast surface seismic CDP gathers transverse the same vertical layers (figure 3.1a). The second factor is the signal to noise ratio; the complexity of the crosswell wavefield makes wavefield separation a top priority in reflection velocity analysis. These signal to noise considerations are examined in more detail in chapter 5.

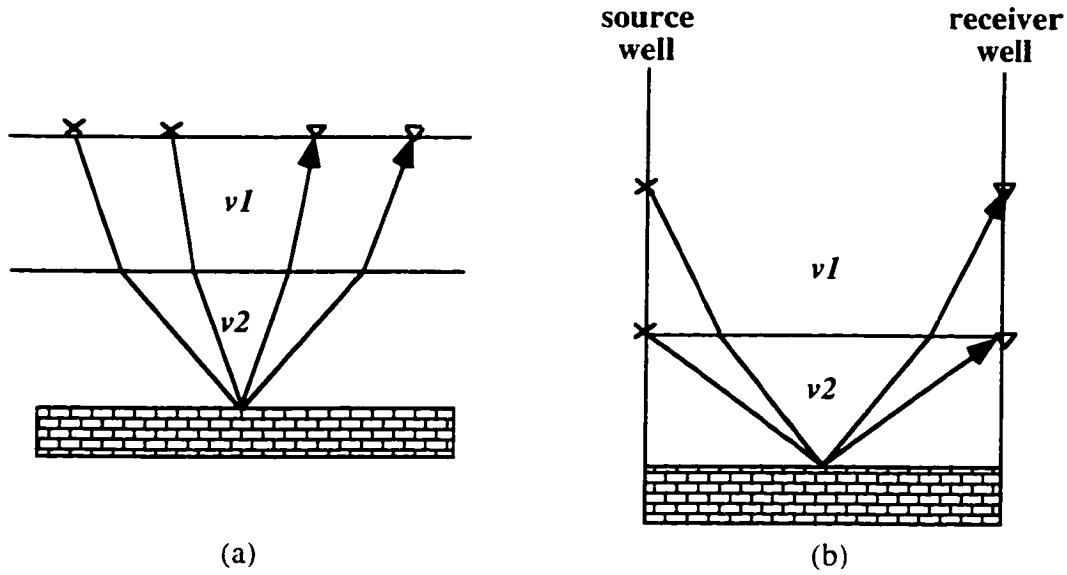


Figure 3.1: Surface Seismic (a) and Crosswell (b) CDP gathers in variable velocity media. The crosswell CDP gathers transverse different layers while the surface seismic CDP gathers transverse the same layers.

3.2 VELOCITY ANALYSIS IN A CONSTANT VELOCITY MEDIUM

In chapter 2, we defined moveout corrections for CDP gathers. These moveout corrections were defined by assuming that the velocity of the medium was known. In reality the velocity is unknown. This leads to the concept of reflection velocity analysis, well defined in surface seismic reflection imaging. To examine reflection velocity analysis for crosswell reflection imaging, we need to consider how the CDP moveout changes as a function of the velocity used for the moveout corrections. We first consider a constant velocity medium, and later extend the concept to a variable velocity medium. As was shown in the previous chapter, the traveltide equation in a constant velocity medium for a crosswell reflection CDP gather is given by

$$t^2 = \frac{r^2(z_R)[1 + \sin(2\alpha(z_R))] + x_{off}^2}{v^2}. \quad (3.1)$$

The CDP gather is obtained by holding the coordinate $\alpha(z_R)$ constant in the crosswell polar coordinate system and collecting traces corresponding to varying values of $r(z_R)$. The HNMO correction to the reflection traveltide is defined to be

$$t_{ho}^2 = t^2 - \frac{1}{v^2} x_{off}^2. \quad (3.2)$$

We perform velocity analysis by estimating the velocity v by v_e . This gives us the estimated HNMO corrected traveltime:

$$(t_{ho}^2)_e = t^2 - \frac{1}{v_e^2} x_{off}^2. \quad (3.3)$$

Substituting equation (3.1) into equation (3.3), we obtain the estimated HNMO traveltime:

$$(t_{ho}^2)_e = \frac{1}{v^2} \cdot \{r^2(z_R)[1 + \sin(2\alpha(z_R))]\} + \left(\frac{1}{v^2} - \frac{1}{v_e^2} \right) \cdot x_{off}^2. \quad (3.4)$$

The moveout or derivative with respect to $r(z_R)$ of the estimated HNMO traveltime is given by

$$\frac{\partial(t_{ho})_e}{\partial r(z_R)} = \frac{\frac{1}{v^2} \cdot \{r(z_R)[1 + \sin(2\alpha(z_R))]\}}{\sqrt{\frac{1}{v^2} \cdot \{r^2(z_R)[1 + \sin(2\alpha(z_R))]\} + \left(\frac{1}{v^2} - \frac{1}{v_e^2} \right) \cdot x_{off}^2}}. \quad (3.5)$$

When $v_e = v$ equation (3.5) reduces to

$$\left. \frac{\partial(t_{ho})_e}{\partial r(z_R)} \right|_{v=v_e} = \frac{\sqrt{1 + \sin 2\alpha(z_R)}}{v}. \quad (3.6)$$

which is the equation of a straight line. From equations (3.4) and (3.5), we can see that if $v_e > v$, then the HNMO estimated traveltime is under corrected (figure 3.2(a)), and if $v_e < v$, then the HNMO estimated traveltime is over corrected (figure 3.2(b)). If $v_e = v$, then $(t_{ho})_e = t_{ho}$, which is a straight line (figure 3.2(c)).

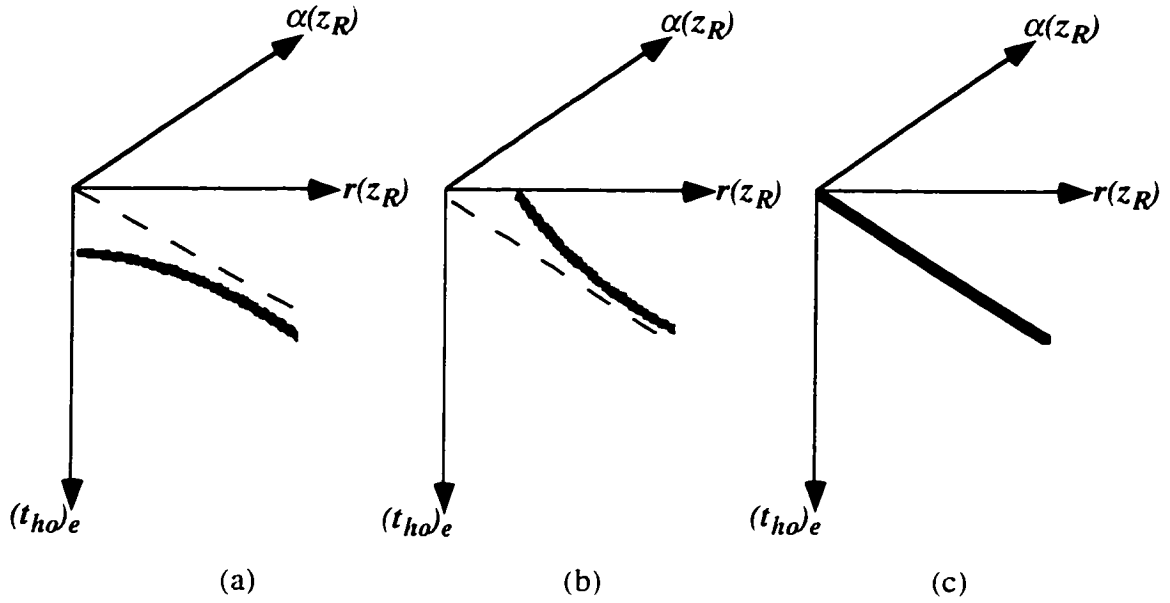


Figure 3.2: CDP - HNMO gathers when the velocity estimate is too large ($v_e > v$) (a), when the velocity estimate is too small ($v_e < v$) (b), and when the velocity estimate is correct ($v_e = v$) (c). The dashed line shows the correct moveout curve, and is the asymptote of the hyperbolas.

The same procedure is followed for the VLMO correction. The VLMO correction is defined as

$$t_o = t_{ho} - \frac{1}{v} \cdot r(z_R) \sqrt{1 + \sin(2\alpha(z_R))}. \quad (3.7)$$

We again perform the velocity analysis procedure on the VLMO correction. Since the VLMO correction is performed after the HNMO correction, we rewrite equation (3.7) as

$$(t_o)_e = (t_{ho})_e - \frac{1}{v_e} \cdot r(z_R) \sqrt{1 + \sin(2\alpha(z_R))}. \quad (3.8)$$

Substituting equation (3.4) into equation (3.8) we obtain the traveltme equation after both moveout corrections (HNMO and VLMO) have been performed:

$$(t_o)_e = \sqrt{\frac{1}{v^2} \cdot \{r^2(z_R)[1 + \sin(2\alpha(z_R))]\} + \left(\frac{1}{v^2} - \frac{1}{v_e^2}\right) \cdot x_{off}^2} - \frac{1}{v_e} \cdot r(z_R) \sqrt{1 + \sin(2\alpha(z_R))}. \quad (3.9)$$

The moveout or derivative of the estimated CDP - VLMO traveltimes is given by

$$\frac{\partial(t_o)_e}{\partial r(z_R)} = \frac{\frac{1}{v^2} \cdot \{r(z_R)[1 + \sin(2\alpha(z_R))]\}}{\sqrt{\frac{1}{v^2} \cdot \{r^2(z_R)[1 + \sin(2\alpha(z_R))]\} + \left(\frac{1}{v^2} - \frac{1}{v_e^2}\right) \cdot x_{off}^2}} - \left\{ \frac{1}{v_e} \cdot \sqrt{1 + \sin 2\alpha(z_R)} \right\}. \quad (3.10)$$

When $v_e = v$ equation (3.10) reduces to

$$\left. \frac{\partial(t_o)_e}{\partial r(z_R)} \right|_{v_e=v} = 0. \quad (3.11)$$

From equations (3.9) and (3.10), we can see that if $v_e > v$, then the VLMO estimated traveltimes are under corrected (figure 3.3(a)), and if $v_e < v$, then the VLMO estimated traveltimes are over corrected (figure 3.3(b)). If $v_e = v$, then $(t_o)_e = t_o = 0$ (figure 3.3(c)).

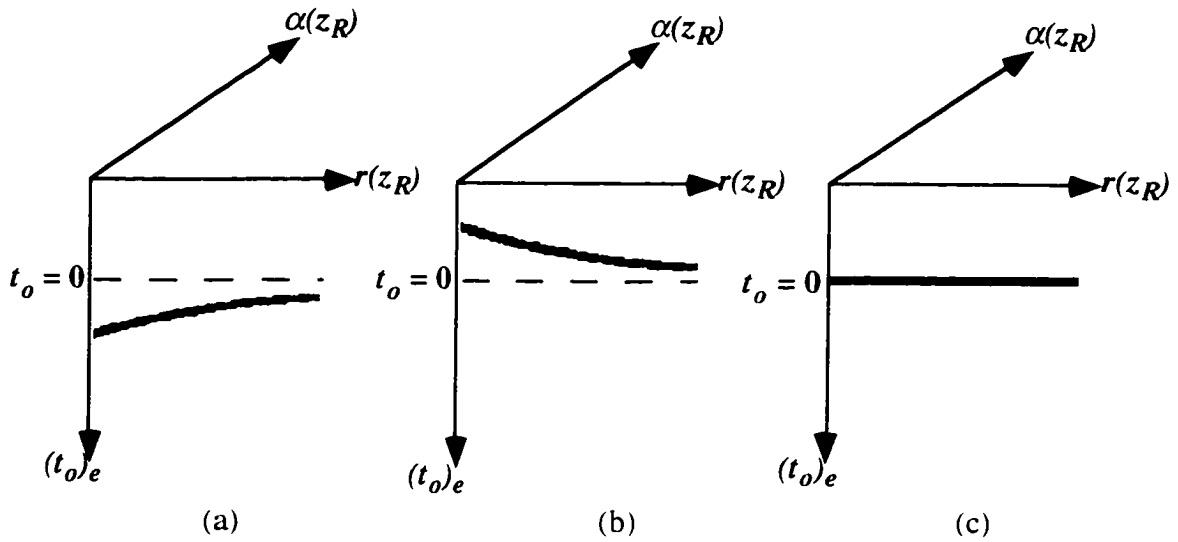


Figure 3.3: CDP - VLMO gathers when the velocity estimate is too large ($v_e > v$) (a), and when the velocity estimate is too small ($v_e < v$) (b), and when the velocity estimate is correct ($v_e = v$) (c). The dashed line shows the correct moveout curve, and is the asymptote of the hyperbolas.

3.3 VARIABLE VELOCITY REFLECTION TRAVELTIME EQUATIONS

In general we never have a constant velocity medium, as was discussed in the previous section. Therefore we have to determine how the moveout equations and the reflection velocity analysis procedure change for a variable velocity medium. To derive a variable

velocity traveltimes equation for the crosswell reflection geometry, we adapt the previously derived surface seismic reflection traveltimes equation for a variable velocity medium to the crosswell geometry. Figure 3.4 shows the reflection geometry for surface seismic in a variable velocity medium.

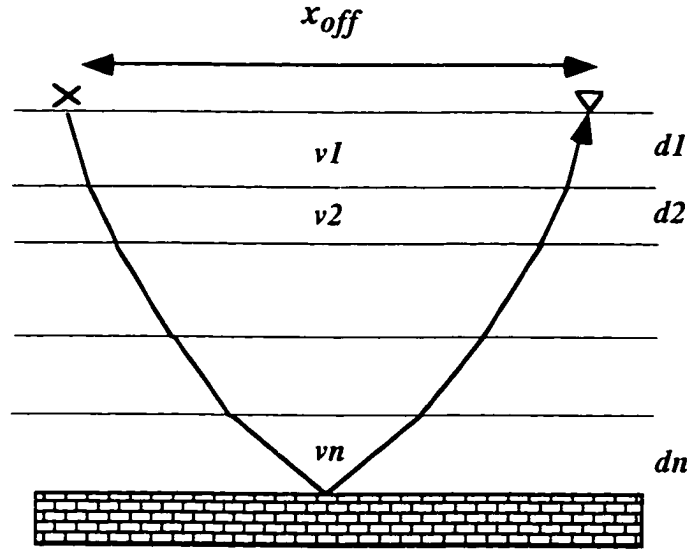


Figure 3.4: Surface seismic reflection geometry for variable velocity media. The variable v designates layer velocity and d designates layer thickness.

The surface seismic reflection traveltimes for a 1-d variable velocity medium is written in terms of a Taylor Series expansion about zero source-receiver offset (Yilmaz, 1987), (Aki & Richards, 1980):

$$t^2 = C_0 + C_1 x_{off}^2 + C_2 x_{off}^4 + C_3 x_{off}^6 + \dots + C_n x_{off}^{2n} + \dots \quad (3.12)$$

where x_{off} is the full source-receiver offset. The coefficients are given by (Taner and Koehler, 1969):

$$C_0 = (t_o)^2, \quad (3.13)$$

where t_o is the vertical two way traveltimes down to the reflecting layer, and

$$C_1 = \frac{k_1}{k_2}, \quad (3.14)$$

$$C_2 = \frac{k_2^2 - k_1 k_3}{4k_2^4}, \quad (3.15)$$

$$\text{and } C_3 = \frac{2k_1 k_3^2 - k_1 k_2 k_4 - k_2^2 k_3}{8k_2^7}, \quad (3.16)$$

where

$$k_q = 2 \sum_{i=1}^{i=n} v_i^{2q-3} d_i, \quad q = 1, 2, \dots \quad (3.17)$$

where v_i is the velocity of the i th layer and d_i is the thickness of the i th layer. We can extend this derivation to the variable velocity reflection crosswell geometry (figure 3.5(a)). Using the method of images, figure 3.5(b) shows a raypath that yields the identical traveltime. Figure 3.5(c) shows a surface seismic raypath that has twice the traveltime of a crosswell experiment where the offset is twice the well spacing. Therefore we can write

$$t_{xwell}(x_{off}) = \frac{t_{surfseis}(2 \cdot x_{off})}{2}, \quad (3.18)$$

where $t_{xwell}(x_{off})$ is the traveltime for the crosswell experiment shown in figure 3.5(a) and $t_{surfseis}(2 \cdot x_{off})$ is the traveltime of the surface seismic experiment shown in figure 3.5(c), where the source - receiver offset is twice the well spacing in the crosswell geometry. Therefore we can adapt equation (3.10) to the crosswell geometry:

$$t^2 = D_0 + D_1 x_{off}^2 + D_2 x_{off}^4 + D_3 x_{off}^6 + \dots + D_n x_{off}^{2n} + \dots, \quad (3.19)$$

where after some algebra we find the crosswell coefficients in terms of the surface seismic coefficients:

$$D_0 = (t_{ho})^2, \quad (3.20)$$

$$D_1 = C_1, \quad (3.21)$$

$$D_2 = 4C_2, \quad (3.22)$$

$$\text{and } D_3 = 16C_3, \quad (3.23)$$

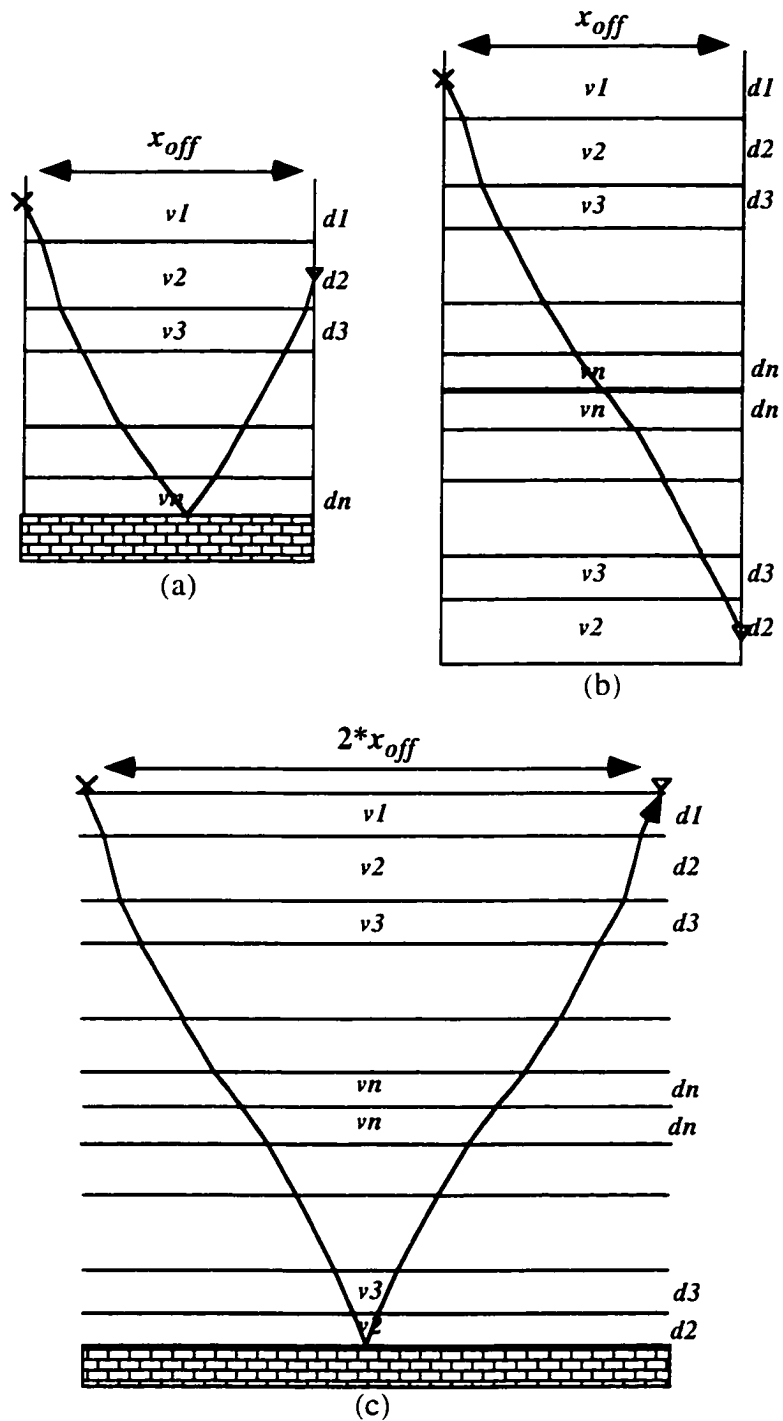


Figure 3.5: Crosswell reflection geometry for variable velocity media (a), a raypath with equal traveltime using the method of images (b), and a surface seismic reflection raypath (c) that has twice the traveltime as the crosswell raypaths in (a) and (b).

where we rewrite k_q for the crosswell case as

$$k_q = 2 \sum_{i=1}^{i=n_t} v_i^{2q-3} d_i. \quad (3.24)$$

where n_t is the number of layers transversed from the source to the reflector and back to the receiver. t_{ho} is the vertical raypath length contribution to the total traveltime. It is defined as:

$$t_{ho} = \sum_{i=1}^{i=n_t} \frac{d_i}{v_i}. \quad (3.25)$$

3.3.1 Evaluating the Crosswell Traveltime Taylor Series Expansion

It is useful to evaluate the terms in equation (3.19) to see their individual contributions to the total traveltime of the crosswell reflection geometry. We consider a simplified experiment to evaluate these terms. Figure 3.6 shows a two layer model where we allow the velocity of the second layer to change relative to the first layer. We also allow the well spacing to change, while keeping the layer thicknesses constant. We define the total vertical distance traveled by z_t , where $z_t = |z_R - z_L| + |z_R - z_S|$. In the case of the experiment shown in figure 3.6, $z_t = 4$. This allows us to determine the size of the terms in equation (3.19) by examining how they change as a function of velocity contrast and well spacing relative to layer thickness.

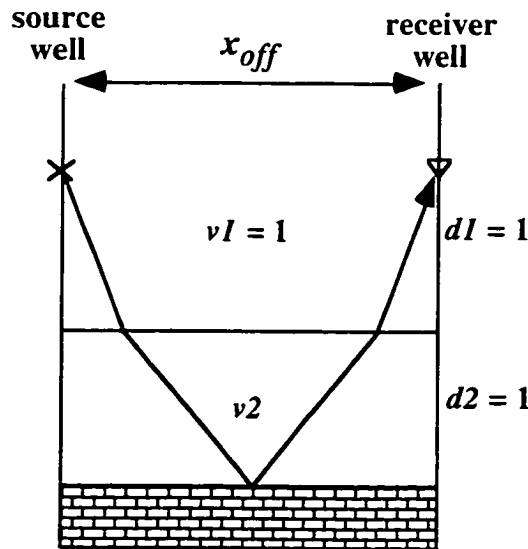


Figure 3.6: Crosswell experiment used to evaluate the Taylor Series expansion in equation (3.19).

Figure 3.7 shows the traveltime contributions using the first two terms of equation (3.19), and the true traveltime. We see that the traveltime estimated by the first two terms is virtually identical to the true traveltime for a large range of velocity contrasts for well offsets which are less than or equal to the total vertical offset (z_t) between the source and receiver and the reflector (figure 3.7(a) and (b)). For very large contrasts ($x_{off} \gg z_t$), the difference in traveltime using the first two terms of equation (3.19) and the true traveltime is still very small for moderate changes in velocity ($< 20\%$) (figure 3.7(d)). This analysis allows for the approximation of using only the first two terms in equation (3.19) to define the crosswell reflection traveltime in a variable velocity medium:

$$t^2 = (t_{ho})^2 + D_1 x_{off}^2. \quad (3.26)$$

3.4 VARIABLE VELOCITY MOVEOUT CORRECTIONS

The most important aspect of using equation (3.26) to represent the crosswell reflection traveltime in a variable velocity medium is being able to define the HNMO and VLMO corrections in a variable velocity medium in a similar mathematical fashion to the constant velocity HNMO and VLMO corrections discussed in section 2.7.2. In this section we examine more closely the two terms on the right hand side of equation (3.26) to define these moveout corrections in a variable velocity medium. We can rewrite equation (3.25) as

$$t_{ho} = \left(\frac{1}{v} \right)_{ave} z_t, \quad (3.27)$$

where

$$\left(\frac{1}{v} \right)_{ave} = \left(\frac{1}{z_t} \right) \cdot \left(\sum_{i=1}^{i=n_t} \left(\frac{1}{v} \right)_i d_i \right), \quad (3.28)$$

which is the average velocity over the transversed layers, and n_t is the total number of layers transversed from the source to the reflector and back to the receiver. We can rewrite equation (3.27) in terms of our the crosswell polar coordinate system defined in Section 2.5:

$$t_{ho} = \left(\frac{1}{v} \right)_{ave} \cdot r(z_R) \sqrt{1 + \sin(2\alpha(z_R))}, \quad (3.29)$$

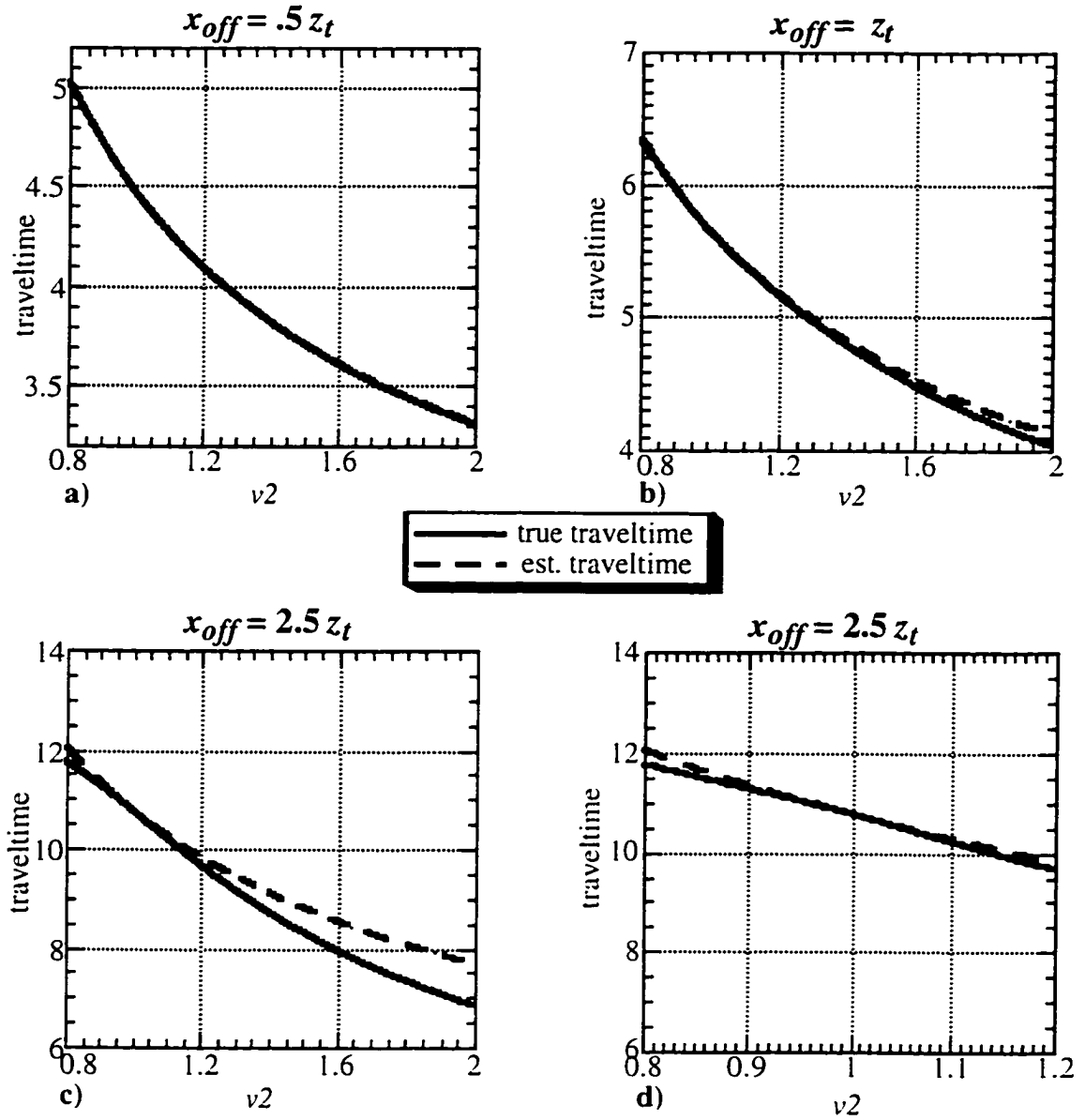


Figure 3.7: Traveltimes computed for the geometry shown in figure 3.6 for a two layer velocity ratio range of 0.8 to 2 for well spacings .5 (a), 1 (b), 2.5 (c) times the total vertical offset. Figure (d) shows a comparison over a smaller range of velocities for a well spacing 2.5 times the total vertical offset.

where

$$\left(\frac{1}{v}\right)_{ave} = \left(\frac{1}{r(z_R)\sqrt{1 + \sin(2\alpha(z_R))}} \right) \cdot \left(\sum_{i=1}^{i=n_t} \left(\frac{1}{v}\right)_i d_i \right). \quad (3.30)$$

From equation (3.21), we see that $D_1 = C_1$. The coefficient C_1 , given by equation (3.14) is defined as the inverse of the rms velocity squared of the transversed layers in surface

seismic. Therefore the coefficient D_1 is defined as the inverse of the square of the rms velocity of the transversed layers for a crosswell reflection raypath (figure 3.5(a)):

$$D_1 = \frac{1}{v_{rms}^2}, \quad (3.31)$$

where

$$v_{rms} = \sqrt{\frac{\sum_{i=1}^{i=n_t} v_i d_i}{\sum_{i=1}^{i=n_t} \left(\frac{1}{v_i}\right) d_i}} = \sqrt{\frac{v_{ave}}{\left(\frac{1}{v}\right)_{ave}}}. \quad (3.32)$$

Now substituting equations (3.29) and (3.31) into equation (3.26) we obtain the traveltime equation for crosswell reflection data in a variable velocity medium:

$$t^2 = \left(\frac{1}{v}\right)_{ave}^2 \cdot \{r^2(z_R)[1 + \sin(2\alpha(z_R))]\} + \frac{1}{v_{rms}^2} x_{off}^2. \quad (3.33)$$

or

$$t^2 = \left(\frac{1}{v}\right)_{ave}^2 z_t^2 + \frac{1}{v_{rms}^2} x_{off}^2. \quad (3.34)$$

We see that equation (3.33) has the same form as equation (3.1) except that v_{ave} and $1/v_{rms}$ have replaced the constant velocity v . This allows us to define the variable velocity HNMO and VLMO corrections for crosswell reflection data. The variable velocity HNMO correction is defined as:

$$t_{ho}^2 = t^2 - \frac{1}{v_{rms}^2} x_{off}^2. \quad (3.35)$$

The variable velocity VLMO correction is defined as:

$$t_o = t_{ho} - \left(\frac{1}{v}\right)_{ave} \cdot r(z_R) \sqrt{1 + \sin(2\alpha(z_R))}. \quad (3.36)$$

or

$$t_o = t_{ho} - \left(\frac{1}{v} \right)_{ave} z_t, \quad (3.37)$$

where $t_o = 0$, as was the case for constant velocity, since the VLMO correction puts the source and receiver at the same depth as the reflector (figure 2.8(b)). Therefore we use the rms velocity for the HNMO correction and the average velocity for the VLMO correction in a variable velocity medium. We can also define one joint quantity which can be applied to both the HNMO and VLMO corrections. We can rewrite equation (3.34) as:

$$t^2 = \frac{1}{v_{st}^2} (z_t^2 + x_{off}^2), \quad (3.38)$$

where v_{st} is defined as the stacking velocity applied to the HNMO and VLMO corrections to correct the reflection data to $t_o = 0$. Therefore, we can replace the two quantities shown in equations (3.35) and (3.37) with the single quantity v_{st} . The stacking velocity v_{st} has the value:

$$v_{st} = \sqrt{\frac{z_t^2 + x_{off}^2}{\left(\frac{1}{v} \right)_{ave}^2 z_t^2 + \frac{1}{v_{rms}^2} x_{off}^2}}. \quad (3.39)$$

Therefore the stacking velocity is a function of the well and total vertical offset. When the vertical offset is large relative to the well offset ($z_t \gg x_{off}$), the stacking velocity is approximately equal to $\left(\frac{1}{v} \right)_{ave}$ (figure 3.8a). When the well offset is large relative to the vertical offset ($x_{off} \gg z_t$), the stacking velocity is approximately equal to $\frac{1}{v_{rms}}$ (figure 3.8b).

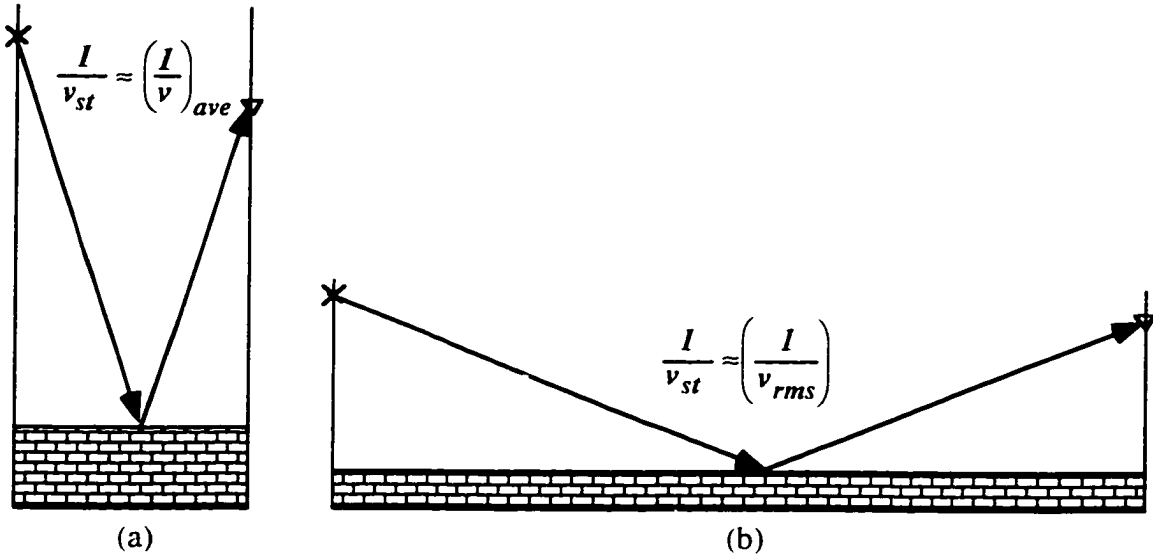


Figure 3.8: The value of the stacking velocity given by equation (3.39) when ($z_t \gg x_{off}$) (a), and when ($x_{off} \gg z_t$) (b).

By showing that we can closely approximate the true reflection traveltime by equation (3.26), and by replacing the series of interval velocities with a single stacking velocity, we can replace the original medium with a new medium (figure 3.9), and make the following conclusions:

- 1) Fermat's principle tells us that the raypath location does not change with small changes in traveltime. Therefore straight rays still accurately yield the true CDPs for small changes in velocity. Therefore we can use common ratio gathers to determine the CDPs (figure 3.9).
- 2) We can replace the medium with a single stacking velocity which is a function of the rms velocity and average of the inverse of the velocity to perform the HNMO and VLMO corrections respectively (figure 3.9).

3.5 VARIABLE VELOCITY REFLECTION VELOCITY ANALYSIS

By defining the HNMO and VLMO corrections for a variable velocity medium in the previous section, we can extend the concept of velocity analysis discussed in section 3.2 to a variable velocity medium. Performing velocity analysis in a variable velocity medium is a multiple step process. As was shown in figure 3.1(b), source - receiver pairs with the same CDP transverse different horizontal layers. Therefore each source - receiver pair for a given CDP will need to have a separate HNMO and VLMO stacking velocity assigned. We

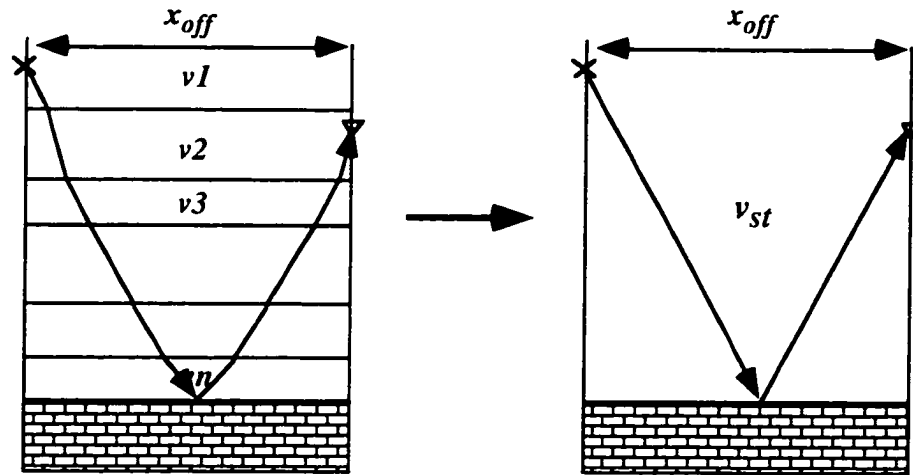


Figure 3.9: Replacement of a variable velocity medium with a single stacking velocity. This allows for the use of common ratio gathers to define CDPs and the use of a single stacking velocity to perform the HNMO and VLMO corrections.

start with the source - receiver pairs closest to the reflector (small radial distances) by applying an HNMO and VLMO stacking velocity that will align the reflection at $t_o = 0$ in CDP - VLMO gathers (the CDP gather after the VLMO correction). This stacking velocity is applied to all radial distances. We then adjust this stacking velocity as a function of the radial distance until we have aligned the reflection for all the radial distances that we plan to use in the final stack. Figure 3.10 shows the reflection velocity analysis procedure for a variable velocity medium.

3.5.1 Synthetic Example

A full waveform synthetic was generated using the velocity model shown in figure 3.11. The well spacing is 600 ft. and the Nyquist frequency is 2000 Hz. Sources and receivers were placed from 1600 ft. - 2600 ft. with 10 ft. spacing. Velocity analysis was performed on a reflection point 65 ft. from the source well at a depth of 2600 ft. (figure 3.11). The first objective is to assign a single stacking velocity at smaller radial distances that will align the reflection at $t_o = 0$. We do not perform velocity analysis on the smallest radial distances, since these correspond to the largest angles of incidence (figure 3.10), and experience substantial stretch due to the non-linear HNMO correction. The HNMO correction is similar to the surface seismic NMO correction (figure 2.8(a)), and incurs the same stretch due to the non-linear moveout correction. The step by step velocity analysis procedure is shown in figures 3.12. We start with the initial constant stacking velocity model in figure 3.12(a) and continue to refine this model through increasing radial

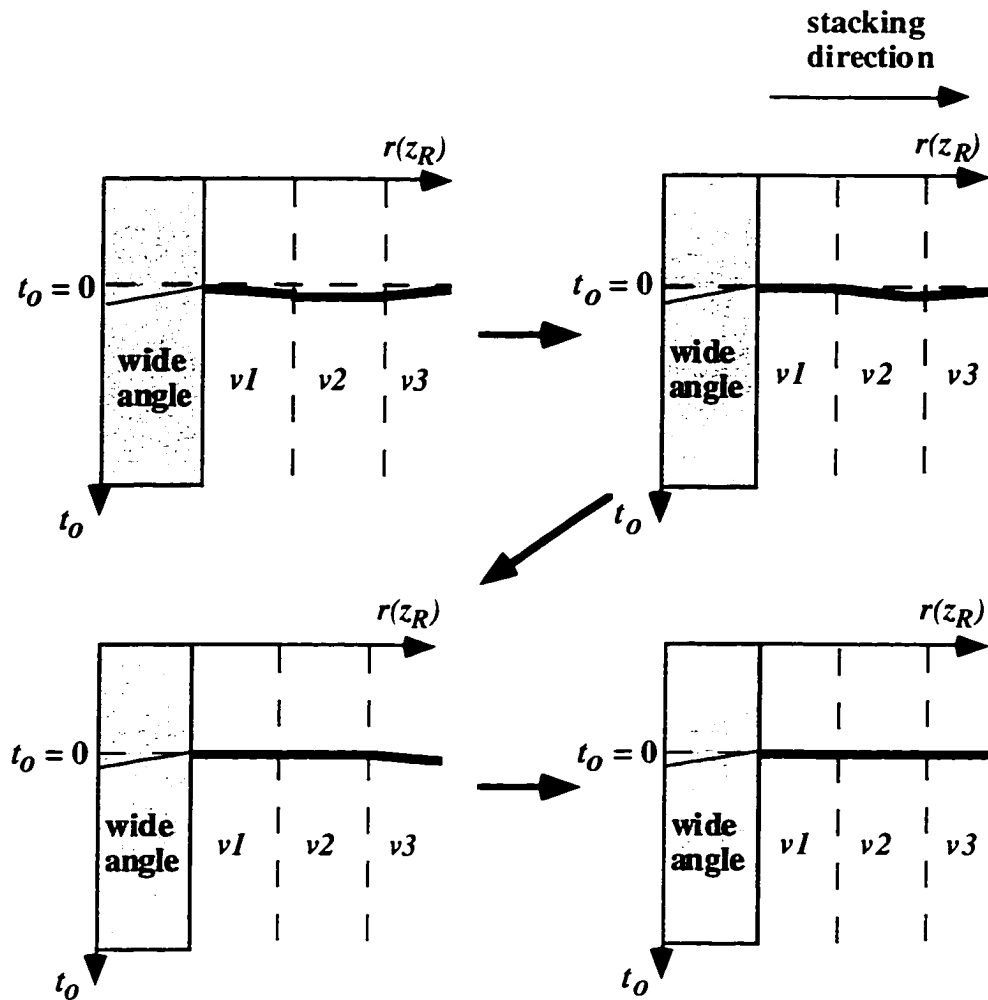


Figure 3.10: Crosswell reflection velocity analysis procedure. We start with small radial distances which correspond to source-receiver pairs closest to the reflection and align the reflection until all radial distances to be used in the final stack are aligned.

distances until we have aligned the entire reflection at $t_o = 0$. We use the same stacking velocity based on equation 3.38 for the HNMO and VLMO corrections, since we only know the final moveout of the CDP-VLMO gather ($t_o = 0$). We determine specific radial distances to assign stacking velocity values due to observing the moveout of the reflection in the CDP-VLMO gather. The moveout of the reflection changes due to velocity contrasts, and large changes in the radial distance. In between the radial distances where we assign stacking velocities, we linearly interpolate the stacking velocities for the other radial distances. We use equations (3.5) and (3.8) as justification for this, since as long as we are close to the correct stacking velocity, the moveout is close to linear over small ranges of radial distances. In the synthetic example, some of the stacking velocity assignments corresponded to radial distances where there was a change in velocity, others were within a

layer due to a large change in the radial distance, where a linear approximation was insufficient to model the hyperbolic moveout. A total of 9 stacking velocities were assigned for this CDP. We also compare the values of the stacking velocities determined from the reflection velocity analysis with the true stacking velocities based on equation (3.39) (figure 3.13). We see that the stacking velocities obtained from the velocity analysis procedure compare very favorably to the actual stacking velocities as a function of radial distance. Two reasons for the small difference are the non-linear stretch due to the HNMO correction, and the small approximation in using straight rays to determine the source-receiver pairs for the CDP gather. The large change in the slope at the radial distance of 503 ft. corresponds to the change in interval velocity at 2100 ft. relative to the stacking velocity at this depth (interval velocity = 19 kft/sec, stacking velocity = 16.1 kft/sec). We don't see the same change at the boundary of the layer at 2200 ft. (radial distance = 402 ft). The stacking velocity at the radial distance of 500 ft. is approximately 15.9 kft/sec, while the interval velocity is 17 kft/sec.

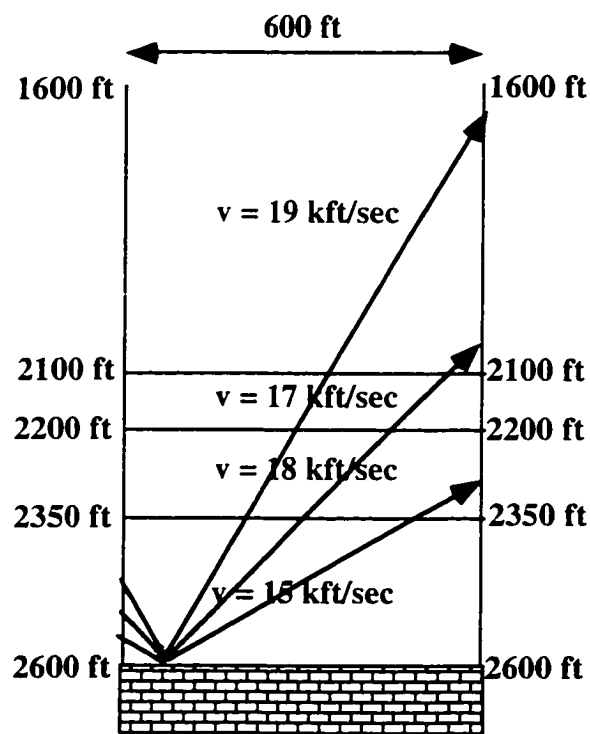


Figure 3.11: Model used for synthetic velocity analysis.

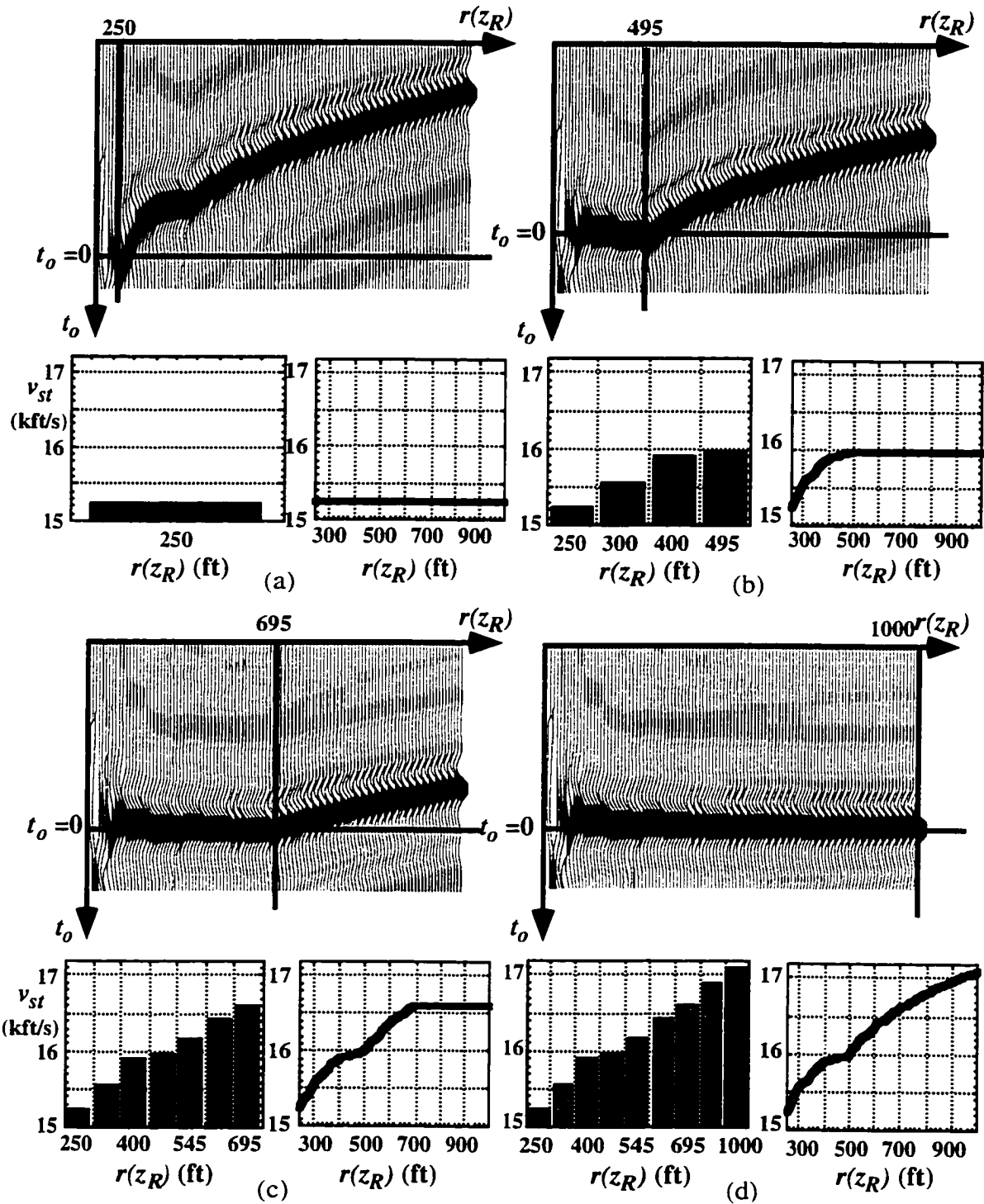


Figure 3.12: Velocity analysis results on a synthetic CDP-VLMO gather after the application of 1(a), 4(b), 7(c), and 9(d) stacking velocities. The graphs on the left of each figure show the radial distances at which velocity analysis was performed. The graphs on the right of each figure show the stacking velocities applied at all radial distances.

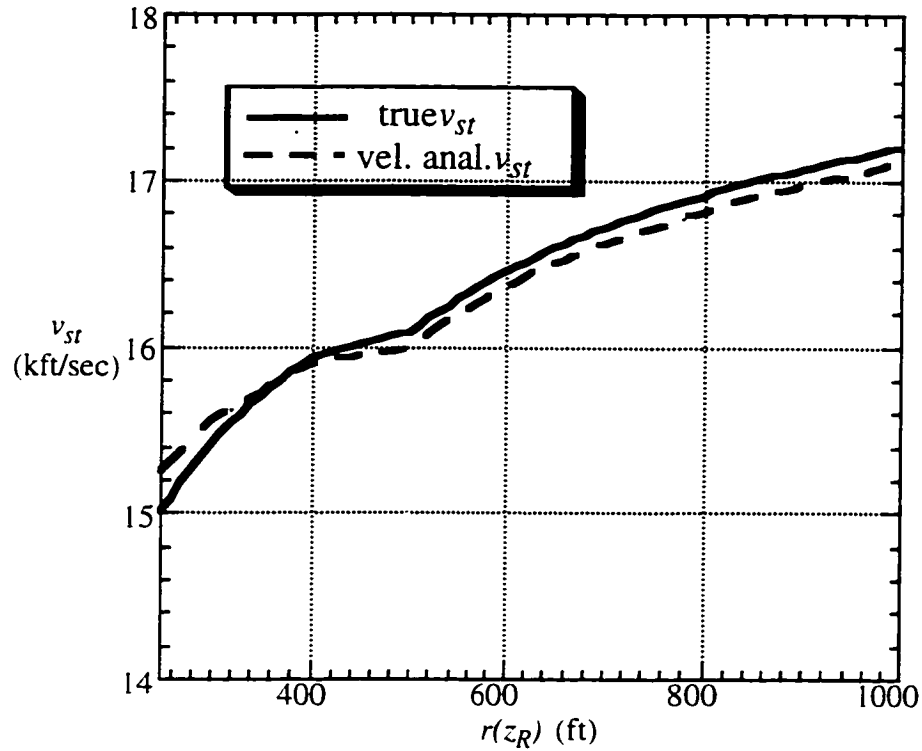


Figure 3.13: Comparison between velocity analysis stacking velocities and the true stacking velocities for the synthetic model in figure 3.11. The large change in the slope at the radial distance of 503 ft. corresponds to the change in interval velocity at 2100 ft. relative to the stacking velocity at this depth.

3.6 ESTIMATING REFLECTION DEPTH

As we have seen in both Chapter 2 and the preceding sections in this chapter, the crosswell reflection imaging problem is parameterized by reflection depth. The velocity analysis procedure depends on knowing the reflection depth. In section 3.1, we attempted to find the correct velocity by examining the moveout of the reflection data assuming that the reflection depth was known. In practice, the actual reflection depth is unknown. However, we can still perform velocity analysis even when the reflection depth is not known. As was shown in equation 3.38, the reflection traveltimes is given by

$$t^2 = \frac{1}{(v_{st})^2} [z_t^2 + x_{off}^2]. \quad (3.40)$$

When we perform velocity analysis we are shifting the reflection event on each seismic trace to a new traveltimes ($t_o = 0$). As we see in equation (3.40), there are two variables that

contribute to the traveltime:

- 1) the reflection depth relative to the source - receiver location; z_t .
- 2) the velocity or stacking velocity of the medium; v_{st} .

Therefore for each seismic trace, we only have one constraint; the traveltime or the stacking velocity determined from the velocity analysis. However, we have two unknowns; the reflection depth and the actual stacking velocity of the medium. We can see this if we rewrite equation (3.40) in terms of an unknown reflection depth:

$$t^2 = \frac{1}{(v_{st})_e^2} [z_t'^2 + x_{off}^2], \quad (3.41)$$

where z_t' is the estimated total vertical offset, which is related to the true vertical offset by

$$z_t' = z_t + 2\Delta z_R, \quad (3.42)$$

where Δz_R is the difference between the true reflection depth and the actual reflection depth (figure 3.14). $(v_{st})_e$ is the estimated stacking velocity determined from reflection velocity analysis using z_t' as the estimated vertical offset. As we see from equation (3.41), the estimated stacking velocity assigned to a source-receiver pair is a function of the estimated vertical offset or the assumed reflection depth. After a little algebra, we can obtain the relationship between the estimated stacking velocity (obtained from velocity analysis based upon the assumed reflection depth) and the true stacking velocity of the medium:

$$(v_{st})_e = v_{st} \sqrt{\frac{(z_t')^2 + x_{off}^2}{(z_t)^2 + x_{off}^2}}, \quad (3.43)$$

or

$$(v_{st})_e = v_{st} \sqrt{\frac{(z_t')^2 + x_{off}^2}{(z_t' - 2\Delta z_R)^2 + x_{off}^2}}. \quad (3.44)$$

When the assumed reflection depth is equal to the true reflection depth (i.e., $z'_t = z_t$ or $\Delta z_R = 0$), equations (3.43) and (3.44) reduce to:

$$(v_{st})_e = v_{st}. \quad (3.45)$$

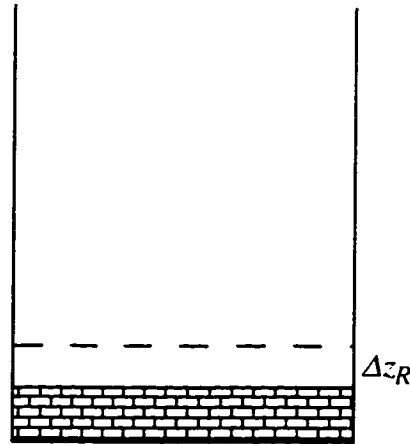


Figure 3.14: Reflection depth error. The dashed line is the assumed reflection depth, and the top of the brick layer is the true reflection depth.

3.6.1 Synthetic Example

To see how the estimated stacking velocity depends on the assumed vertical offset or reflection depth, we examine a constant velocity synthetic example (figure 3.15).

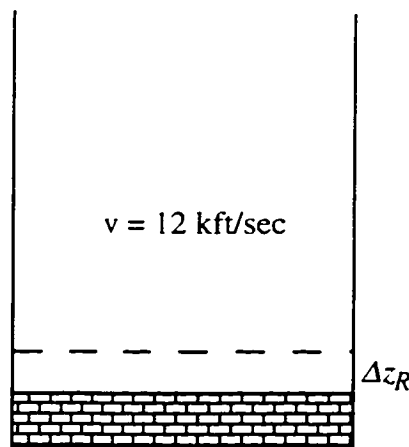


Figure 3.15: Synthetic model to evaluate reflection depth error effect on the stacking velocity and the derivative of the stacking velocity.

We allow the source and receiver apertures to be continuous (sources and receivers at all depths). In order to generalize this example we rewrite equation (3.45) by normalizing the estimated vertical aperture and reflection depth error by the well offset:

$$(v_{st})_e = v_{st} \sqrt{\frac{\left(\frac{\dot{z}_t}{x_{off}}\right)^2 + 1}{\left(\frac{\dot{z}_t}{x_{off}} - \frac{2\Delta z_R}{x_{off}}\right)^2 + 1}}. \quad (3.46)$$

We allow the error in the assumed reflection depth (Δz_R) to vary. Figure 3.16(a) shows the estimated stacking velocity as a function of normalized vertical offset and normalized error in reflection depth. The difference between $(v_{st})_e$ and (v_{st}) increases with increasing reflector depth error. We can also see that the moveout of the curves increases with increasing reflector depth error. We examine this further by taking the derivative of equation (3.46):

$$\frac{\partial(v_{st})_e}{\partial\left(\frac{\dot{z}_t}{x_{off}}\right)} = v_{st} \cdot \frac{\left\{ \left(\frac{\dot{z}_t}{x_{off}}\right)\left(\frac{2\Delta z_R}{x_{off}}\right)^2 - \left(\frac{\dot{z}_t}{x_{off}}\right)^2\left(\frac{2\Delta z_R}{x_{off}}\right) + \left(\frac{2\Delta z_R}{x_{off}}\right) \right\}}{\left[\sqrt{\left(\frac{\dot{z}_t}{x_{off}}\right)^2 + 1} \left[\left(\left(\frac{\dot{z}_t}{x_{off}}\right) - \left(\frac{2\Delta z_R}{x_{off}}\right) \right)^2 + 1 \right]^{\frac{3}{2}} \right]}. \quad (3.47)$$

When $\Delta z_R = 0$, equation (3.47) reduces to

$$\frac{\partial(v_{st})_e}{\partial\left(\frac{\dot{z}_t}{x_{off}}\right)} = 0. \quad (3.48)$$

for all vertical offsets or source-receiver pairs. In figure 3.15(b) we plot equation (3.47) for different errors in assumed reflection depth. We see that the derivative is larger for larger errors in the reflection depth. Therefore in a constant velocity medium our objective is to find the reflection depth that minimizes the derivative of the estimated stacking velocity.

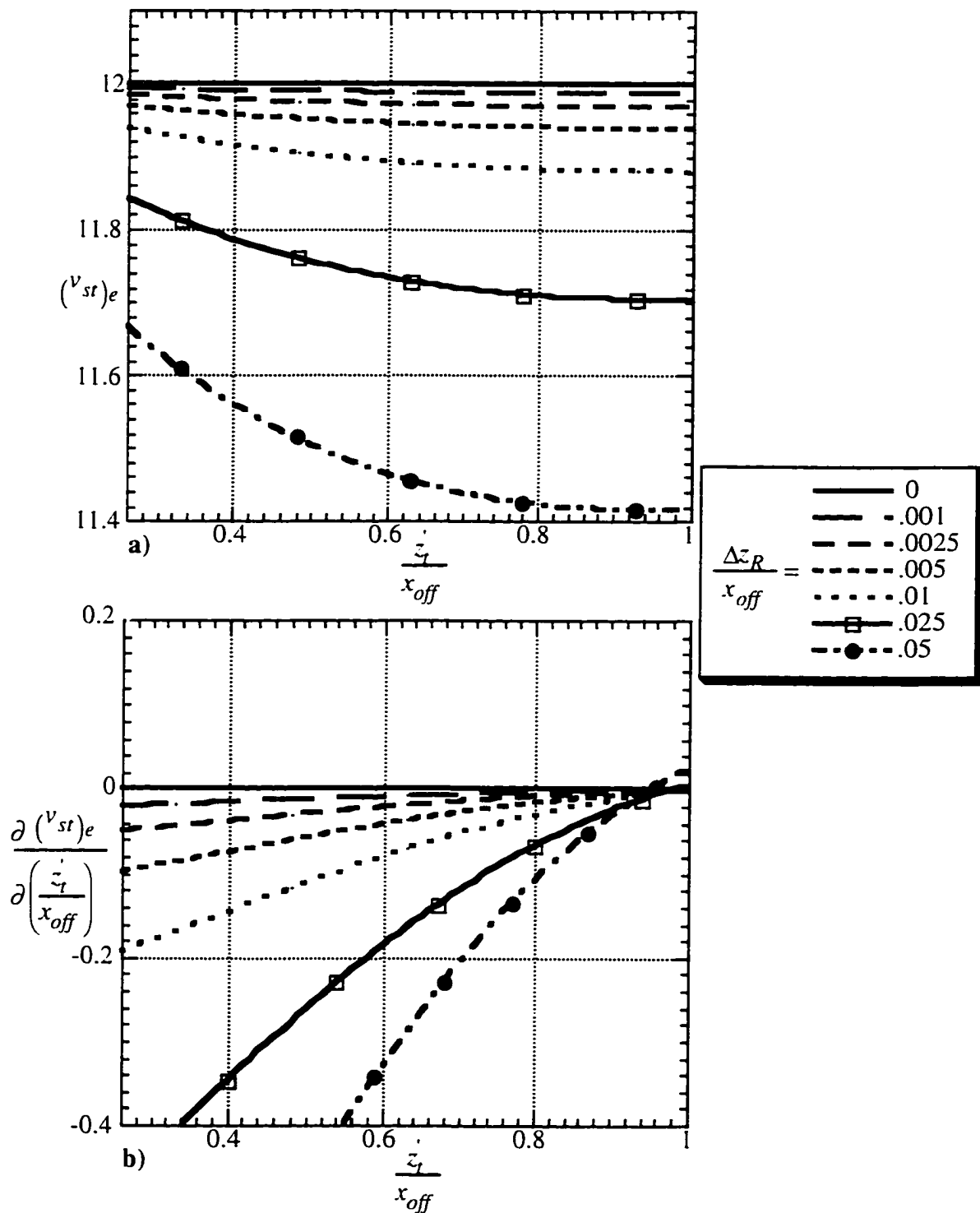


Figure 3.16: Stacking velocity as a function of normalized vertical offset and normalized reflection depth error (a), and the derivative of the stacking velocity with respect to normalized vertical offset (b). The error in the stacking velocity and the magnitude of the derivative of the stacking velocity increase with increasing error in reflection depth.

3.6.2 Variable Velocity

In the previous section we demonstrated a method to solve for the reflection depth in a constant velocity medium. In a variable velocity medium, the analysis becomes more complicated. Equation (3.46) stays the same for a variable velocity medium. However, equation (3.47) has an additional term in variable velocity media:

$$\frac{\partial(v_{st})_e}{\partial\left(\frac{\dot{z}_t}{x_{off}}\right)} = v_{mo} \cdot \left\{ \frac{\left(\frac{\dot{z}_t}{x_{off}}\right)\left(\frac{2\Delta z_R}{x_{off}}\right)^2 - \left(\frac{\dot{z}_t}{x_{off}}\right)^2\left(\frac{2\Delta z_R}{x_{off}}\right) + \left(\frac{2\Delta z_R}{x_{off}}\right)}{\left[\sqrt{\left(\frac{\dot{z}_t}{x_{off}}\right)^2 + 1}\right]\left[\left(\left(\frac{\dot{z}_t}{x_{off}}\right) - \left(\frac{2\Delta z_R}{x_{off}}\right)\right)^2 + 1\right]^{\frac{3}{2}}}\right\} + \frac{\partial(v_{st})}{\partial\left(\frac{\dot{z}_t}{x_{off}}\right)} \cdot \frac{\sqrt{\left(\frac{\dot{z}_t}{x_{off}}\right)^2 + 1}}{\sqrt{\left(\frac{\dot{z}_t}{x_{off}} - \frac{2\Delta z_R}{x_{off}}\right)^2 + 1}}. \quad (3.49)$$

where $\frac{\partial(v_{st})}{\partial\left(\frac{\dot{z}_t}{x_{off}}\right)}$ is the true change in the stacking velocity as a function of relative vertical

and horizontal offset. The first term in equation (3.49) is due to the error in the estimated reflection depth. The second term is due to the change in the stacking velocity as a function of vertical offset, and is modified by the error in reflection depth. If the reflection depth is correct ($\Delta z_R = 0$), then equation (3.49) reduces to:

$$\frac{\partial(v_{st})_e}{\partial\left(\frac{\dot{z}_t}{x_{off}}\right)} = \frac{\partial(v_{st})}{\partial\left(\frac{\dot{z}_t}{x_{off}}\right)}. \quad (3.50)$$

Therefore, if we obtain the correct reflection depth the derivative of the stacking velocities obtained from reflection velocity analysis will equal the true stacking velocities of the medium. However, since we do not know the true stacking velocities of the medium, we

cannot use the derivative of the estimated stacking velocity to determine the reflection depth. If we are to determine the reflection depth in a variable velocity medium, we must estimate the true stacking velocity of the medium through an additional piece of information, such as the sonic logs or direct arrival traveltime tomography. We can define a new term $(v_{st})_c$, which is a calculated stacking velocity based on sonic log or tomographic interval velocity information. We use this quantity to estimate the true stacking velocity of the medium:

$$(v_{st})_c \equiv (v_{st}). \quad (3.51)$$

To summarize, we have three quantities:

- 1) (v_{st}) is the true stacking velocity of the medium.
- 2) $(v_{st})_e$ is the estimated stacking velocity from reflection velocity analysis.
- 3) $(v_{st})_c$ is computed from previously determined interval velocities of the medium such as tomography or sonic logs.

We can define the quantity

$$\frac{\partial(v_{st})}{\partial\left(\frac{z_t}{x_{off}}\right)} = \frac{\partial(v_{st})}{\partial\left(\frac{z_t}{x_{off}}\right)} - \frac{\partial(v_{st})_c}{\partial\left(\frac{z_t}{x_{off}}\right)}. \quad (3.52)$$

Therefore we want to minimize the value of $\frac{\partial(v_{st})}{\partial\left(\frac{z_t}{x_{off}}\right)}$, which we call the adjusted stacking

velocity derivative. The accuracy to which this gives us the true reflection depth depends on how accurately $(v_{st})_c$ yields the true stacking velocity of the medium.

3.6.3 Synthetic Example

To evaluate reflection depth estimation in a variable velocity medium, we examine the synthetic model shown in figure 3.17. The synthetic has two layers. The first layer has a

velocity of 12 kft/sec. We examine the cases where the second layer has a velocity of 13 kft/sec and 15 kft/sec. We have a continuous aperture of sources and receivers. In figure 3.18 we see the value of the adjusted stacking velocity derivative (equation 3.52) when the derivatives of the calculated stacking velocities are within 95 % of the derivative of the true stacking velocities. In figure 3.19 we see the value of the adjusted stacking velocity derivative when we are able to calculate the derivative of the true stacking velocities within 99 % of their actual value. If we use the criterion of minimizing the magnitude of the derivative, we would obtain a small error in the reflection depth, but still a very accurate estimate (i.e. for the 95 % case with a second layer velocity of 13 kft/sec, we would have a reflection depth error of approximately $.005 x_{off}$ - this would be 5 ft. for a 1000 ft. well spacing).

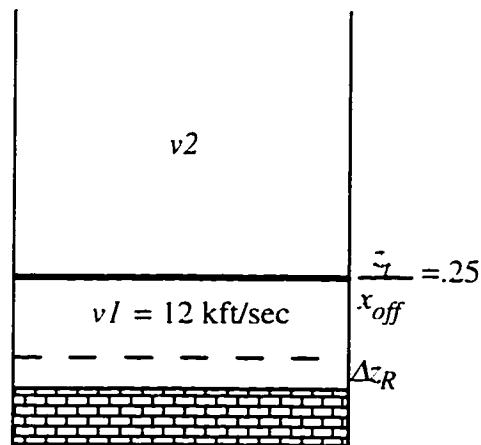


Figure 3.17: Synthetic model to evaluate the stacking velocity and the derivative of the stacking velocity for a variable velocity medium. The values of v_2 are 13 and 15 kft/sec.

3.7 CONCLUSIONS

We have shown that we can perform velocity analysis on crosswell reflection data in a similar fashion to surface seismic reflection data. The crosswell reflection velocity analysis problem is more complicated than surface seismic due to the transversal of different layers for a given CDP. We were able to examine how the velocity estimate relative to the true velocity affects the shape of the CDP traveltimes moveout curves. We were able to extend these concepts to variable velocity media. A synthetic example helped to verify the mathematical theory, and demonstrated the crosswell reflection velocity analysis procedure. We also examined the effect that the assumed reflection depth has on the stacking velocity estimate, and the need to use prior information to estimate the reflection depth in a variable velocity medium. The velocity analysis procedure gives us a powerful tool to provide an

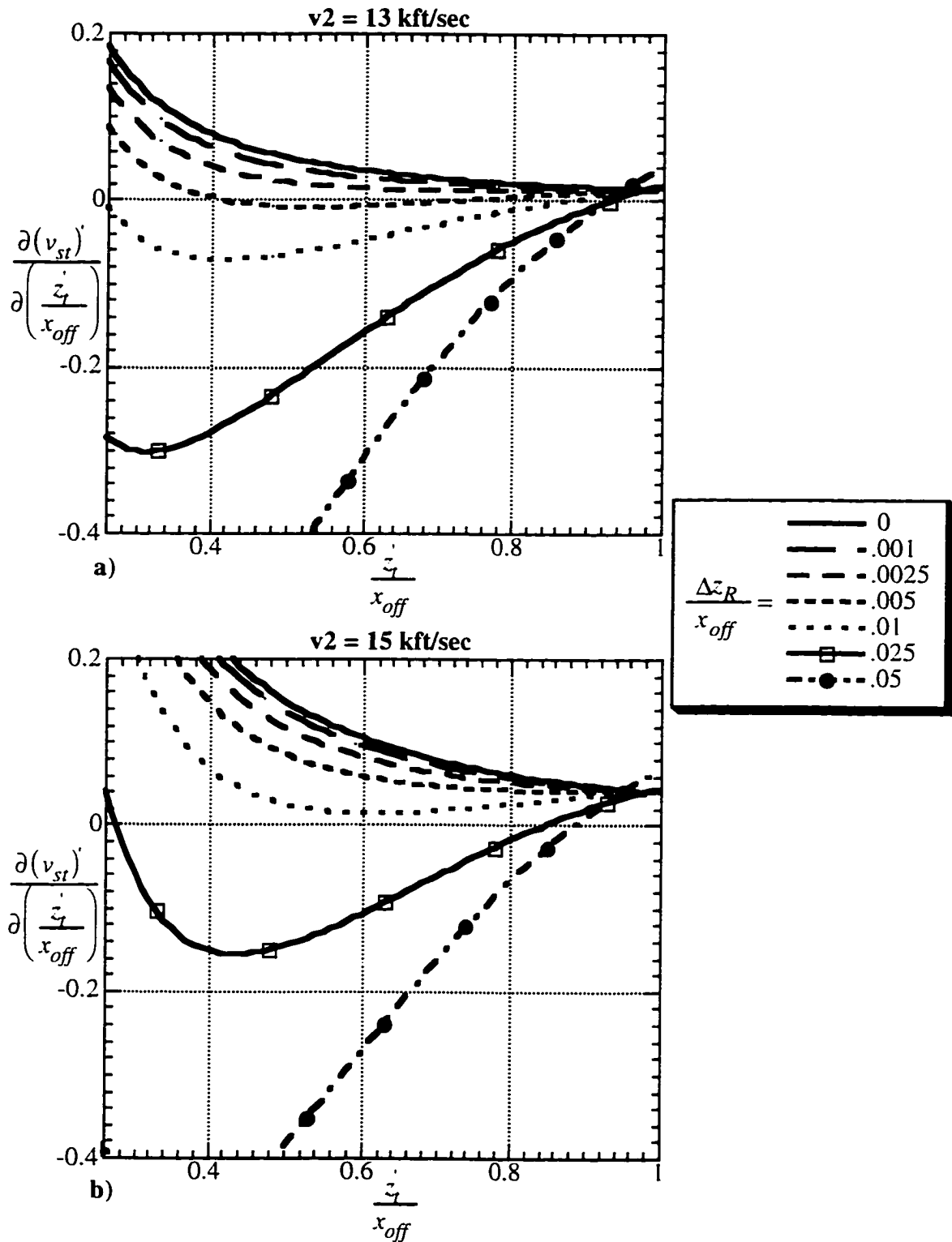


Figure 3.18: The adjusted derivative of the stacking velocity as a function of normalized vertical offset and normalized reflection depth error for the variable velocity medium shown in figure 3.17 when the calculated stacking velocity derivative is 95% of the true stacking velocity derivative. The second layer velocity is (a) 13 kft/sec and (b) 15 kft/sec.

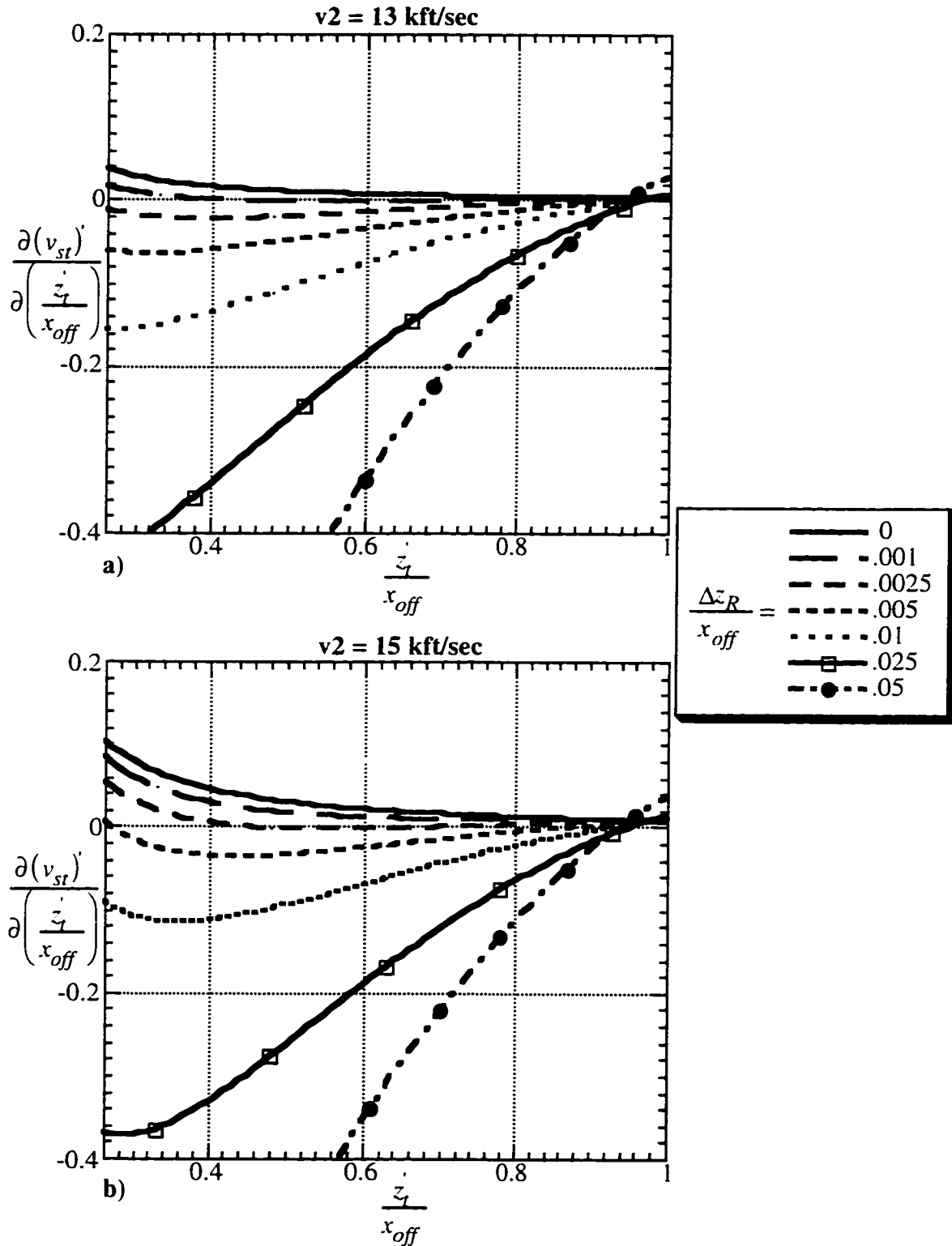


Figure 3.19: The adjusted derivative of the stacking velocity as a function of normalized vertical offset and normalized reflection depth error for the variable velocity medium shown in figure 3.17 when the calculated stacking velocity derivative is 99% of the true stacking velocity derivative. The second layer velocity is (a) 13 kft/sec and (b) 15 kft/sec.

accurate stacking velocity model for crosswell reflection imaging, which is examined in detail in chapter 4 on a synthetic data set, and chapter 5 on a field data set.

Chapter 4

Crosswell CDP Reflection Imaging - Synthetic Data Set

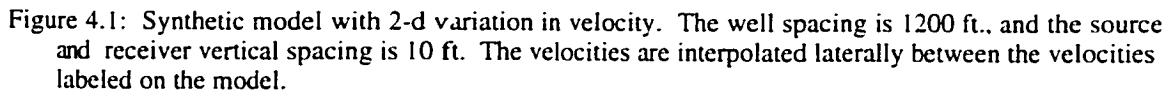
4.1 INTRODUCTION

In chapter 2 we derived a CDP coordinate system for the sorting of crosswell reflection data. In chapter 3, we derived a reflection velocity analysis procedure based on this coordinate system. In this chapter, we combine the CDP sorting and velocity analysis procedure into a complete reflection imaging algorithm, and apply this algorithm to a synthetic data set. The algorithm developed takes the data from its raw form in Common Source Gathers (CSG) and Common Receiver Gathers (CRG) to a final reflection image.

4.2 DATA SET DESCRIPTION

A data set with 2-d velocity variation was generated by a finite difference program with ProMAX software. An acoustic wavefield was created with a central frequency of 350 Hz, and a Nyquist frequency of 1400 Hz. Figure 4.1 shows the geometry of the data set. The well separation is 1200 ft, and the source and receiver spacing is 10 ft. As well as horizontal layers with different velocities, the model has three types of horizontal variation in velocity:

- 1) Constant linear change in the velocity from the source to the receiver well.
- 2) Change in the linear velocity slope from the source well to the receiver well.
- 3) A velocity discontinuity.



In order to produce a final reflection image from raw crosswell data, we have to perform a number of different operations on the data. Figure 4.2 shows the complete reflection imaging procedure based upon the CDP sorting and velocity analysis procedures developed in chapter 2 and chapter 3. The data in its raw form is first pre-processed in CSGs and CRGs to enhance upgoing and downgoing reflection data. The pre-processed data is used to find the stacking velocities that will optimize the stack of the reflection data for CDP gathers. The pre-processed reflection data and the set of CDP stacking velocities serve as the input to the CDP reflection imaging algorithm. The data is then mapped into image space by a point to point mapping operator. The data is then stacked over CDPs to give a final reflection image for the entire crosswell survey. This algorithm is discussed in detail in subsequent sections in this chapter.

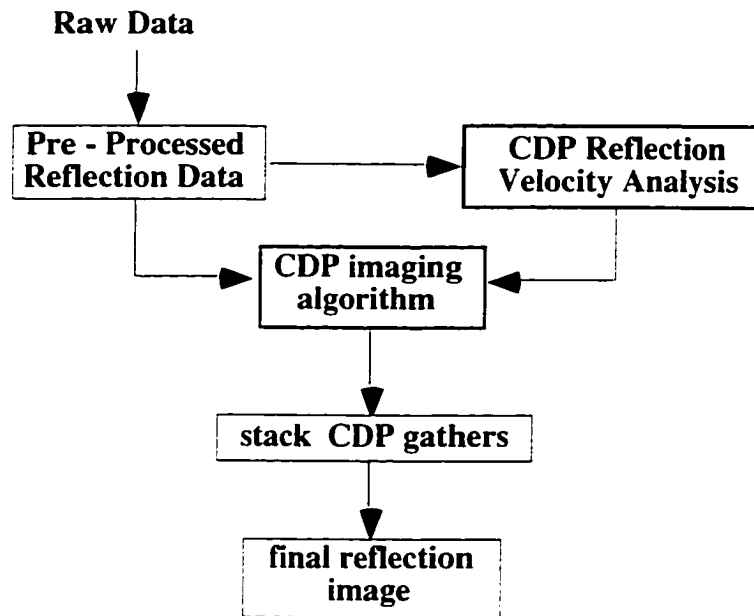


Figure 4.2: Crosswell reflection imaging algorithm. This procedure takes the data from its recorded time series to the final reflection image.

4.4 RAW DATA

In figure 4.3 we see three CSGs of the synthetic wavefield at 2000 ft., 2400 ft., and 2800 ft. respectively. We primarily see two wavemodes; the direct arrival and the reflected arrivals. The reflected arrival branches off from the direct arrival for reflection CDPs at the source well at the reflection depth. In the CSG at 2000 ft. we see only upgoing reflections, and in the CSG at 2800 ft. we see only downgoing reflections. In the CSG at 2400 ft, we see both downgoing and upgoing reflections.

4.5 PRE-PROCESSED REFLECTION DATA

Before we can use the crosswell reflection data for velocity analysis and imaging, we have to attempt to remove as much of the rest of the wavefield as possible. On this synthetic data set the pre-processing consists of two steps:

- 1) Removal of the direct arrival.
- 2) Enhancing all upgoing or downgoing reflection events (figure 4.4).

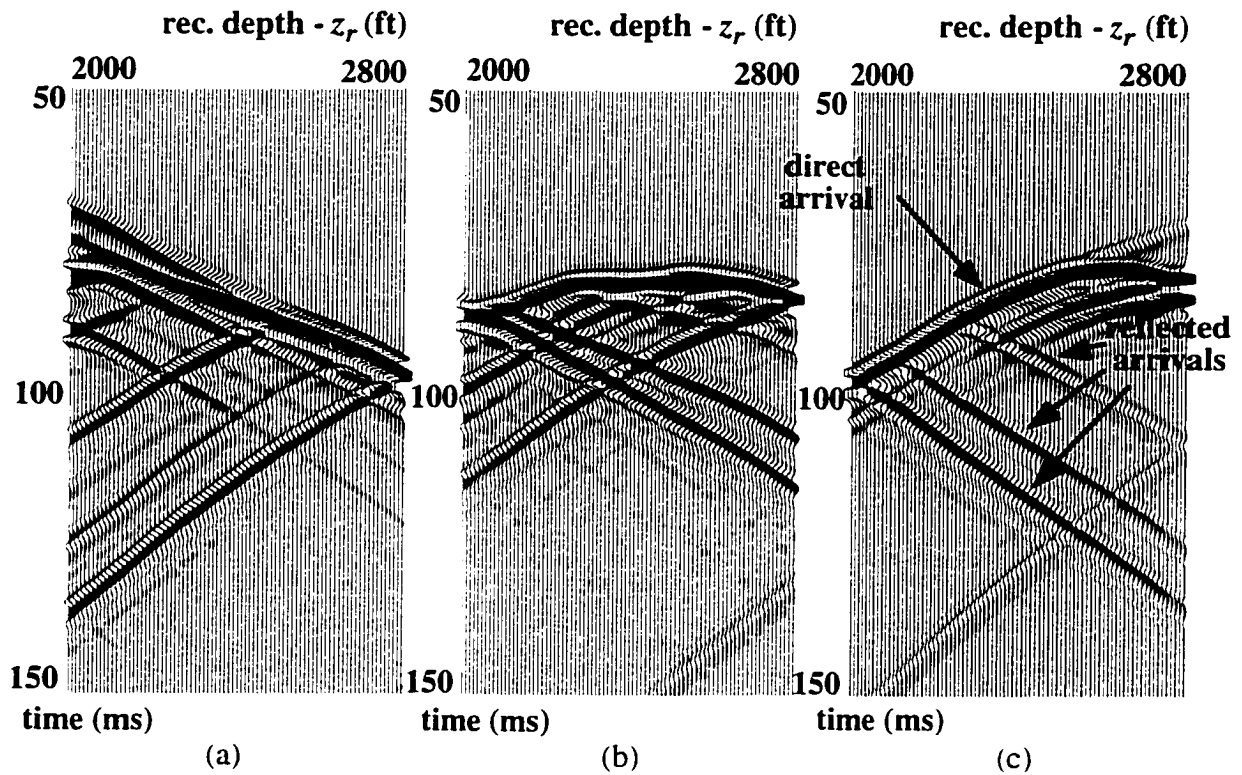


Figure 4.3: CSGs at 2000 ft. (a), 2400 ft. (b), and 2800 ft. (c). The two wavemodes seen are the direct and reflected arrivals.

Removal of the direct arrival requires:

- 1) Picking the direct arrival travel time from the raw data.
- 2) Aligning the direct arrival.
- 3) Subtracting the direct arrival through a trace mix.

Enhancement of the reflections requires:

- 1) An f-k filter (figure 4.5) to separate upgoing and downgoing reflections.

The direct arrival traveltimes are determined by picking the peak of the first break arrival in both source gathers and receiver gathers. The picking must be done in both gathers in order to enhance the reflection data for all reflection points from the source well to the receiver well (Lazaratos, 1993). The traces are then shifted by the picked traveltimes to a

common reference time so that all of the direct arrivals are aligned. A 2-d mixing operator is then applied to the data to subtract the direct arrival from the rest of the wavefield. To separate upgoing and downgoing reflections we use an f-k filter. A positive f-k filter pass allows for upgoing reflections to be enhanced (figure 4.6(a)), and a negative f-k filter pass allows for downgoing reflections to be enhanced (figure 4.6(b)).

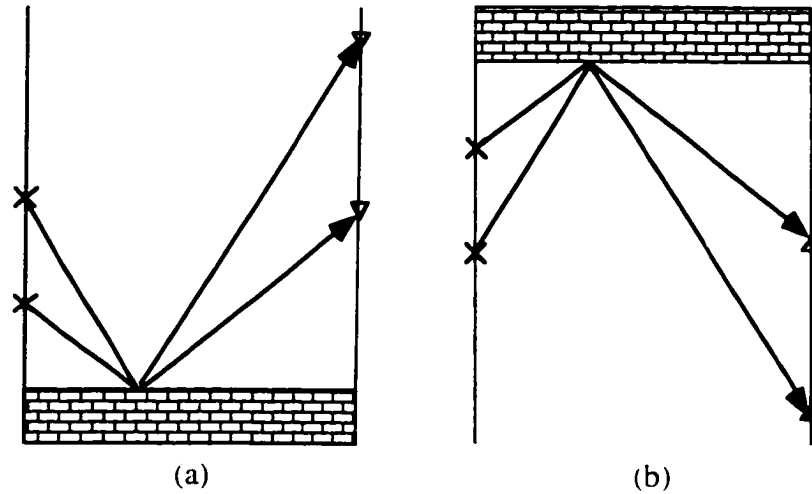


Figure 4.4: Upgoing reflection events (a), and downgoing reflection events (b).

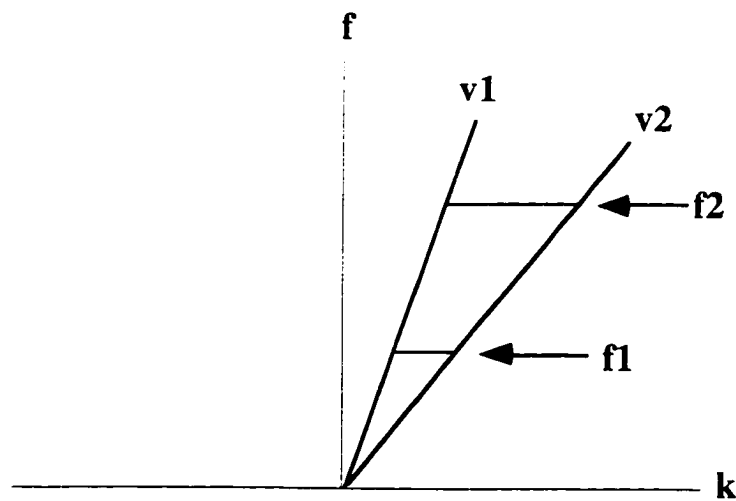


Figure 4.5: Pie-slice f-k filter. Velocity slopes and a frequency range are defined for a pass or rejection region.

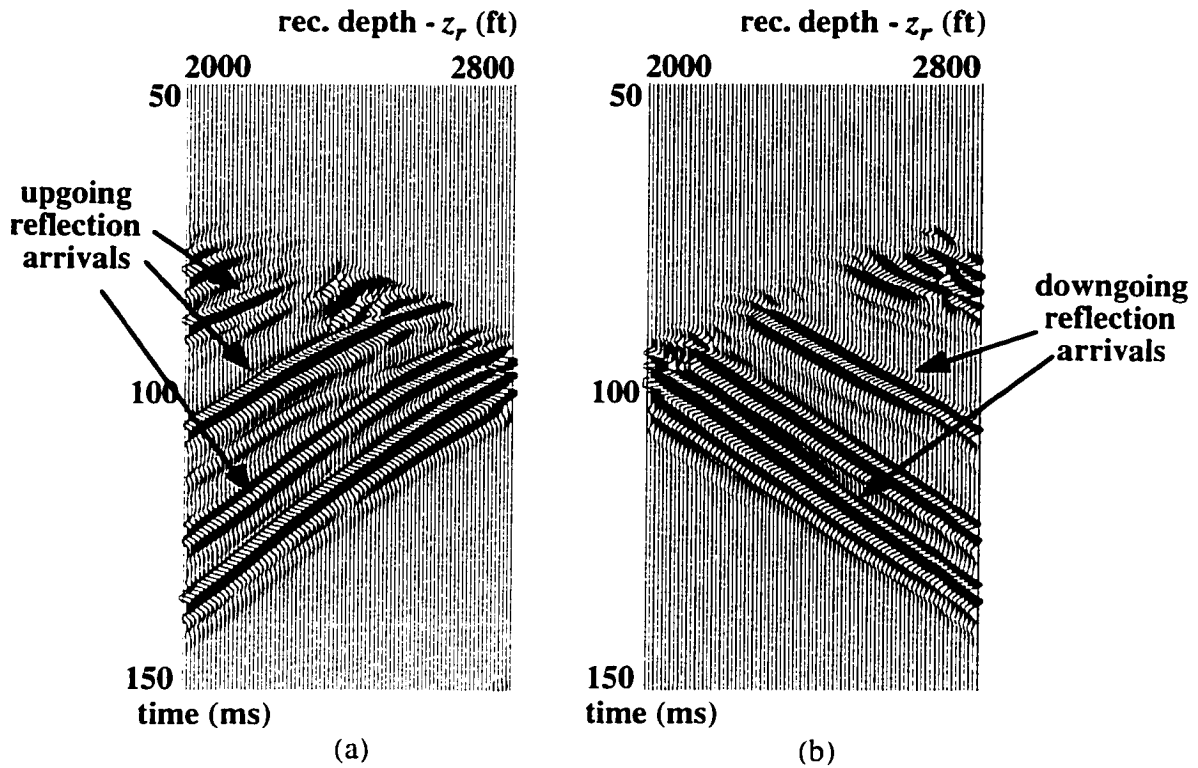


Figure 4.6: CSGs after pre-processing to enhance reflection data. The CSG at 2000 ft. (a) is pre-processed for upgoing reflections, and the CSG at 2800 ft. (b) is pre-processed for downgoing reflections.

4.6 REFLECTION VELOCITY ANALYSIS

Once we have pre-processed the data for reflections, we can perform reflection velocity analysis to align the phase of the reflection data for stack. This consists of several steps (figure 4.7). We perform this loop for multiple CDP locations to obtain stacking velocity vectors for the entire survey. We need to perform velocity analysis for numerous CDPs locations due to the raypath locations for various CDPs (figure 4.8).

4.6.1 CDP Sorting of the Reflection Data

After being pre-processed for reflections, the reflection data is sorted into the crosswell CDP coordinate system (Section 2.5.2). Figure 4.9 shows four CDP gathers 45, 55, 65, and 75 from the source well respectively for a reflection depth of 2000 ft. A 10 ft. bin for sorting the CDP gathers is used. We see a strong reflection event starting at about 82 ms. The reflection event is discontinuous in these gathers due to the CDP binning. The CDP binning causes the radial distance coordinate to have gaps for a single CDP gather.

Therefore we look at several CDP gathers at once when performing CDP reflection velocity analysis. Over the reflection segments, we see small hyperbolic moveout in the reflection event (section 2.6.2).

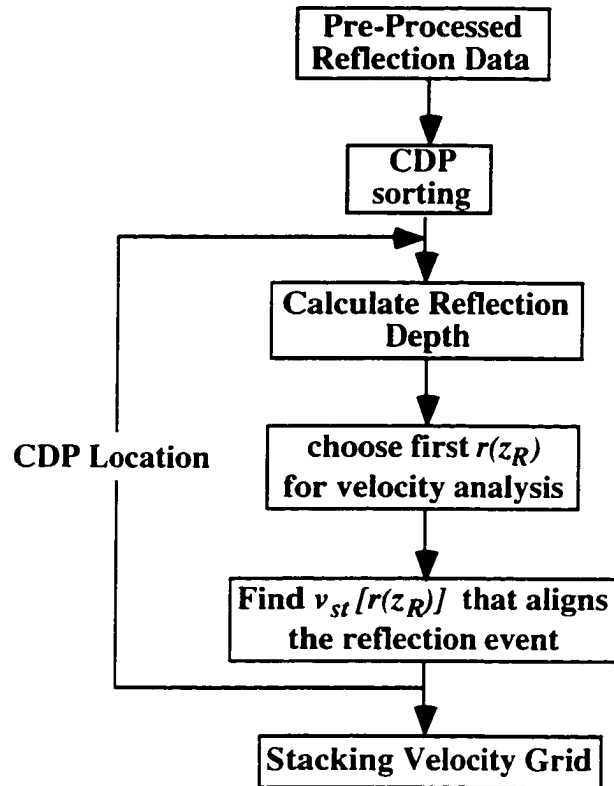


Figure 4.7: Reflection Velocity Analysis Algorithm.

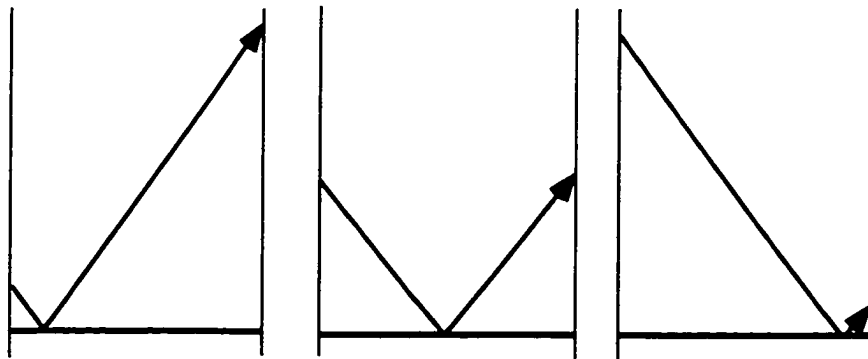


Figure 4.8: CDP locations and their respective raypaths. Different areas of the medium are sampled.

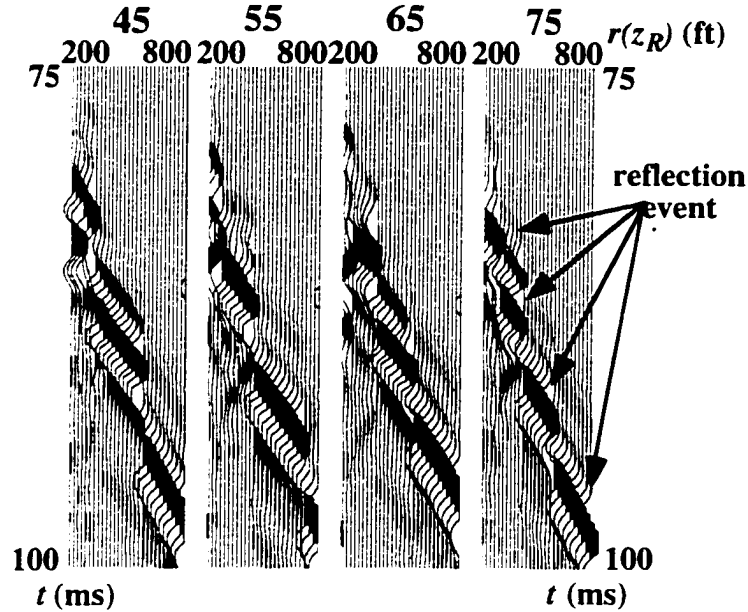


Figure 4.9: CDP gathers 45, 55, 65, and 75 ft. from the source well for a reflection depth of 2000 ft. We see a strong reflection event starting at about 82 ms at small radial distances. The reflection event is discontinuous within individual CDP gathers due to CDP binning. This causes gaps in the radial distance coordinate for a single CDP gather. The first row of numbers is the CDP distance from the source well. The second row of numbers is the radial distance for a given CDP gather.

4.6.2 Reflection Depth Determination

Once we have chosen the CDP reflection point location, we need to make an estimate of the reflection depth at the chosen CDP location. As was discussed in section 3.6, we need some type of prior information to estimate the reflection depth in variable velocity media. In figure 4.10(a) we see the moveout curve for a CDP gather (section 2.6.2). At $r(z_R) = 0$ this corresponds to the direct arrival traveltimes (a raypath traveling straight across the survey at the reflection depth). Therefore we can estimate the reflection depth by tying the reflection event to the direct arrival in CDP gathers. In figure 4.10(b) we see the CDP moveout curve when the assumed reflection depth is different from the true reflection depth. We see that the reflection at $r(z_R') = 0$ has a different traveltimes than when we have the correct reflection depth. If we use the direct arrival traveltimes to estimate the velocity, we can calculate the error in the reflection depth:

$$\Delta z_R = \sqrt{\frac{v_{st}^2 \cdot t_{r(z_R')=0}^2 - x_{off}^2}{2}}, \quad (4.1)$$

where Δz_R is the difference between the assumed reflection depth and the actual reflection depth, and $t_{r(z_R')=0}$ is the reflection traveltime at $r(z_R')=0$. We use direct arrival traveltime tomography to estimate v_{st} , as was discussed in section 3.6. At $r(z_R')=0$ the stacking velocity used is the velocity at the assumed reflection depth. We do not have reflection data at $r(z_R)=0$ unless we have continuous source and receiver coverage. Therefore we use the traveltime of the reflection data at the smallest radial distance that the reflection data is visible as opposed to the traveltime at $r(z_R')=0$. We then use the velocity from the direct arrival traveltime to calculate the stacking velocity. We can now solve for the total vertical offset:

$$\tilde{z}_t = \sqrt{(v_{st})_c^2 \cdot t_{r_{min}}^2 - x_{off}^2}, \quad (4.2)$$

where \tilde{z}_t is the total vertical offset (section 3.4) between the reflector and the source and receiver, $(v_{st})_c$ is the calculated stacking velocity from direct arrival tomography (section 3.6), and r_{min} is the smallest radial distance in the gather (the source and receiver pair that is closest vertically to the reflection for this CDP gather). This allows us to solve for the error in reflection depth by:

$$\Delta z_R = \frac{\tilde{z}_t - \tilde{z}_t'}{2}, \quad (4.3)$$

where \tilde{z}_t' is the total vertical offset based on the assumed reflection depth.

In figure 4.11, we see CDP gathers for reflection points 45, 55, 65, and 75 ft. from the source well based on an assumed reflection depth of 2020 ft. We pick the traveltime of the CDP gather at 45 ft. at the smallest radial distance in the gather ($r_{min} = 240.21$ ft). This corresponds to the source at 2030 ft. and the receiver at 2260 ft., giving a total assumed vertical offset of 250 ft ($\tilde{z}_t' = 250$ ft.) The picked reflection traveltime on this trace is (figure 4.11) is 82.3 ms. We use the 1-d tomogram shown in figure 4.12 to estimate v_{st} . We calculate $(v_{st})_c$ to be 14.125 kft/sec for this vertical offset. Using equation 4.2, we calculate the true vertical offset to be 297.7 ft. ($\tilde{z}_t = 297.7$ ft.). Using equation 4.3, we calculate the difference between the assumed reflection depth and the true reflection depth to be -23.85 ft ($\Delta z_R = -23.85$ ft.). Therefore we calculate the true reflection depth to be 1996.15 ft. The true reflection depth is 2000 ft. Therefore in this example we have been able to estimate the reflection depth within 3.85 ft.

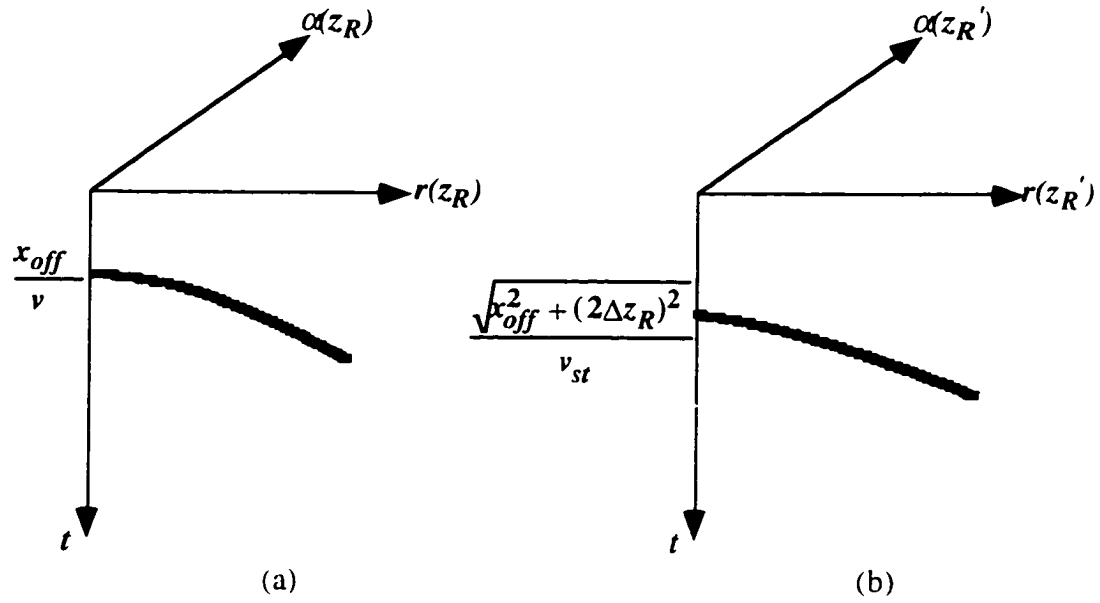


Figure 4.10: CDP gather when we have assumed the correct reflection depth (a), and when the assumed reflection depth (z_R') is different from the true reflection depth (z_R) (b).

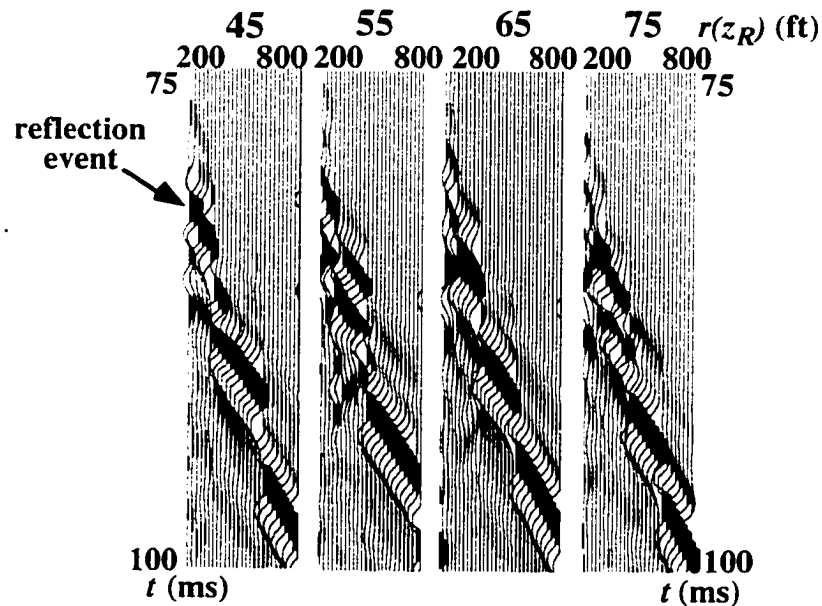


Figure 4.11: CDP gathers 45, 55, 65, and 75 ft. from the source well for an assumed reflection depth of 2020 ft. We pick the traveltide of the reflection at the smallest available radial distance and use direct arrival traveltide tomography to estimate the true reflection depth.

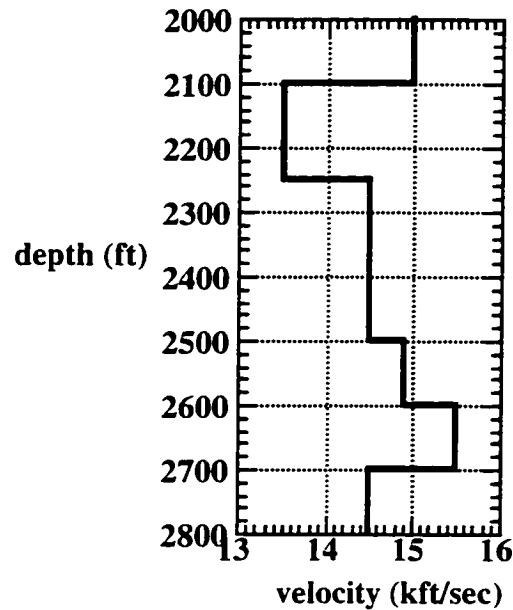


Figure 4.12: 1-d tomogram of the synthetic model.

4.6.3 Alignment of the Reflection Event

Once we have estimated the depth of the reflection to be 1996 ft., we can perform reflection velocity analysis (section 3.5). We start the reflection event alignment at a radial distance of 450 ft. The reflection event at radial distances smaller than this have considerable waveform distortion due to the wide angles of incidence (section 3.5). We perform velocity analysis for the reflection event for all the remaining radial distances (figure 4.13). We apply two stacking velocities at two different radial distances and interpolate the stacking velocities for the other radial distances (figure 4.14). The increase in stacking velocity is expected due to the increase in the interval velocity at the depth of 2500 ft at the receiver well.

4.6.4 Stacking Velocity CDP grid

We perform the reflection depth and velocity analysis procedure for many different CDP locations to obtain a grid of stacking velocity vectors for the entire crosswell survey (figure 4.15). We have estimated the depths of the CDP by the procedure described in section 4.6.2. We were able to estimate all of the reflection depths within 8 ft. of their true reflection depth, except for a few CDPs on the source well side of the image on the reflection at 2700 ft. The largest reflector depth error was 13 ft. at the CDP 450 ft. from the source well. The stacking velocities compare very favorably to the interval velocities of

the medium (figure 4.1), and increase and decrease expectedly with increases and decreases in the interval velocities. This also gives us evidence that these events are primary reflections as opposed to other wave modes, such as head waves. Some CDPs required more stacking velocity assignments than others due to transversal of more layers with different velocities. For example CDPs in the middle of the survey are transversing regions with many different velocities due to the 2-d variation in velocity. As we see from figure 4.15, one of the main differences between crosswell and surface seismic velocity analysis is that at each CDP we obtain a vector of stacking velocities for crosswell, where we only obtain one stacking velocity for a surface seismic CDP (figure 4.16).

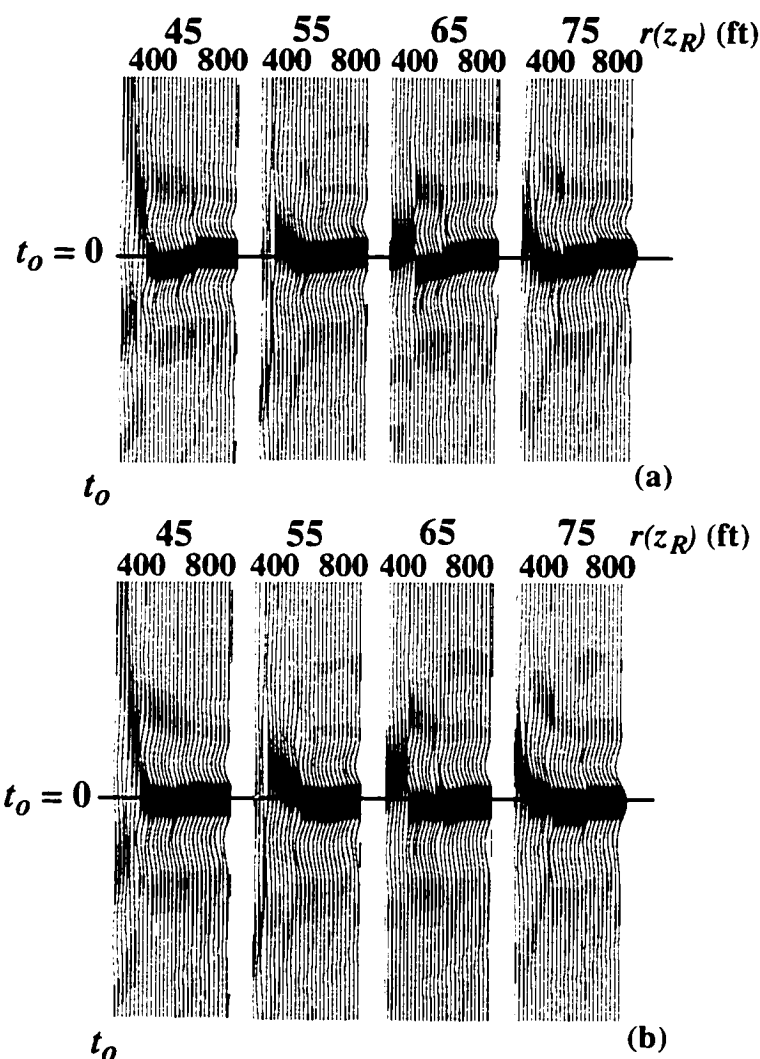


Figure 4.13: CDP-VLMO gathers (CDP gathers after we have performed the HNMO and VLMO corrections) 45, 55, 65, and 75 ft. from the source well for a reflection depth of 1996 ft., after we have assigned one stacking velocity (a) and two stacking velocities (b). The reflection event is now aligned for stack after assigning stacking velocities at two radial distances and interpolating for other radial distances. The first row of numbers is the CDP distance from the source well, and the second row of numbers is the radial distance for a given CDP.

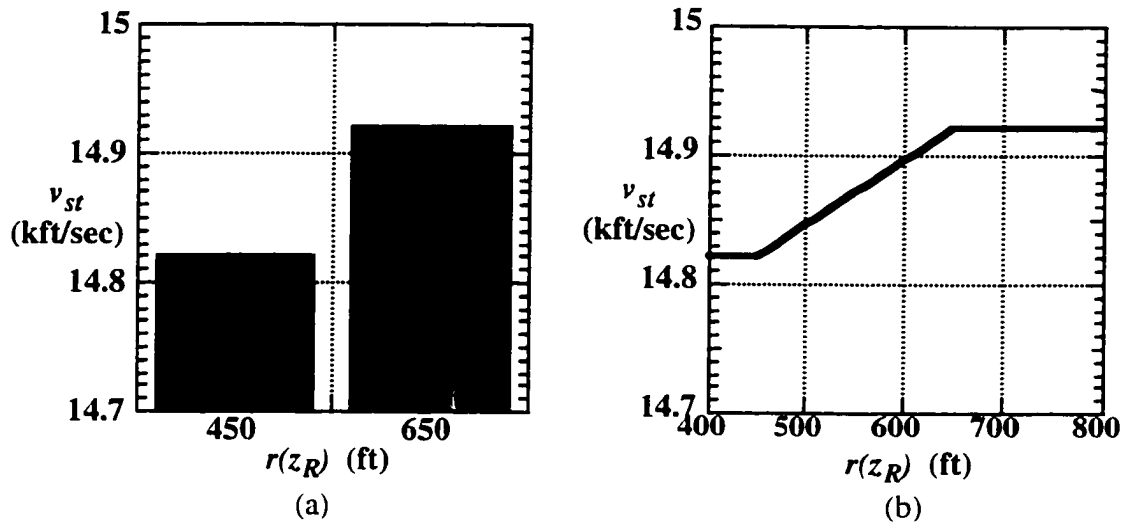


Figure 4.14: Stacking velocities for specific radial distances (a), and for all radial distances (b), which were obtained from velocity analysis on the CDP gathers shown in figure 4.13.

4.7 CDP IMAGING ALGORITHM

Once we have the complete grid of stacking velocity vectors, we can then perform reflection imaging on the entire survey. The full algorithm is shown in figure 4.17. The pre-processed reflection data and the stacking velocity grid serve as the input data for the CDP imaging algorithm. Once the data has been run through the reflection imaging algorithm it is ready to be stacked to give a final reflection image. As was discussed in section 4.5, we can pre-process the data in different gathers for different types of events. Figure 4.18 shows the domain and wavefield that is used for imaging different parts of the survey.

4.7.1 Starting Reflection Depth and Reflection Depth Loop

As has been discussed consistently throughout this thesis, the crosswell CDP reflection gathers are parameterized by the reflection depth; z_R . Therefore we perform the imaging algorithm over a set of all reflection depths that we want to image. The parameterization by reflection depth means that each seismic trace only contributes a single sample to the image space for one particular reflection depth (figure 4.19). On this data set, the reflection depth increment is 2 ft.

4.7.2 CDP sorting

For each reflection depth in the loop, we have to perform CDP sorting (section 2.5.2), since the CDP sorting is parameterized by reflection depth.

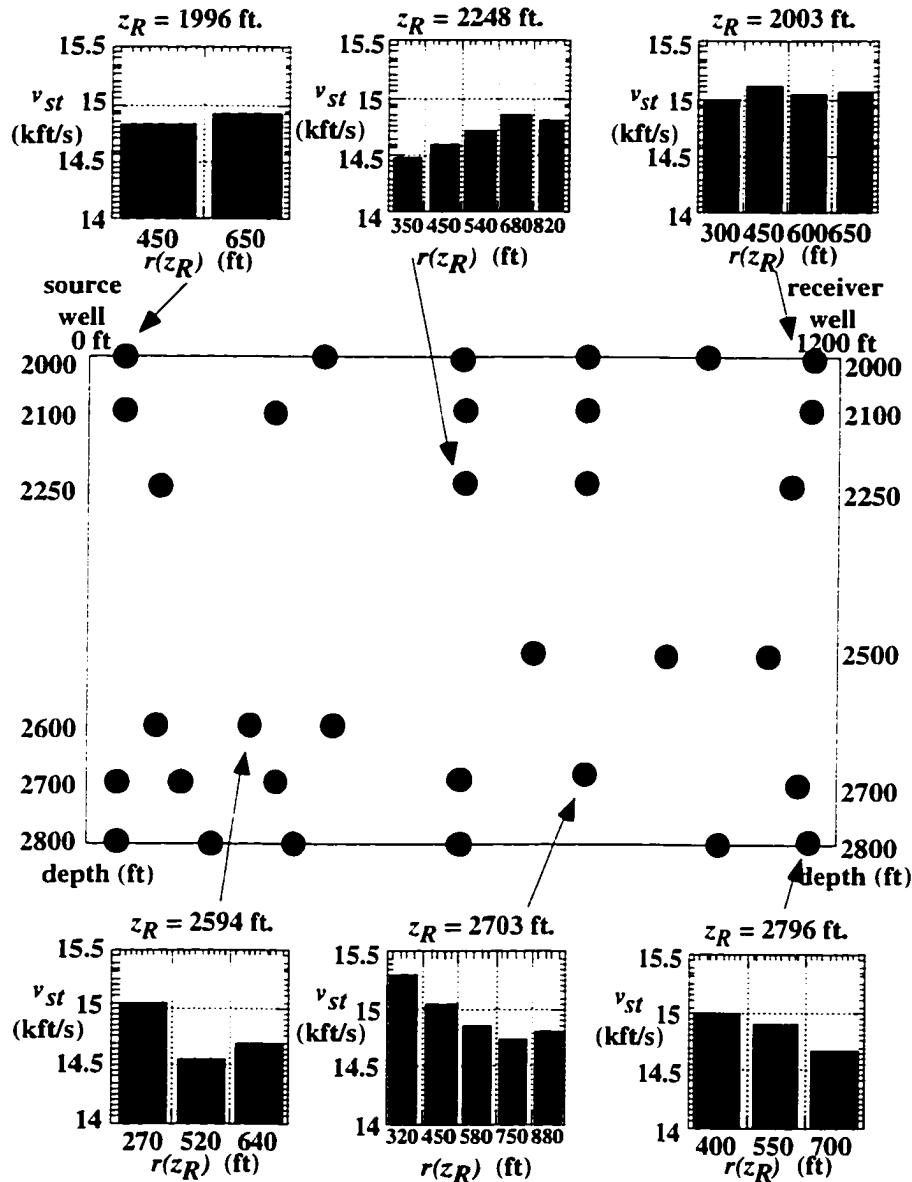


Figure 4.15: Stacking velocity grid for the entire survey. Each black dot shows where CDP velocity analysis was performed. Stacking velocity vectors are shown for certain CDPs.

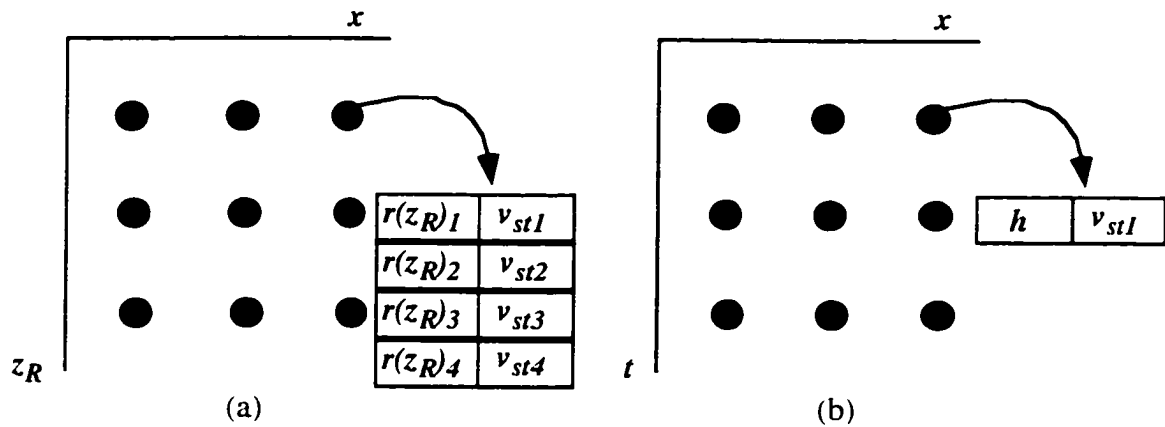


Figure 4.16: CDP reflection velocity analysis results for crosswell (a), and surface seismic (b). Crosswell yields a vector of stacking velocities, while surface seismic yields one stacking velocity for a CDP.

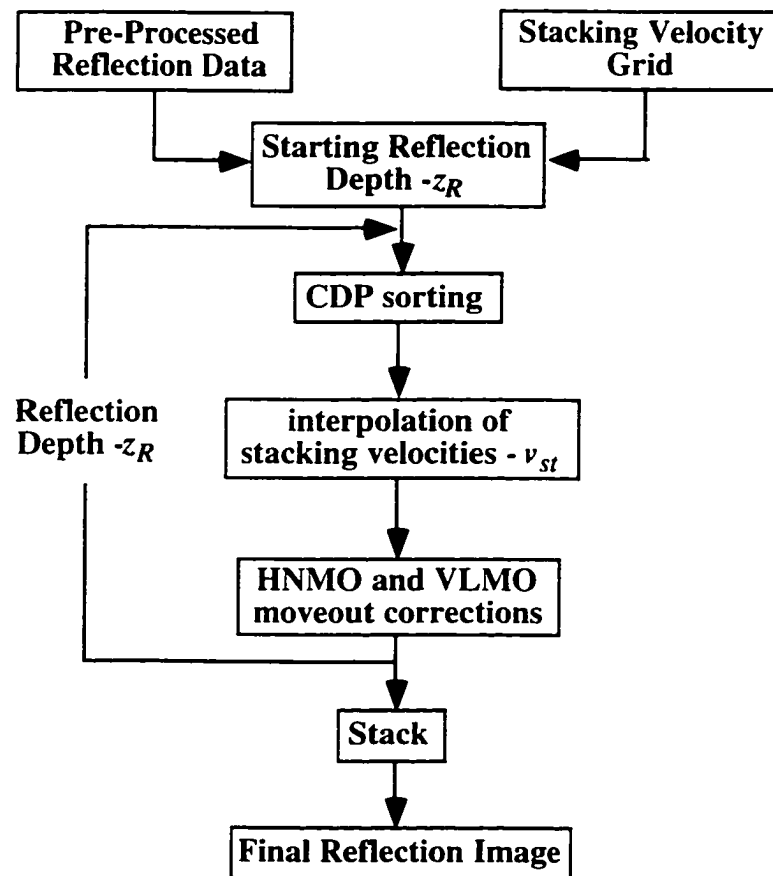


Figure 4.17: CDP reflection imaging algorithm. The input to the algorithm is the pre-processed reflection data and the stacking velocity grid. The output of the algorithm is CDP sorted imaged reflection data ready to be stacked to obtain the final reflection image.

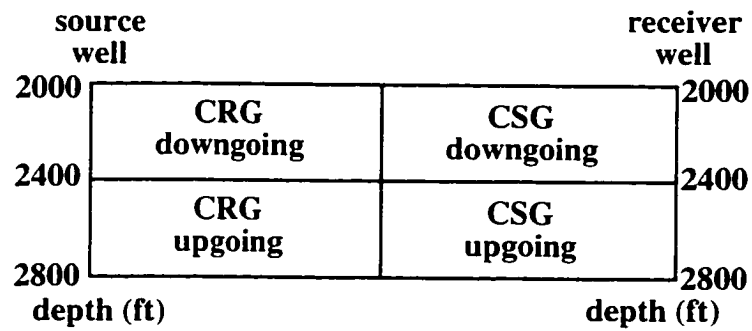


Figure 4.18: Types of pre-processing that are performed for reflection imaging on different regions of the survey.

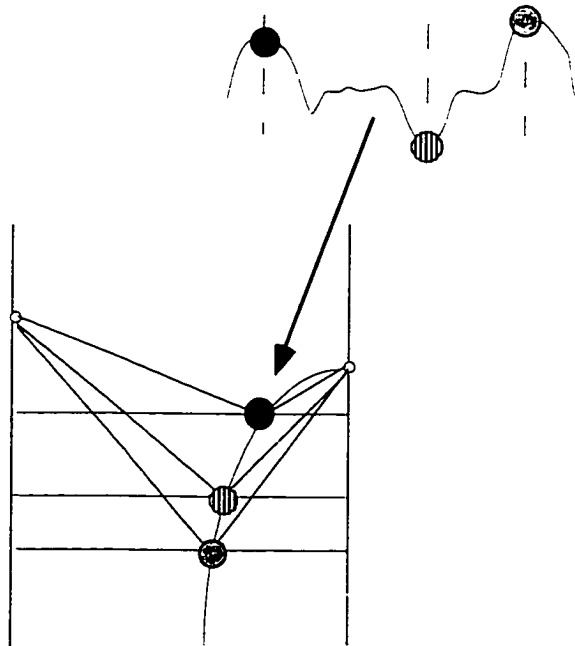


Figure 4.19: Each sample on a time trace corresponds to a reflection depth in image space. Each trace contributes one sample for each reflection depth.

4.7.3 Interpolation of Stacking Velocities

In figure 4.15, we showed the CDP locations where we performed velocity analysis. We need to use these stacking velocity vectors to interpolate stacking velocities for all CDPs. We do this by interpolating both laterally and vertically the stacking velocities for constant radial distance values (figure 4.20).

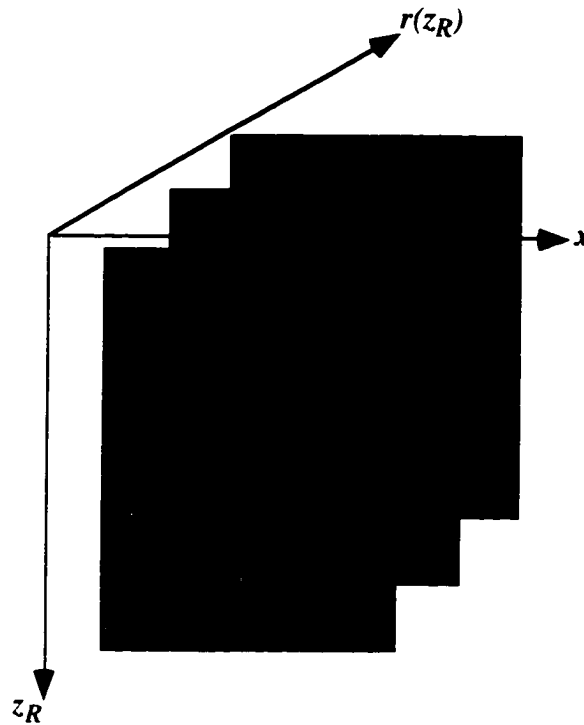


Figure 4.20: 3-d interpolation of stacking velocities. The stacking velocities are interpolated vertically and horizontally for constant values of radial distance.

4.7.4 HNMO and VLMO corrections

Once we have calculated stacking velocities for all CDPs, we perform the HNMO and VLMO moveout corrections that were discussed in section 2.7.2 for all CDPs. After these moveout corrections have been performed, all of the data is now in image space, and is ready to be stacked.

4.8 STACK OVER CDP GATHERS AND FINAL REFLECTION IMAGE

The data are stacked over CDP gathers to obtain a final reflection image (figure 4.21). All the reflectors, both with positive and negative reflectivity, have been imaged very close

to their correct locations. This is primarily due to the large number of CDP velocity analysis locations (figure 4.15). The large number of velocity analysis CDPs allows us to take into account the 2-d velocity variation of the model (figure 4.1). There are some differences in the quality of the imaging on some of the individual reflections. The reflection at depth 2100 ft. shows a little more curvature than some of the other reflections. This is due to the use of fewer velocity analysis CDPs on this reflection. The

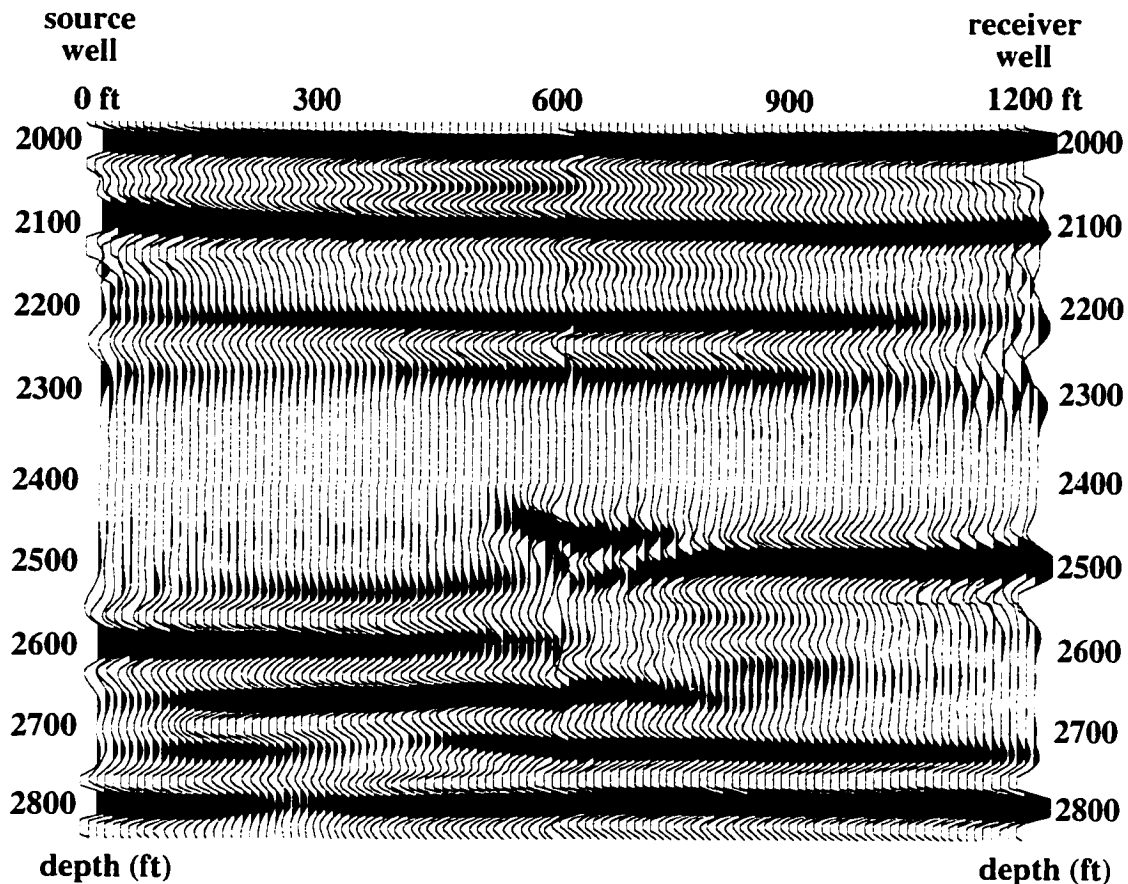


Figure 4.21: Final reflection image stack. The locations of the positive and negative reflections correlate closely with the original model shown in figure 4.1.

discontinuous reflection events at 2500 ft and at 2600 ft. have a decrease in their amplitudes toward their truncation point. This is because the point to point mapping algorithm used to image the reflection data (figure 4.19) does not collapse the Fresnel zone, therefore limiting lateral resolution. The reflection with negative reflectivity at 2700 ft. becomes very weak near the receiver well. This is due to the small velocity contrast near the receiver well at this depth, as well as destructive interference caused by a side lobe from the reflection at 2800 ft. The small pull-up in the reflections at the CDP location 400 on the reflection at

2700 ft. and CDP location 300 on the reflection at 2800 ft. is due to the raypath transversing the velocity discontinuity in the middle of the survey between depths 2500 ft. and 2600 ft. Since we use straight raypaths this also causes a slight weakening of the amplitudes on the reflection at 2800 ft. at CDP location 300. The straight rays do not take into account the velocity discontinuity, causing a small error in the calculation of the CDP gathers. Therefore the CDP reflection imaging algorithm can deal well with small gradual 2-d variations in velocity, but has slightly less ability to deal with velocity discontinuities.

4.9 CONCLUSIONS

In this chapter we have developed a complete reflection imaging algorithm where we started with raw data and obtained a final reflection image stack. We used the CDP sorting and velocity analysis procedures developed in chapters 2 and 3 as the framework to develop the reflection imaging algorithm. We implemented this algorithm on a synthetic data set with 2-d variation in velocity, which included wavefield separation, CDP velocity analysis and imaging, and CDP stacking. The final stacked image correlated well with the original model. The strength of the algorithm is that we can take into account small gradual 2-d variations in velocity by performing velocity analysis over a 2-d grid of CDPs. The mapping and straight ray approximation of the algorithm causes some small problems with reflection coherency when there is a velocity discontinuity.

Chapter 5

Crosswell CDP Reflection Imaging - Field Data Set

5.1 INTRODUCTION

Crosswell reflection imaging is a relatively new field in the crosswell seismology experiment. A number of reflection images have already been obtained using crosswell data (Lazaratos, (1993), Mo (1993), Van Schaack (1997), Stewart (1991)). Each of these reflection imaging algorithms had methods for wavefield separation, sorting, obtaining a velocity model, and imaging and stacking. The work in this chapter seeks to use many of the aspects in these other reflection imaging algorithms; including wavefield separation and point to point mapping (Lazaratos, 1993), and looking at the moveout of the reflection data to find the velocity model for stacking (Stewart 1991). Additionally, we attempt to improve upon all of these previous methods by examining the moveout of the reflection data in CDP gathers to find the best velocity model for reflection imaging. The benefits of this methodology are:

- 1) It optimizes the stack of the reflection data by finding the stacking velocities that the reflection data itself indicates are best for stack.
- 2) It can take into account 2-d variation in the stacking velocities.
- 3) It can handle wider well spacing where we are more likely to have 2-d changes in the stacking velocities.

In the previous chapter, we developed a new algorithm for reflection imaging based on the CDP coordinate system and reflection velocity procedure developed in chapters 2 and 3. In this chapter the same algorithm is applied to a wide offset ($x_{off} = 1225$ ft) field data crosswell survey. While we are applying the same algorithm to the real data survey as was performed on the synthetic data set, the field crosswell data has additional problems in dealing with the wavefield separation, due to the complexity of the field data. Wavefield separation and filtering is used three times during the reflection imaging procedure: pre-processing, velocity analysis, and imaging and stack.

5.2 FIELD DATA DESCRIPTION

Figure 5.1 shows the geometry for the field data set. The data was collected by a private oil company. The well separation is 1225 ft, and the source and receiver spacing is 10 ft. with a total of 500 ft of vertical aperture. The source gathers from 4850 ft. to 4985 ft. had a receiver spacing of 5 ft. Typical seismograms had a Nyquist frequency of approximately 1000 Hz.

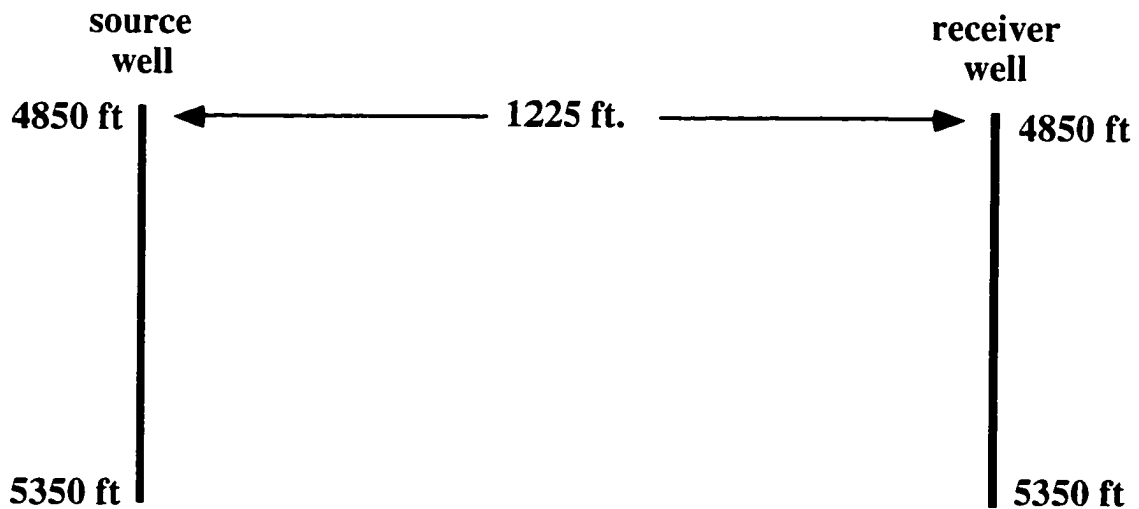


Figure 5.1: Data set geometry.

5.3 PRE-PROCESSED REFLECTION DATA

As was discussed in section 4.5, we need to perform wavefield separation to isolate the reflection data from the rest of the crosswell wavefield. We perform the same procedure as detailed in section 4.5, including removal of the direct arrival and separation into upgoing and downgoing reflections. On the real data example, we then apply an additional f-k filter

to further attenuate noise. Typical types of noise in crosswell data include converted reflections and tube wave noise. Figure 5.2(a) shows a CRG of the raw data, and then after pre-processing with enhancement for downgoing reflections with an additional f-k filter applied to further attenuate noise (figure 5.2(b)).

5.4 REFLECTION VELOCITY ANALYSIS

As was discussed in section 4.6, we perform velocity analysis to align the phase of the reflection data for stack. This consists of several steps shown in figure 4.7. We again want to select a number of CDPs for the survey that will give us a complete and accurate stack for the entire survey.

5.4.1 CDP Sorting of the Reflection Data

We start the reflection velocity analysis procedure by sorting the data into CDP gathers or common ratio gathers as was described in detail in Chapter 2. Figure 5.3 shows four CDP gathers for an assumed reflection depth of 4760 ft. located 240, 260, 280, and 300 ft. from the source well respectively. A 20 ft. bin for sorting the CDP gathers was used. We see a strong reflection event starting at about 90 ms at a radial distance of 320 ft. and increasing in traveltime for larger radial distances (larger distance between the reflector and the source and receiver).

5.4.2 Reflection Depth Estimation

As was shown in section 4.6.1, we need to determine the reflection depth at the chosen CDP location. As was shown in section 4.6.2 and discussed in section 3.8, we need some type of additional information in order to find the reflection depth. As was demonstrated in section 4.6.2, we can tie the reflection traveltime to the direct arrival traveltime in a CDP gather at a radial distance of zero, which is at the reflection depth (figure 4.10). We consider the CDP gathers shown in figure 5.4. The assumed reflection depth of 4760 ft. is only a preliminary estimate. We obtained this preliminary estimate of the reflection depth by considering the CDP gathers after a single stacking velocity has been applied for all radial distances. Figure 5.4 shows three different assumed reflection depth and stacking

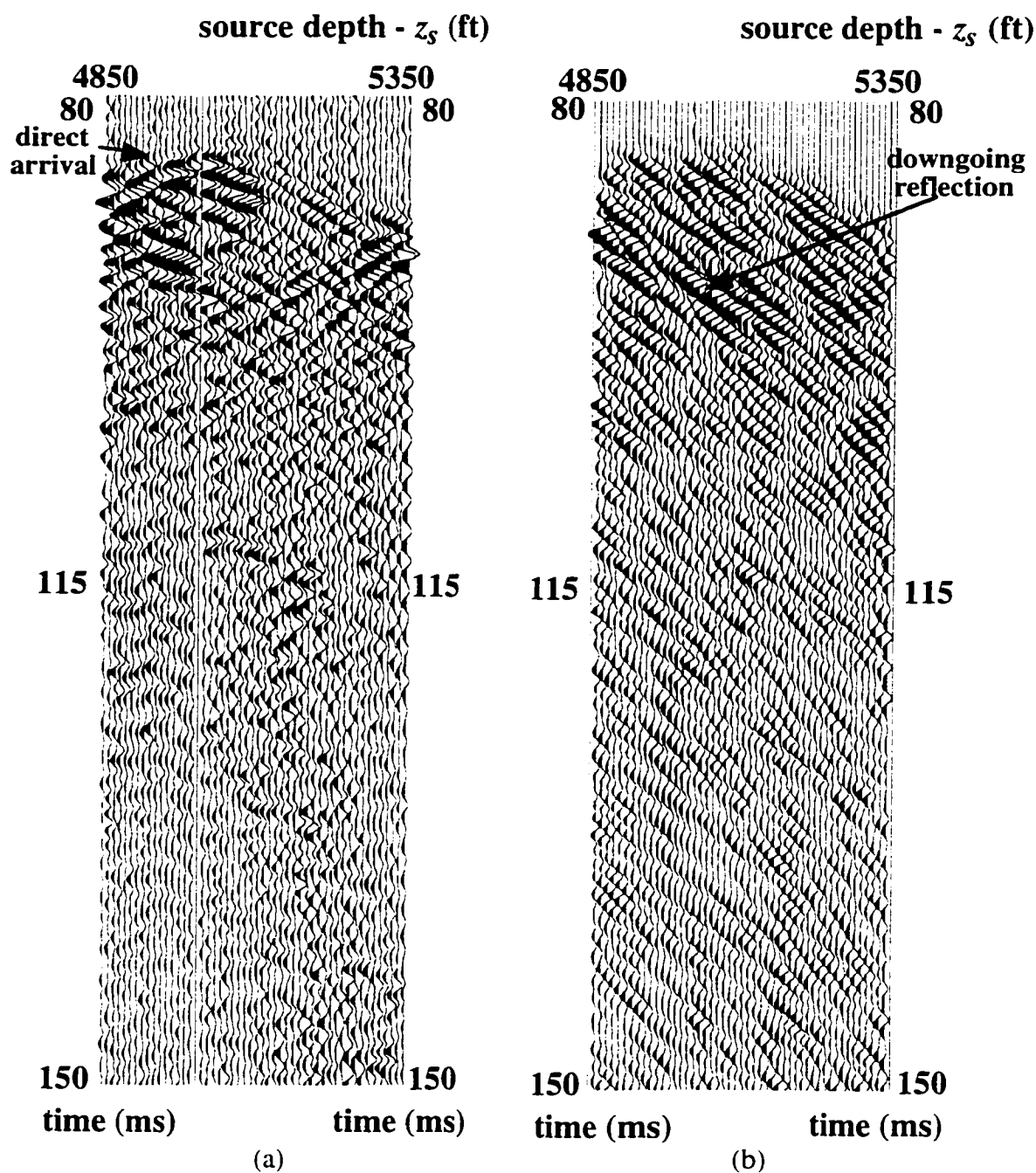


Figure 5.2: CRG at 4905 ft. of the field data (a), and after pre-processing to enhance downgoing reflections and attenuation of additional noise (b).

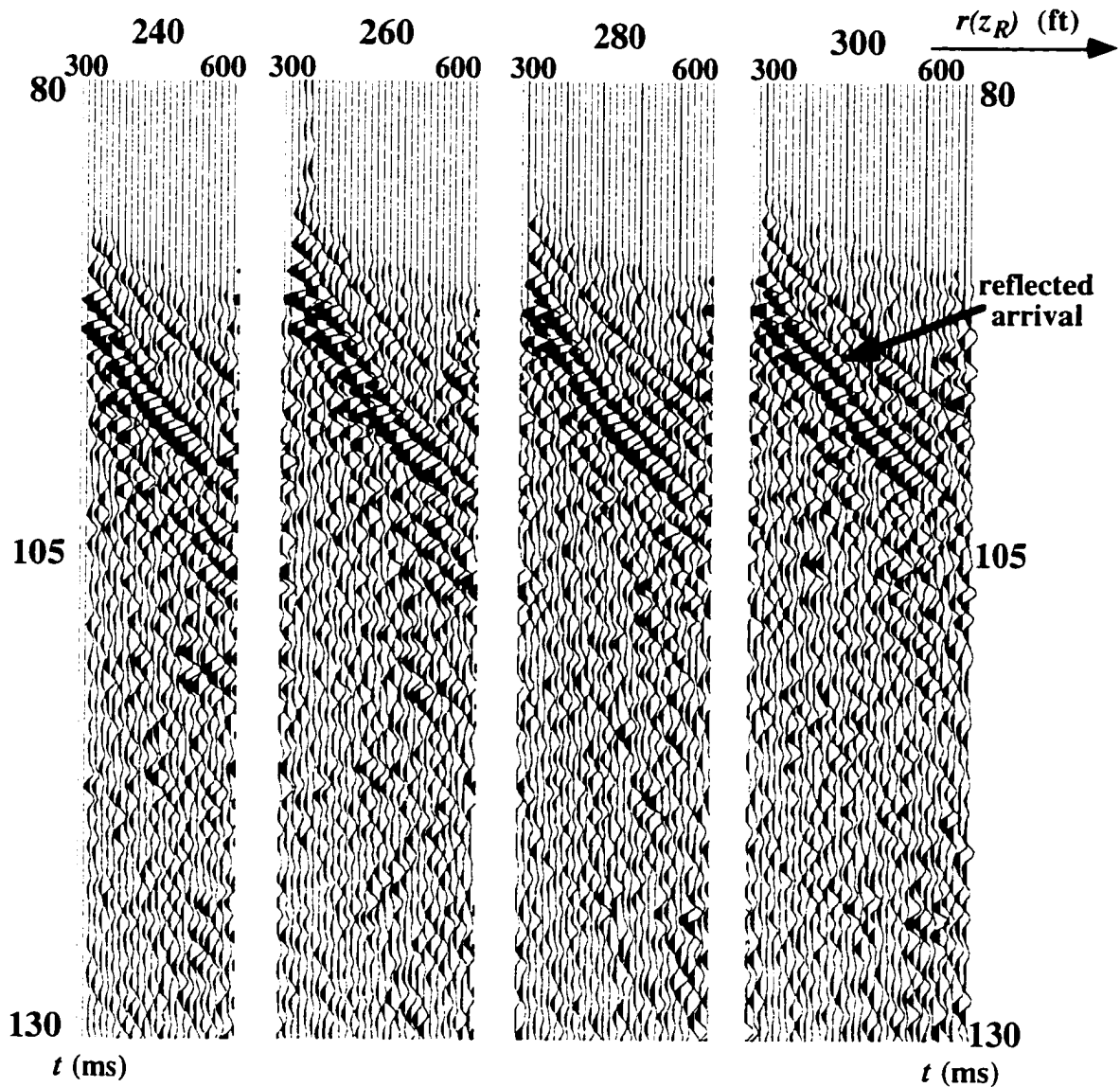


Figure 5.3: CDP gathers located at 240, 260, 280, and 300 ft. from the source well for the assumed reflection depth of 4760 ft. We see a reflection event that starts at about 90 ms for smaller radial distances. The first row of numbers corresponds to the CDP location, and the second row of numbers corresponds to the radial distances at each CDP.

velocity pairs for CDP - VLMO gathers. The reflection depths used were 4720, 4760, and 4800 ft. We need to examine the moveout of the reflection event, the coherency of the reflection event, and the visibility of the reflection event in the CDP gathers to estimate which reflection depth serves as the best approximation. From these CDP gathers we can estimate the reflection depth to be 4760 ft. The estimate at 4720 ft. shows less coherency in the reflection event due to CDP smear, particularly at the CDPs locations 240 ft. and 260 ft. from the source well. The estimate at 4800 ft. shows too much moveout in the reflection event as well as less coherency.

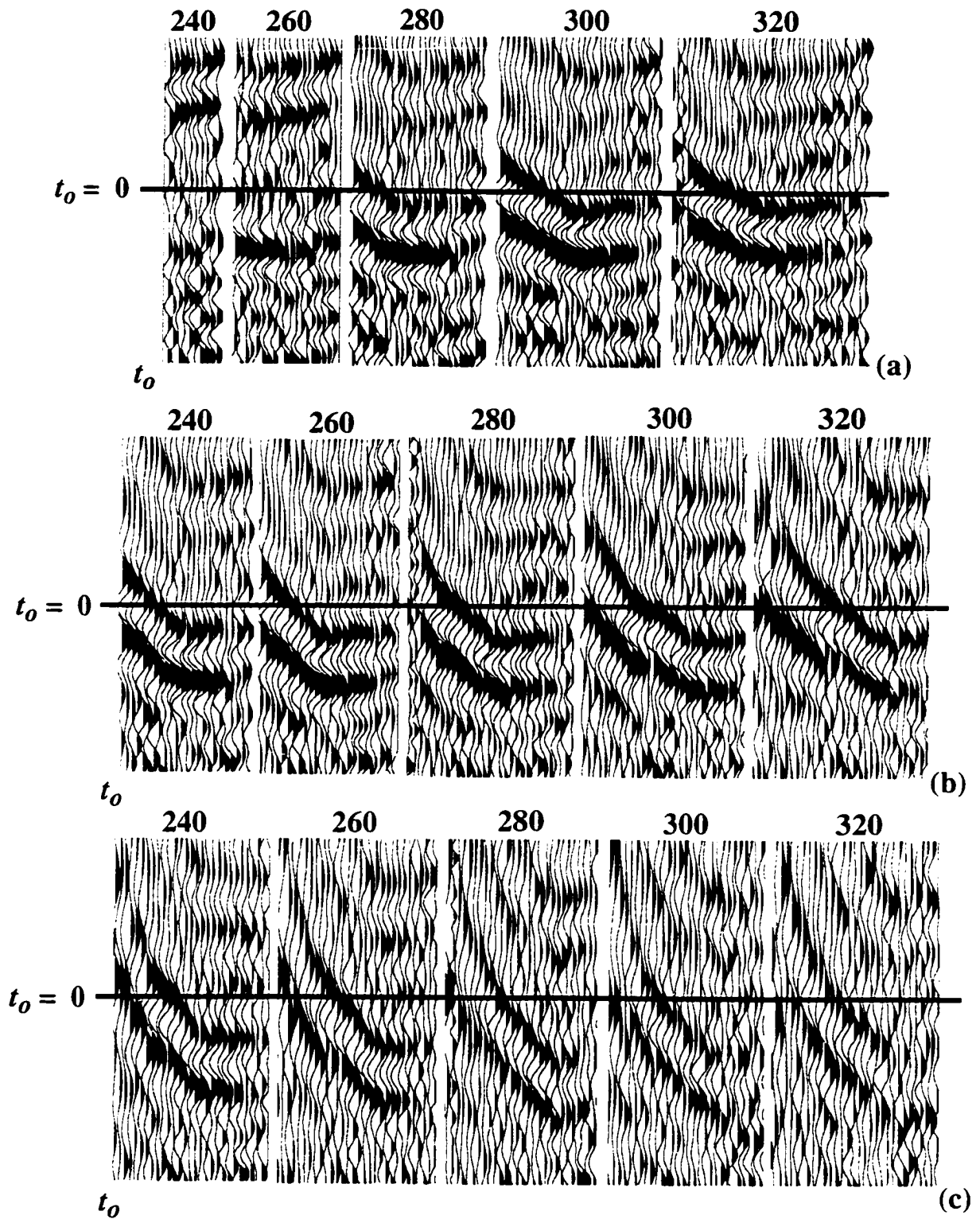


Figure 5.4: CDP-VLMO gathers for assumed reflection depths 4720 (a), 4760 (b), and 4800 (c) ft. We use the moveout and coherency of the reflection event to estimate the reflection depth from the reflection data itself.

Estimating the reflection depths for reflections below or above the survey makes using direct arrival tomography more difficult since direct arrivals only extend over the duration of the survey. Unfortunately on this data set, the available sonic log information was incomplete. A 1-d tomogram model is shown in figure 5.5. We use the velocity at the top of the tomogram to extend the velocity model to higher depths. As was discussed in section 4.6.2, we use the first visible reflection event traveltimes at the smallest radial distance, and the direct arrival tomogram velocity to estimate the stacking velocity. We use equation 4.2 to solve for the total vertical offset, by using the tomogram velocities in figure

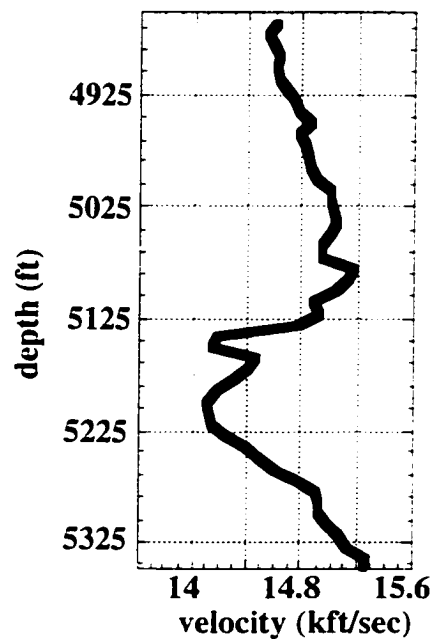


Figure 5.5: 1-d tomogram velocity model calculated from the direct arrival traveltimes.

5.5 to estimate the stacking velocity: $(v_{st})_c$ (section 3.6). We use the CDP gather at 280 ft. in figure 5.4. The radial distance of the first trace in this gather is 323 ft. (the source depth is 4855 ft. and the receiver depth is 5075 ft.). This corresponds to an estimated total vertical offset of 410 ft. The reflection traveltimes is 89.03 ms on this trace. The stacking velocity down to the reflection is estimated to be 14.71 kft/sec from the tomogram in figure 5.5. Equation 4.2 gives us the total vertical offset to be 421.35 ft. Equation 4.3 gives us a revised reflection depth estimate of 4754 ft. (rounded to the nearest integer).

5.4.3 Alignment of the Reflection Event

Once we have estimated the depth of the reflection, we can perform reflection velocity analysis as it was described in section 3.5. Figure 5.6 shows the reflection event at 4754 ft. after 1, 2, and 3 stacking velocities have been applied. We do not perform velocity analysis at the smaller radial distances since these correspond to large angles of incidence which yield a large stretch due to the non-linear HNMO correction as was described in section 3.5. Unlike the synthetic data set, we cannot be certain if the negative cycle or positive cycle represents the actual reflection event. Therefore it is possible that the alignment is along a side lobe. However as we see in figure 5.6 by aligning the side lobe we are also aligning the negative phase below it and the next positive cycle. Figure 5.7 shows the stacking velocities that were applied at this CDP location.

5.4.4 Velocity Analysis for CDPs in the middle of the survey

The signal to noise ratio of the reflection arrival decreases for CDPs further from either of the wells due to being buried deeper in the wavefield (Lazaratos, 1993). This often makes velocity analysis for CDPs in the middle of the survey more difficult. Figure 5.8(a) shows a CDP - VLMO gather for a reflection event at 4758 ft for a CDP 600 ft from the source well. Figure 5.8(b) shows the same CDP gather after the application of an f-k filter enhancing zero moveout. The f-k filter improved the coherency of the reflection event. Applications of additional filters are often necessary to resolve reflection events at CDPs midway between the wells. Figure 5.9 shows another CDP in the middle of the wells (620 ft. from the source well) for reflection depth 5188 ft. This gather did not require an f-k filter to resolve the reflection for velocity analysis. This is due to the reflection being a very strong event.

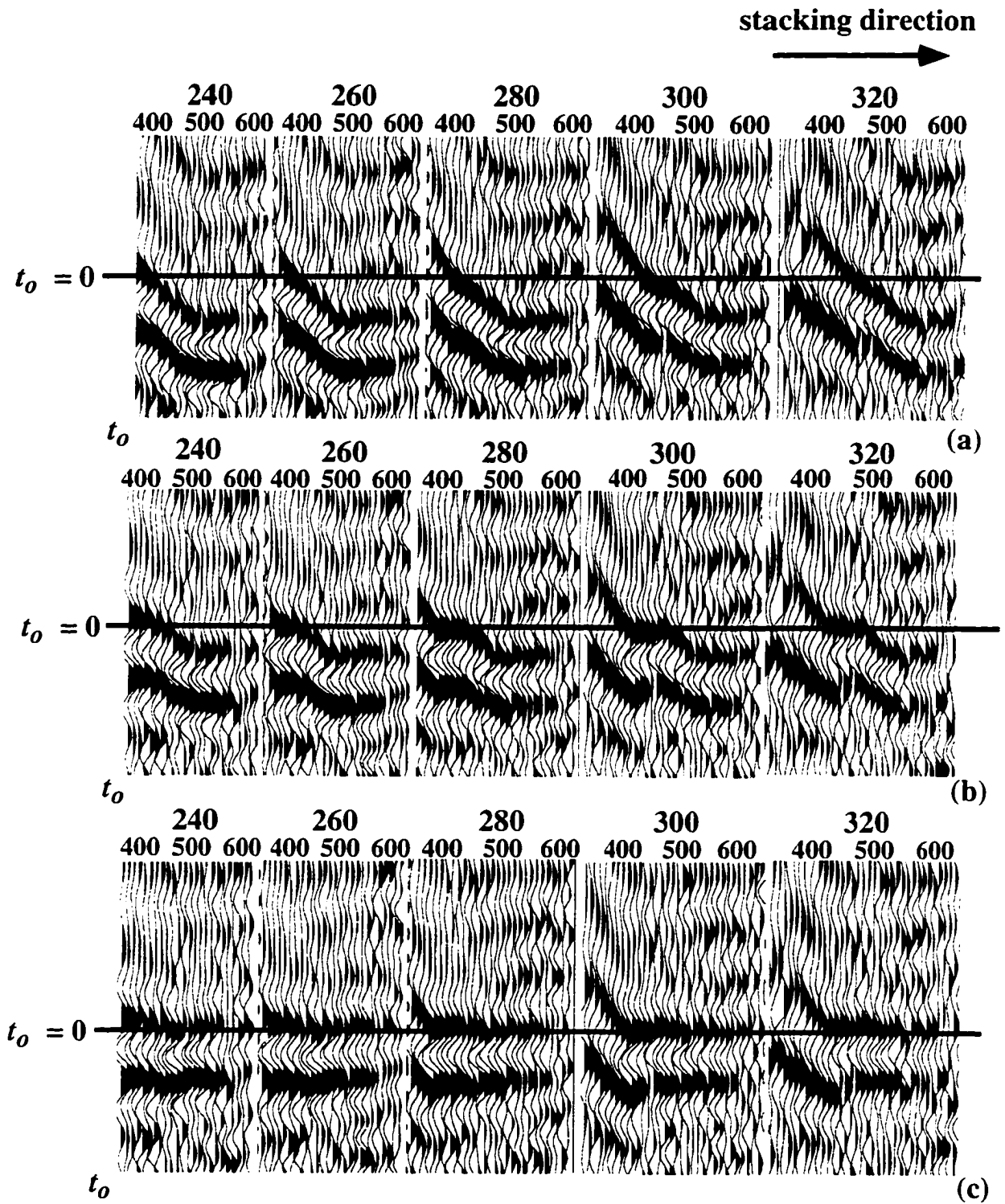


Figure 5.6: CDP gathers after the VLMO correction located at 240, 260, 280, 300, and 320 ft. from the source well for reflection depth 4754 ft. after 1(a), 2(b), and 3(c) stacking velocities were applied. The first row of numbers corresponds to the CDP location. The second row of numbers corresponds to the radial distance at each CDP. The units are feet.

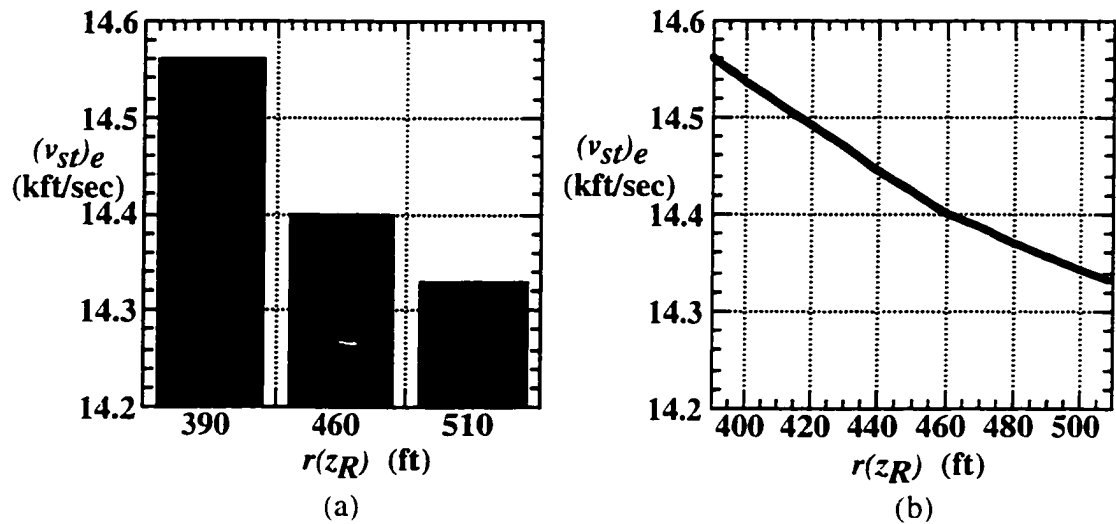


Figure 5.7: Stacking velocities for CDP depth 4754 ft, 280 ft. from the source well, for the radial distances where we performed velocity analysis (a), and all for all radial distances (b).

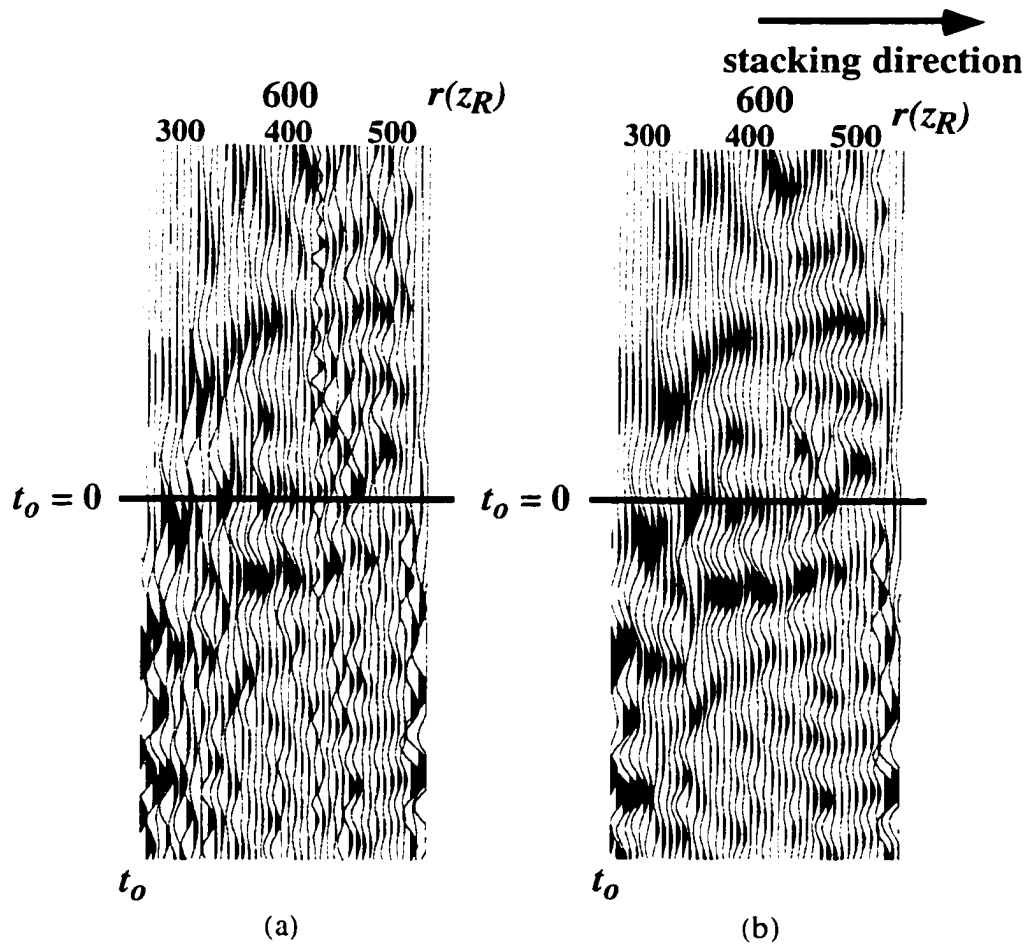


Figure 5.8: CDP - VLMO gather for reflection depth 4758 ft, 600 ft. from the source well with no additional filter (a), and an f-k filter enhancing zero moveout (b). The f-k filter has enhanced the reflection event at $t_o = 0$.

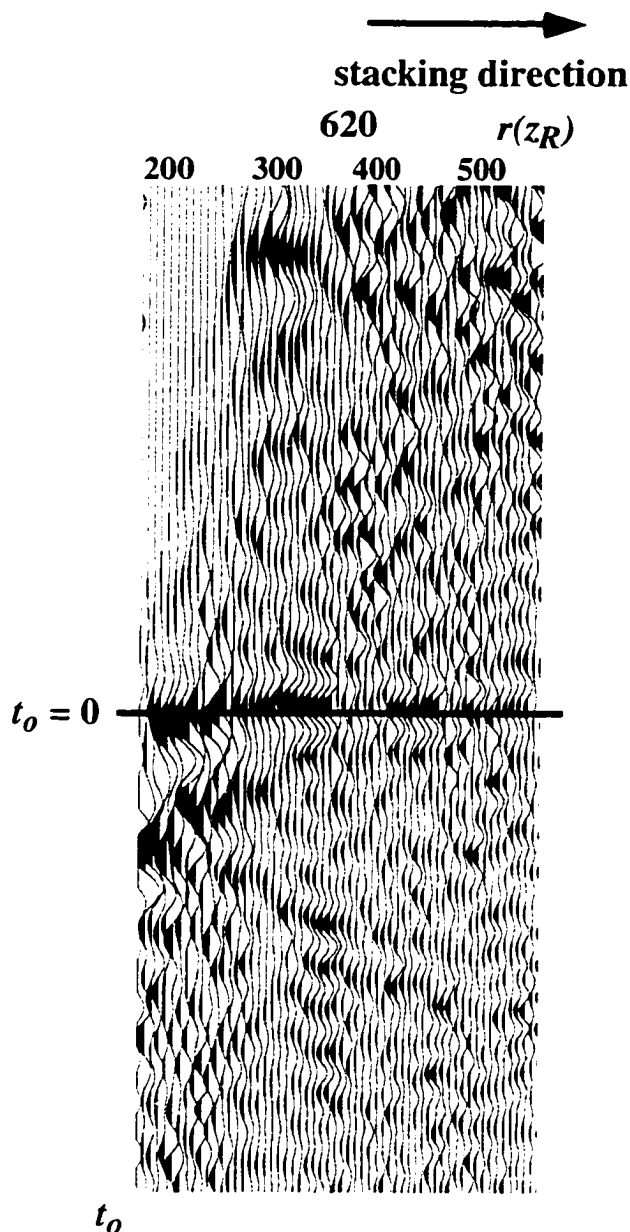


Figure 5.9: CDP - VLMO gather for reflection depth 5188 ft, 620 ft. from the source well.

5.4.5 Stacking Velocity Grid

As was discussed in section 4.6.4 we need to perform reflection velocity analysis at CDPs of varying lateral location and depth in order to obtain a coherent reflection stack for the entire survey. Figure 5.10 shows the locations of CDPs used for velocity analysis for the entire survey. As was discussed in section 4.6.3 the stacking velocities are linearly interpolated between CDPs for each radial distance.

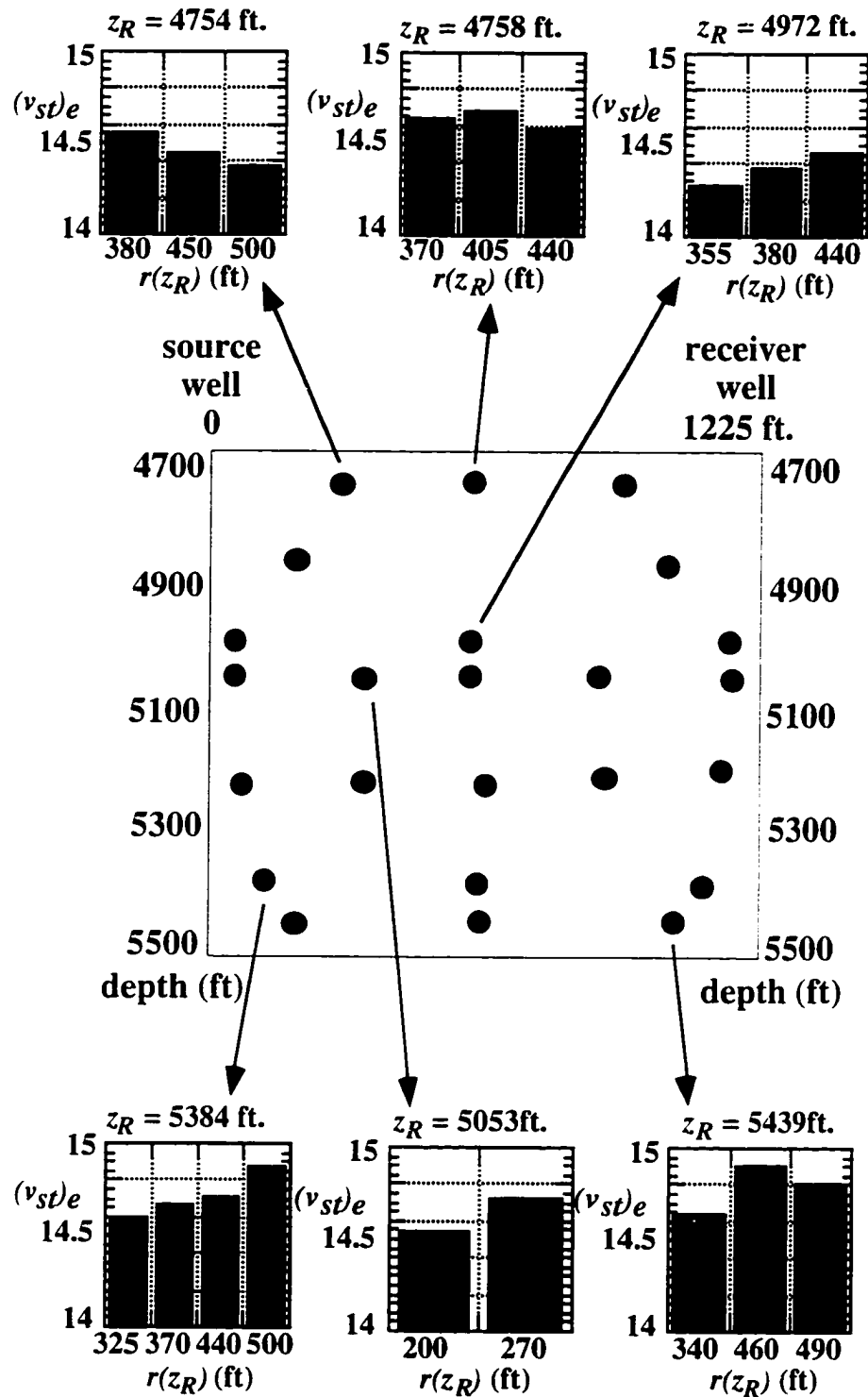


Figure 5.10: CDP stacking velocity grid for the entire survey.

5.7 FINAL REFLECTION IMAGE STACK

As was discussed in section 4.7 the data is mapped from time to image space using a point to point mapping operator. The stacking velocities are interpolated between CDPs as was discussed in section 4.7.3. As was discussed in section 4.7 the image uses data pre-processed for reflections in both CSGs and CRGs for both upgoing and downgoing reflections. Additionally on this data set, the middle depth sections (between 5030 ft. and 5330 ft.) were imaged separately due to the very wide angles of incidence of the reflection raypaths. As was discussed previously, the data is stretched when mapped due to the angle of incidence of the reflection raypath. The vertical wave number for a given frequency component after it has been mapped is given by (Lazaratos, 1993):

$$k_z = 2 \frac{w}{v} \cos \phi, \quad (5.1)$$

where w is the frequency component, and ϕ is the angle of incidence of the reflection raypath. The change in the vertical wave number as a function of the incidence angle can be determined by taking the derivative of equation (5.1):

$$\frac{\partial k_z}{\partial \phi} = -2 \frac{w}{v} \sin \phi. \quad (5.2)$$

From equation 5.2 we see that the stretch in the waveform increases more rapidly with increasing incidence angle (the vertical wave number decreases more rapidly). On this data set the middle depth section of the image has reflections with incidence angles of 70 degrees, where reflection data above and below the survey have angles of incidence between 45 and 60 degrees.

The reflection depth increment in the CDP imaging algorithm (section 4.7) is 2 ft. The data is binned in 6 ft. CDP gathers for stack. As was discussed previously, we used f-k filters to enhance the data for certain CDPs in the velocity analysis procedure. After the data is mapped into image space, we apply global 2-d Fourier filters (now k_x - k_z filters) before stack in each of the 6 ft. CDP gathers. We have also applied additional bandpass and moderate f-k filtering to enhance the final stack. The final stack is shown in figure 5.11.

For comparison, we obtained a stack using the XSP-CDP mapping method (figure 5.12) (Lazaratos, 1993). The XSP-CDP method uses a 1-d tomogram for the velocity model (figure 5.5). Clearly the images are quite different, with the CDP sorting and velocity analysis imaging method giving a much more coherent overall stack. In particular,

the CDP sorting and velocity analysis method yielded numerous continuous reflections from the source well to the receiver well, where the XSP-CDP method failed to give the same reflector coherency. Previous tomographic information indicated small 2-d variation in seismic velocity ($<10\%$) (figure 5.13). As we demonstrated in the previous chapter, the CDP imaging method can generate coherent reflection images in regions with 2-d variation in velocity by finding stacking velocities that optimize the reflection data for stack over a 2-d grid of CDPs. One other difference between the two images are the events in the middle and bottom depths parts of the image. The raytracing in the XSP-CDP imaging method does not allow for the raypaths to connect for the very wide angles of incidence corresponding to this part of the image, therefore there is limited reflector information. The bottom part of the CDP image shows more coherent reflections, but an overall lower frequency. This is partially due to the alignment of the reflection data in CDP gathers. The reflection alignment acts to filter out noise and makes the reflection appear as a single event.

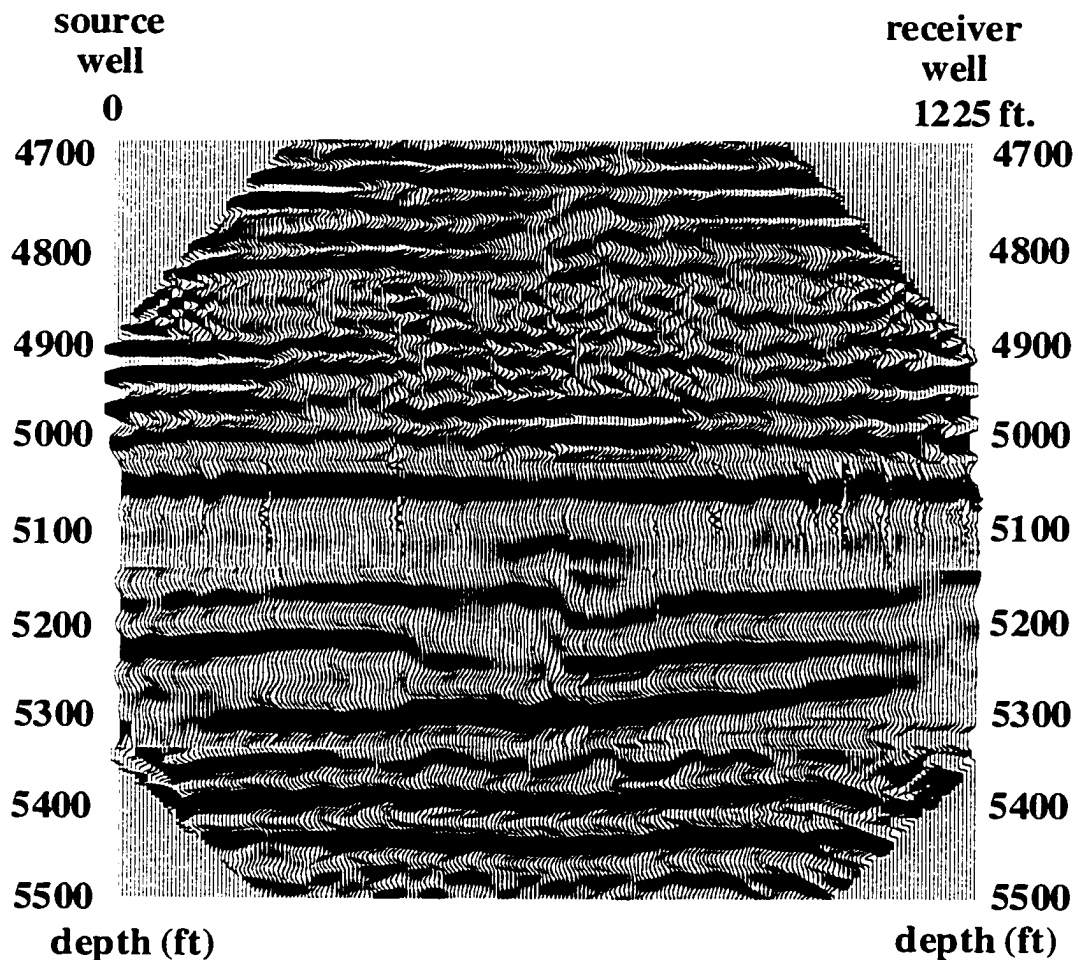


Figure 5.11: Final reflection image stack using CDP sorting and reflection velocity analysis.

Individual reflection events can appear as multiple events if the misalignment of the reflection data in CDP gathers is greater than half a wavelength. The lower frequency is also due to additional bandpass and f-k filtering performed during the mapping procedure in CDP gathers.

Despite the differences in the qualities of the stacks, there are similarities in the type of structure indicated by the two images. The top part of both images (between 4700 - 5000 ft.) indicate flat events. The middle depth part (5100 - 5250 ft.) of both images shows more complicated structure with reflection events dipping upward toward the receiver well.

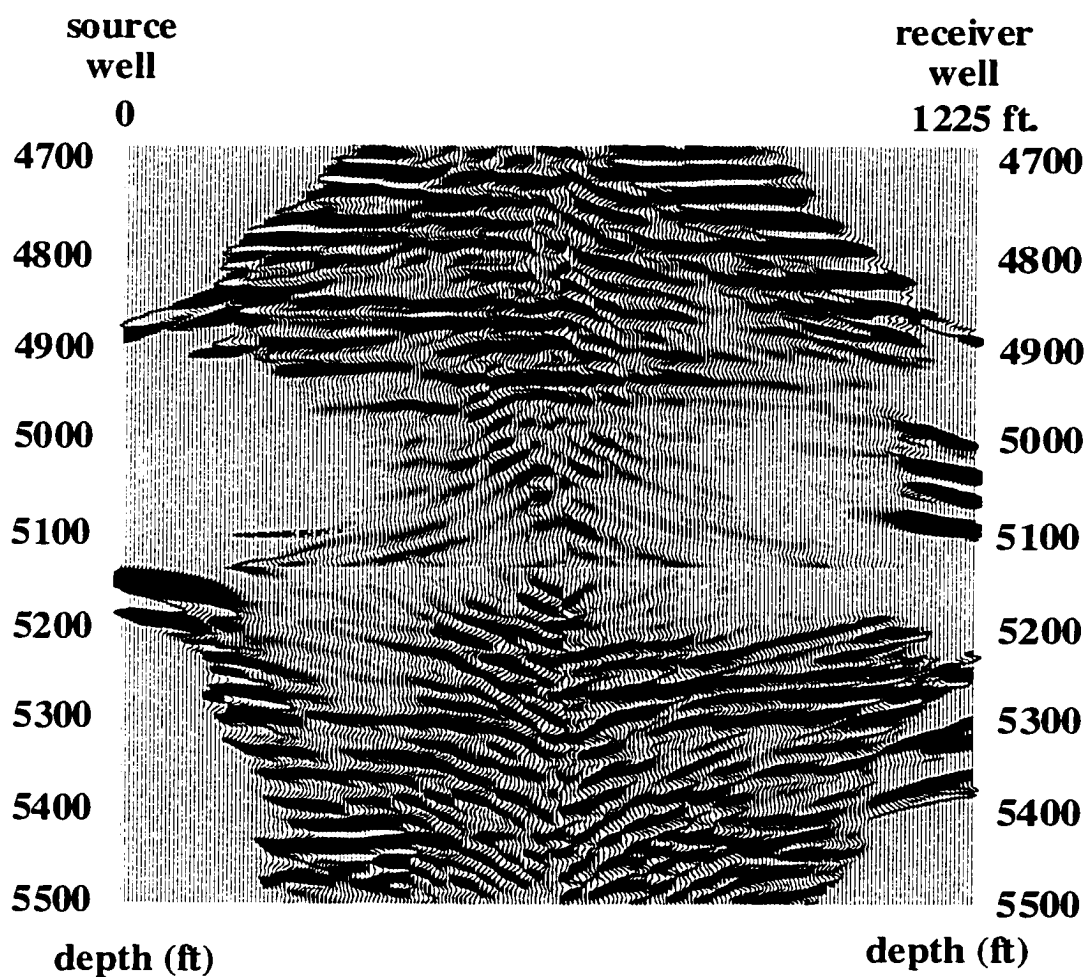


Figure 5.12: Final reflection image stack using XSP-CDP reflection imaging.

We also compare the CDP reflection image to the 2-d tomogram. The tomogram was generated by a SIRT algorithm. We see 2-d velocity variation in the tomogram. We see some correlation in the basic geological structure of the CDP sorting and velocity analysis reflection image to the tomogram. The velocity variation is small over the top part of the image (4825-5050 ft), particularly laterally. The reflection image indicates primarily 1-d structure in this part of the image. The tomogram has a strong change in the velocity at approximately 5070 ft. and the reflection image has a strong reflection event at this depth. Below this reflection event the tomogram has 2-d velocity variation, and the reflection image indicates 2-d structure. However, the reflection image gives us higher resolution of the structure of the medium. There are two reasons for this:

- 1) Each seismic trace can potentially contain several reflected arrivals, while only containing one direct arrival.
- 2) The wave equation gives us the full waveform reflection data information, while an integral gives us the direct arrival traveltimes information.

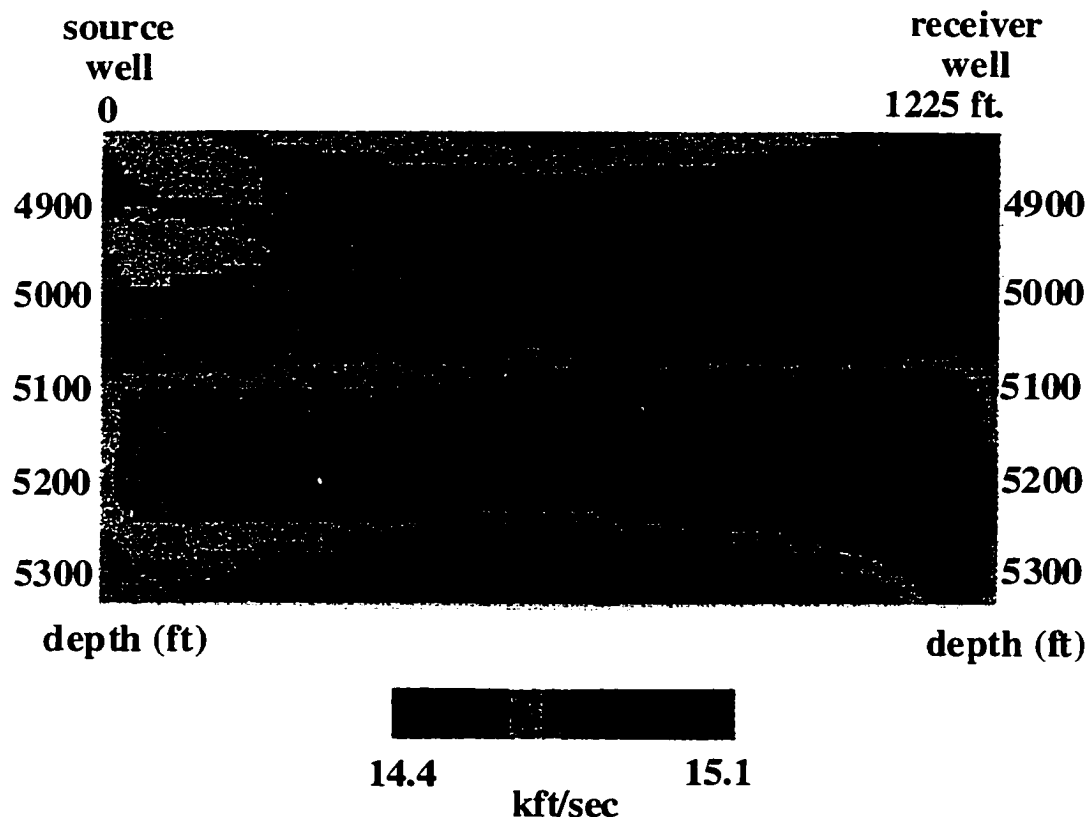


Figure 5.13: 2-d tomogram generated using SIRT. The tomogram and the CDP reflection image indicate the same general geological structure.

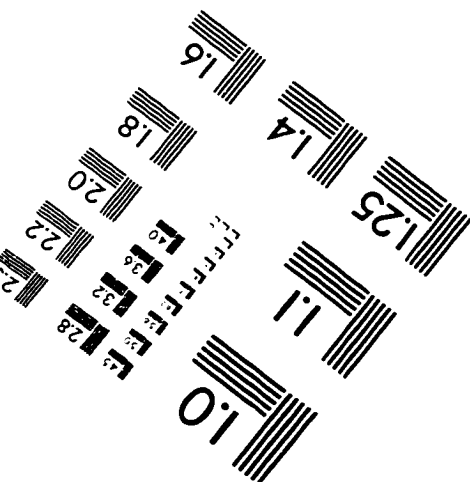
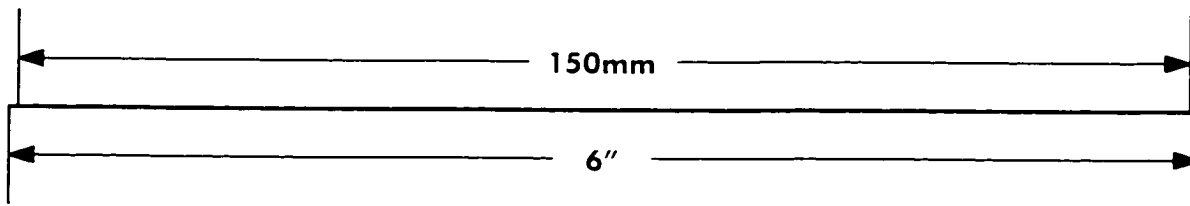
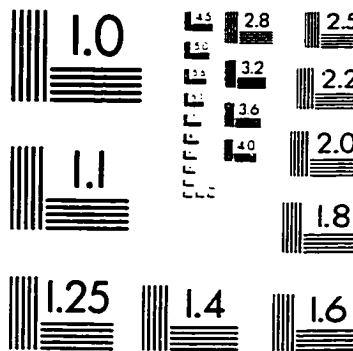
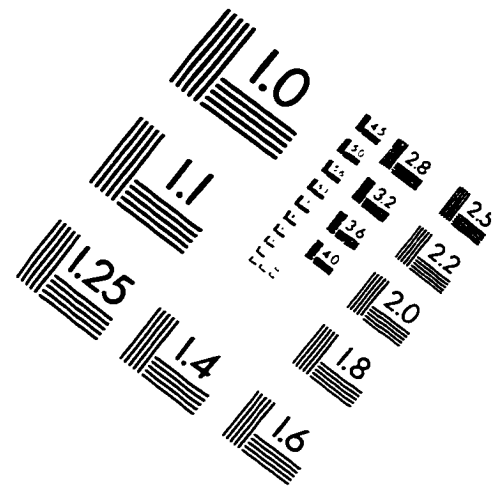
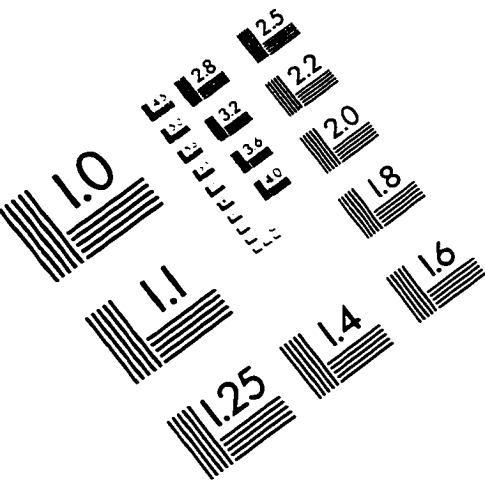
5.8 CONCLUSIONS

We have taken raw field data from a crosswell survey with a wide well offset (1225 ft), and processed it to obtain a final stacked reflection image. We did this using a new CDP reflection imaging algorithm described in chapter 4. It was shown that we could apply the theoretical concepts of Chapters 2 and 3 to a field data set. The final stack yielded a coherent reflection image with numerous continuous reflections that extended from the source well to the receiver well. We compared the CDP reflection velocity analysis based imaging result with the XSP-CDP mapping result. Both reflection imaging methods indicated the same general geological structure. However, the CDP method produced a much more coherent stack than the XSP-CDP method, due to the CDP imaging method's ability to find the stacking velocities that optimized the reflection data for stack over a 2-d grid of CDPs. We also compared the CDP sorting and velocity analysis reflection image to a 2-d SIRT tomogram. The tomogram showed the same general geological structure as the CDP reflection image, with the CDP reflection image giving a higher resolution image of the medium.

References

- Aki & Richards, 1980, Quantitative Seismology, pp. 627-629.
- Claerbout, J., 1985, Imaging the Earth's Interior.
- Harris, J.M., Lazaratos, S.K., Michelena, R., 1990, Tomographic String Inversion, Expanded Abstracts of the 60th Annual Meeting, Society of Exploration Geophysicists, San Francisco pp. 375-378.
- Harris, J.M., Wang, G.Y., 1996, Diffraction Tomography for Inhomogeneities in a Layered Background Medium: Geophysics, Vol. 61, pp. 570-583.
- Lazaratos, S.K., 1993, Crosswell Reflection Imaging, Ph.D. Dissertation, Stanford University.
- Lines, L., Tan, H., Treitel, S., Beck, J., Chambers, R., Eager, J., Savage, C., Queen, J., Rizer, W., Buller, P., Cox, D., Sinton, J., Ballard, J., Kokkoross, G., Track, A., Guerendel, P., Harris, J., Lazaratos, S., and Van Schaack, M., 1995, Integrated Reservoir Characterization: Beyond Tomography: Geophysics, Vol. 60, pp. 354-364.
- Mo, L., 1993, Migration of Crosswell Seismic Data, Expanded Abstracts of the 63rd Annual Meeting, Society of Exploration Geophysicists, Washington D.C., pp. 317-320.
- Qin, F., and Schuster, G.T., 1993, Constrained Kirchhoff Migration of Crosswell Seismic Data, Expanded Abstracts of the 63rd Annual Meeting, Society of Exploration Geophysicists, Washington D.C., pp. 99-102.
- Stewart, R.R. and Marchisio, G., 1991, Crosswell Seismic Imaging Using Reflections, Expanded Abstracts of the 61st Annual Meeting, Society of Exploration Geophysicists, Houston, pp. 375- 378.
- Van Schaack, M., 1997, Velocity Estimation for Crosswell Reflection Imaging Using Combined Direct and Reflected Arrival Traveltime Tomography, Ph.D. Dissertation, Stanford University.
- Taner and Koehler, 1969, Estimating Velocity Spectra, Geophysics, pp. 859-881.
- Wyatt, K., and Wyatt, S.B., 1981, Determination of Subsurface Structural Information Using the Vertical Seismic Profile, Expanded Abstracts of the 51st Annual Meeting, Society of Exploration Geophysicists, pp. 1915-1919.
- Yilmaz, 1987, Seismic Data Processing, pp. 159-160.

IMAGE EVALUATION TEST TARGET (QA-3)



APPLIED IMAGE, Inc.
1653 East Main Street
Rochester, NY 14609 USA
Phone: 716/482-0300
Fax: 716/288-5989

© 1993, Applied Image, Inc., All Rights Reserved

